4-1-2005

The Influence Of Local Rivers On The Eastern Cariaco Basin, Venezuela

Laura Lorenzoni
University of South Florida

The Influence Of Local Rivers On The Eastern Cariaco Basin, Venezuela

by

Laura Lorenzoni

A thesis submitted in partial fulfillment
of the requirements for the degree of
Master of Science
College of Marine Science
University of South Florida

Major Professor: Frank E. Muller-Karger, Ph.D.
Kendall L. Carder, Ph.D.
Gabriel A. Vargo, Ph.D.

Date of Approval:
April 1, 2005

Keywords: bottom nepheloid layer, colored dissolved organic matter, subtropical underwater, remote sensing reflectance, anoxic basin

Acknowledgements

If I wanted to thank all the people that have made this possible by enriching my knowledge, lending a hand when in need or just sharing special moments during my stay at the College of Marine Science, I'd have to write another manuscript, with twice the number of pages (including figures). Unfortunately, that is not an option, and I'll have to settle for this short page.

I want to thank first and foremost my husband; who has stood by me, in the good and the bad times. To my family and Gea, I would not be here if it was not for their love, constant support and faith in me.

Dr. Frank Müller-Karger, my advisor, gave me the opportunity to come to the College of Marine Science, and for that I'll be forever grateful. He believed in me and gave me the means to achieve what I aspired. One individual that deserves a very special recognition is Jim Ivey, who always had time for my questions, putting aside his own work to help me get through mine. I also wish to acknowledge Jennifer Cannizzaro, Robyn Comry, Dr. Chuanmin Hu, Dr. Robert Weisberg (and the Ocean Circulation Group), Dr. Peter Howd, Dr. Carlos del Castillo, Dr. Emmanuel Boss, Dr. Collin Roesler and Dr. Dennis Hansell for their help both in the data processing and analysis. I want to thank my committee members, Dr. Ken Carder and Dr. Gabriel Vargo, for their wisdom and support.

To our friends and colleagues at EDIMAR, especially Yrene Astor, Ramón Varela, Glenda Arias, Aitzol Arrellano and Chuchu, without them and the crew of the Hermano Ginés this work would have never been possible. Thank you for bearing with us during those long sampling days and making this project work. To Luchi, Damaris. Marina, Lucia, Michelle, Ester and the entirety of the IMaRS lab, thank you for those helping hands. To my friends, near and far, you mean the world to me.

For those that I failed to mention, I know who you are, and I thank you all so much.

Financial support for this work was provided by The National Science Foundation OCE0118566 and OCE 0326268.

Table of contents

List of tables

Chapter I

Chapter II

List of figures

Chapter I

The Influence of Local Rivers on the Eastern Cariaco Basin, Venezuela

Laura Lorenzoni

ABSTRACT

Two oceanographic cruises were conducted during September 2003 and March 2004 in the eastern half of the Cariaco Basin. Specific objectives were to examine the hydrography of the seasonal upwelling plume characteristic of this region, the spatial distribution of particles in the area, and to help determine the source and relative importance of *in situ* particle production vs. terrigenous particles delivered laterally from the coast. .

During September 2003, average surface salinities within the basin were higher (~36.6) relative to Caribbean Sea waters outside the basin (~35.6). Salinity patterns indicated that the Orinoco and Amazon River plumes did not enter or influenced the basin directly.

The upwelling plume in March 2004 stimulated primary productivity. Beam attenuation and CDOM fluorescence profiles showed marked vertical structure in biomass of microbial populations, particularly near the oxic-anoxic interface typically located between about 250 and 300 m. There is an increasing difference in temperature and salinity between the Cariaco Basin and the adjacent Caribbean Sea below 200 m. Inside the Basin temperatures and salinities were higher by 4^{o}C and 0.5.

The influence of local rivers on the Cariaco Basin was evident during September 2003. Low salinity plumes with high beam attenuation (~ $1m^{-1}$) lined the southern margin of the Basin. The primary rivers that affected the basin were the Unare and Neverí. Their sediment input affected the shelf near the river mouths, and a surrounding radius of up to 40 Km. Their low salinity plumes were carried northwestward toward the CARIACO time series station. In March 2004, there was minimal or no terrigenous input from local rivers. Near the Manzanares River, off the city of Cumaná, and near Cubagua Island, located south of Margarita Island, attenuation due to suspended particles (~0.09 m^{-1}) was observed at depth (70-150 m) during both cruises (~0.09-0.15 m^{-1}). Therefore, sediment transport from the shelf into the basin seems to occur year-round. More observations are necessary to determine the nature and origin of these particles. In March 2004, there was minimal or no terrigenous input

Foreword

The study is based on data collected during two cruises, carried out in September 2003 and March 2004, in the framework of the CARIACO (CArbon Retention In A Colored Ocean) time series project. Specifically, the objective of the study was to identify sources of particulate material that may contribute to sediments accumulating in the Cariaco Basin ($10^{o}30'$ N $64^{o}40'$ W). This knowledge helps explain the paleoclimatology record stored in these sediments.

The thesis is divided into two chapters. The first focuses on oceanographic interactions between the Cariaco Basin and the open Caribbean Sea, and the second on the impact of local rivers and their sediment load on the basin. Each chapter contains an introduction that explains the rationale of the work conducted, as well as methods, results and discussion, and conclusions. An overall conclusion chapter is included at the end of the thesis.

List of symbols

Symbol/Acronym	*Definition*	*Units*
$a(\lambda)$	Absorption coefficient at wavelength λ	m^{-1}
a_{CDM}	Absorption coefficient of colored dissolved and detrital material	m^{-1}
a_d	Absorption coefficient of detritus	m^{-1}
a_g	Absorption coefficient of CDOM	m^{-1}
a_T	Total absorption	m^{-1}
a_w	Absorption coefficient of water	m^{-1}
BNL	Bottom nepheloid layer	-
$c(\lambda)$	Attenuation coefficient at wavelength l	m^{-1}
CDM	Colored dissolved and detrital material	-
CDOM	Colored Dissolved Organic Matter	-
COHRO	Campaña Óptica e Hidrográfica Región Oriental (September 2003)	-
COHRO2	Campaña Óptica e Hidrográfica Región Oriental 2 (March 2004)	-
CSW	Caribbean Surface Waters	-
DOC	Dissolved organic carbon	-
E_d	Downwelling irradiance	$W\ m^{-2}\ nm^{-1}$
FCDOM	CDOM fluorescence	AU
FChl	Chlorophyll fluorescence	AU
INL	Intermediate nepheloid layer	-
K_d	Diffuse attenuation coefficient	m^{-1}
$OD(z_{eu})$	Optical Depth at which 1% downward irradiance is reached	m
PSD	Particle size distribution	-
Rrs	Remote sensing reflectance	-
S	Spectral slope of the exponential fit to a_g	nm^{-1}
SeaWiFS	Sea-viewing Wide Field-of-View Sensor	-
SUW	Subtropical Underwater	-
TACW	Tropical Atlantic Central Waters	-
γ	Hyperbolic slope of c	Dimensionless
λ	Wavelength of light	nm
λ_o	Reference wavelength	nm
ξ	Hyperbolic slope of the PSD	Dimensionless
ζ	Optical depth	Dimensionless

CHAPTER I

HYDROGRAPHY OF THE EASTERN CARIACO BASIN, VENEZUELA

1. Introduction

The Caribbean Sea does not contain a single, uniform water mass. Rather, it contains several water masses that show spatial and temporal changes. Understanding the distribution and variability of these water masses is relevant to the interpretation of the climate record contained in sediments of the Cariaco Basin in the southern margin of the Caribbean Sea. Here we examine this variability by studying hydrographic properties associated with different water masses and patterns in the color of marine waters including factors that change them, such as variation in colored dissolved organic matter concentration.

The upper portion of the water column in the Caribbean Sea, Caribbean Surface Water (CSW; Wust, 1964; Morrison and Nowlin, 1982), is characterized by low salinity (<35.5) and higher concentrations of silicates, as compared to underlying waters, attributed to the influence of the Amazon and Orinoco Rivers. Froelich et al. (1978) concluded that 60% of the freshwater in the Caribbean is from the Amazon River. The Orinoco and Amazon rivers affect the sea surface salinity (SSS) in the tropical Atlantic at great distances from their point of discharge (Muller-Karger et al., 1989; Hu et al., in press). Both rivers reach the Caribbean Sea (Muller-Karger & Varela, 1989; Hellinger & Gordon, 2002). The Orinoco plume grows in August through November (Muller-Karger et al., 1989; Hellweger and Gordon, 2002). Together, these rivers influence surface salinities (Morrison and Smith, 1990) and pigment distribution of the Caribbean Sea (Muller-Karger et al., 1989; Bidigare et al. 1993). SeaWiFS and other surface spectral reflectance (SSR) satellite imagery are able to trace the circulation of Amazon and Orinoco rivers in the near-surface Caribbean waters (Muller-Karger and Varela, 1989, Hu et al, in press). Their joint plumes have been traced with satellite ocean color images at least as far north as Puerto Rico. Though the dispersal of the Orinoco and Amazon is fairly well understood in the open Caribbean, there is a lack of information on what is the effect of these large river plumes on the southern margin of the Caribbean Sea.

Below the CSW, between 75 and 150 m, is the Subtropical Underwater (SUW). The SUW is characterized by a salinity maximum (36.8; Morrison and Smith, 1990). Also of importance are the 18°C Sargasso Sea Water (SSW; located in the central Caribbean between 200 and 400 m, characterized by an oxygen maximum; Kinard et al, 1974), the Tropical Atlantic Central Water (TACW; between 400-700 m and recognizable by an oxygen minimum), and Antartic Intermediate Water (AAIW, below 700 m with low salinity and high silicate content; Morrison and Nowlin, 1982). There is very little known about the spatial and temporal variability, or even the origin, of some of these water masses. Much less is known about their influence on properties around the margin of the Caribbean basin.

The Cariaco Basin (Figure 1.1) is located off the coast of Eastern Venezuela. The Basin is formed by the strike slip fault zones of El Morón and El Pilar (Schubert, 1982). It contains two depressions, the Eastern deep and the Western deep, separated by a sill of

less than 900 m. Each depression reaches depths of ~1400 m. The basin is bound to the south by the Unare platform, to the north by the Tortuga Bank, and to the East and West by continental Venezuela. The Cariaco Basin is connected to the Caribbean Sea through a sill of about 100 m deep, which is cut by the Centinela Channel to the west and the Tortuga Channel to the north, both of a depth of about 140 m.

Processes in the Caribbean Sea affect the exchange of waters with the Cariaco Basin, its productivity and vertical carbon flux (Muller-Karger et al., 2001). The Cariaco Basin is anoxic below 250 m because of decomposition of the flux of particulate organic matter settling from surface waters and the reduced circulation inside the basin. The origins of the basin date back to the Quaternary, and since then it has seen several alternating episodes of anoxia during interglacials and oxicity mostly during glacial times (Peterson et al., 1991; Hughen et al, 1996; Lin et al., 1997; Haug et al., 1998; Peterson et al., 2000). The sediment record extracted to date under the Ocean Drilling Program extends back an estimated 600,000 years (Hughen et al, 1996; Yarincik et al., 2000).

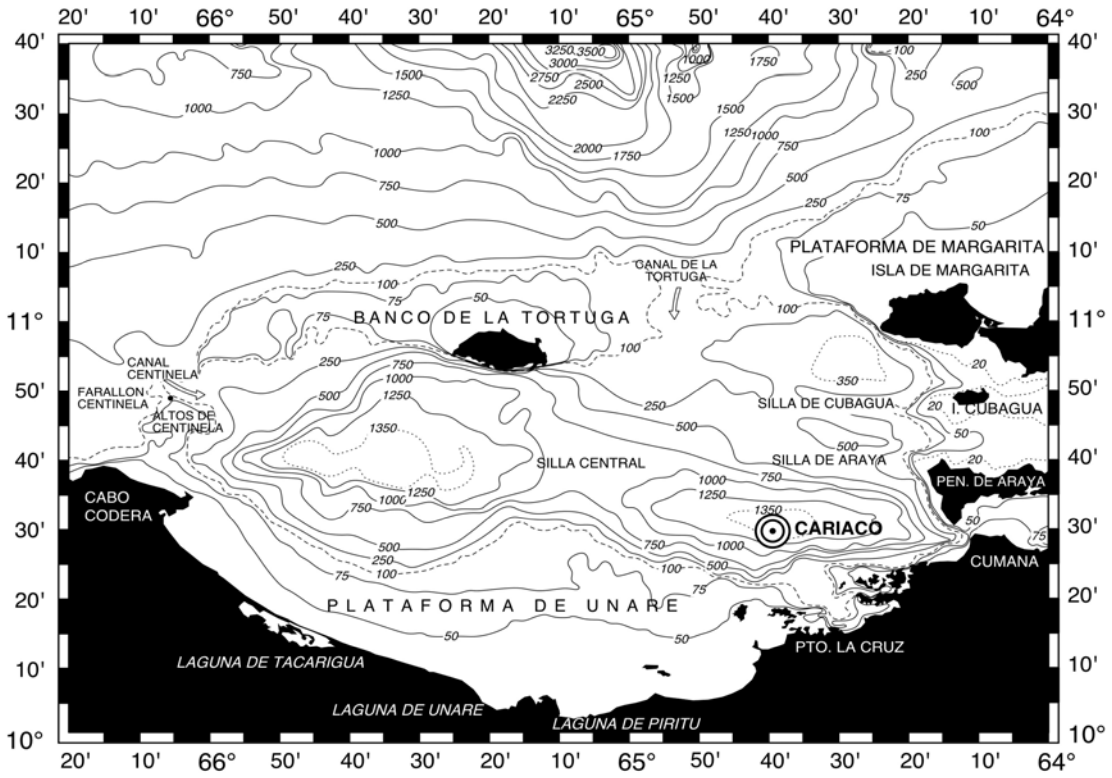

Figure 1.1: Schematic of the Cariaco Basin, showing location of the CARIACO time series station (from Astor et al., 2003).

Due to its present anoxic state and sedimentation rate (1 cm/1000 years), the Cariaco Basin conserves in its sediments a record of processes that cover the present interglacial period (Thunell, 1997; Black et al., 1999; Muller-Karger et al., 2000; Peterson et al., 2000). In order to correctly interpret the record of this and gain insight about past interglacials, it is necessary to have a clear understanding of the processes that occur in the water column of the Cariaco Basin.

The CARIACO project has over 9 years of data which have provided invaluable information on primary productivity and geochemical cycles in the tropics, as well as a better understanding of processes that occur in anoxic environments (Muller-Karger et al., 2001; Astor et al., 2003; Kessler et al., 2004; Muller-Karger et al. 2004). However, the one-location sampling is not enough to gain a full understanding of the processes that affect the basin, and the important role that the Caribbean and large South American Rives may play on the productivity and possible sediment and nutrient transport of the region.

1.1. Objectives

The objective of this chapter is to understand the influence of the Caribbean Sea and large South American Rivers, like the Orinoco, on the Cariaco Basin. More specifically, we want to answer the following questions:

- Which water masses enter the Cariaco Basin from the adjacent Caribbean Sea?
- Do the Orinoco and Amazon rivers contribute dissolved and/or detrital material to the Cariaco Basin? What is the role of small, local rivers?
- What is the vertical distribution of colored dissolved organic matter (CDOM) in the Cariaco basin? Is the Caribbean Sea a source of CDOM to the Basin?

2. Methods

Two cruises were conducted to the Cariaco Basin on board of the *R/V Hermano Gines* (Fundación La Salle de Ciencias Naturales de Venezuela). The first cruise was conducted in September 2003 (COHRO – Campaña Optica e Hidrografica Región Oriental). The objective of this cruise was to study the impact of rivers, both local and distant, specifically the Orinoco and Amazon, on the Cariaco Basin. Stations offshore were separated by a distance of approximately 20 km, but were more closely spaced near the coast (Figure 1.2A). The second cruise was carried out in March 2004 (COHRO2). The objective of the second cruise was to study the distribution of upwelling waters within the Cariaco Basin, and to determine the characteristics of the water entering the basin from the Caribbean Sea during this period. Stations were separated by approximately 20 km in a grid pattern. Eight stations were located outside the basin, north of the Tortugas-Margarita sill (Figure 1.2B). Table 1 provides a list of location and maximum depth sampled in both cruises.

Salinity and temperature profiles were collected using a Seabird SBE25 CTD, deployed at each station in a rosette ensemble. Dissolved oxygen and chlorophyll fluorescence data were obtained with a Seabird SBE 43 oxygen sensor and a Chelsea fluorometer (Chelsea, Inc.) attached to the CTD. The ensemble also had a C-Star transmissometer (WetLabs) that measured beam attenuation at 660 nm (c660). The data were processed using SeaBird's SBE Data Processing software.

CDOM (colored dissolved organic matter) fluorescence (hereafter referred to as FCDOM) was measured during March 2004 only, using a WetStar fluorometer (WetLabs). The excitation and emission wavelengths were set to 370 nm and 460 nm, respectively. A linear relationship between CDOM absorption and fluorescence permitted derivation of an empirical estimate of CDOM absorption throughout the region, similar to the approach used by Vodacek et al. (1997) and Blough and Del Vecchio (2002).

Samples were filtered on board with a 0.2 μm pore-size *anotop* filter, using a glass syringe. Filtrate samples were frozen in acid cleaned amber-colored bottles. Absorption was measured within one month as described below under *Absorption Spectroscopy*.

In September 2003, an absorption/attenuation meter (AC-9, WetLabs) was deployed as part of the vertical hydro-casts. A pump was used to draw water through the absorption and attenuation sensors. At 14 stations, double casts were performed, one with an unfiltered AC-9, and the second using a 0.2 μm filter (Propor PES filter capsules) attached to the inlet of the absorption tube. The instrument was calibrated before, during and after the cruise using distilled water as a reference.

DOC (dissolved organic carbon) samples were collected only during March 2004, by gravity filtering though GF/F precombusted filters, directly from the Niskin bottles and using silicone tubing. Samples and tubing were handled using polyethylene gloves.

Table 1.1: Station location and cast depth for COHRO and COHRO2.

COHRO, September 16-20, 2003				COHRO2, March 15-20, 2004			
Latitude	Longitude	Station	Maximum profiling depth (m)	Latitude	Longitude	Station	Maximum profiling depth (m)
10.83	-64.37	0	225	10.83	-64.36	1	217
10.66	-64.36	1	157	10.66	-64.36	2	160
10.50	-64.36	2	400	10.50	-64.36	3A	400
10.33	-64.55	3	120	10.50	-64.36	3B	1220
10.49	-64.55	4	400	10.45	-64.26	4	120
10.66	-64.55	5	400	10.41	-64.38	5	190
10.83	-64.55	6	220	10.33	-64.55	6	127
10.83	-64.70	7	225	10.40	-64.61	7	160
10.66	-64.71	8	400	10.45	-64.55	8A	521
10.49	-64.66	9	400	10.45	-64.55	8B	798
10.33	-64.71	10	40	10.56	-64.55	9A	400
10.33	-64.88	11	56	10.56	-64.55	9B	1220
10.23	-64.88	12	37	10.76	-64.55	10	400
10.14	-65.03	13	15	10.76	-64.71	11	383
10.19	-64.79	14	26	10.76	-64.88	12	400
10.28	-64.8	15	45	10.60	-64.88	13	403
10.49	-64.88	16	400	10.48	-64.88	14	400
10.66	-64.88	17	400	10.33	-64.71	15	50
10.83	-64.88	18	224	10.28	-64.80	16	50
10.66	-65.05	19	400	10.38	-64.93	17	76
10.49	-65.05	20	400	10.50	-65.05	18	400
10.41	-65.05	21	63	10.63	-65.10	19	400
10.33	-65.05	22	59	10.76	-65.05	20	400
10.23	-65.05	23	25	10.93	-65.05	21	67
10.23	-65.21	24	24	11.05	-65.05	22	75
10.33	-65.21	25	56	11.16	-65.05	23	276
10.41	-65.21	26	75	11.33	-65.05	24	400
10.33	-65.38	27	55	11.33	-64.88	26A	400
10.41	-65.38	28	77	11.33	-64.88	26B	1382
10.49	-65.21	29	113	11.16	-64.88	28	276
10.83	-65.04	30	220	11.05	-64.88	29	123
11.00	-65.04	31	80	10.93	-64.88	30	181
11.00	-64.88	32	130	10.93	-64.71	31	310
11.00	-64.71	33	174	11.05	-64.71	32	90
10.99	-64.54	34	273	11.16	-64.71	33	90
10.44	-64.26	48	70	11.33	-64.71	34	210
10.14	-65.11	49	15	11.33	-64.55	35	380
10.16	-65.21	50	10	11.16	-64.55	36	50
10.41	-64.40	51	180	11.05	-64.55	37	84
				10.93	-64.55	38	350

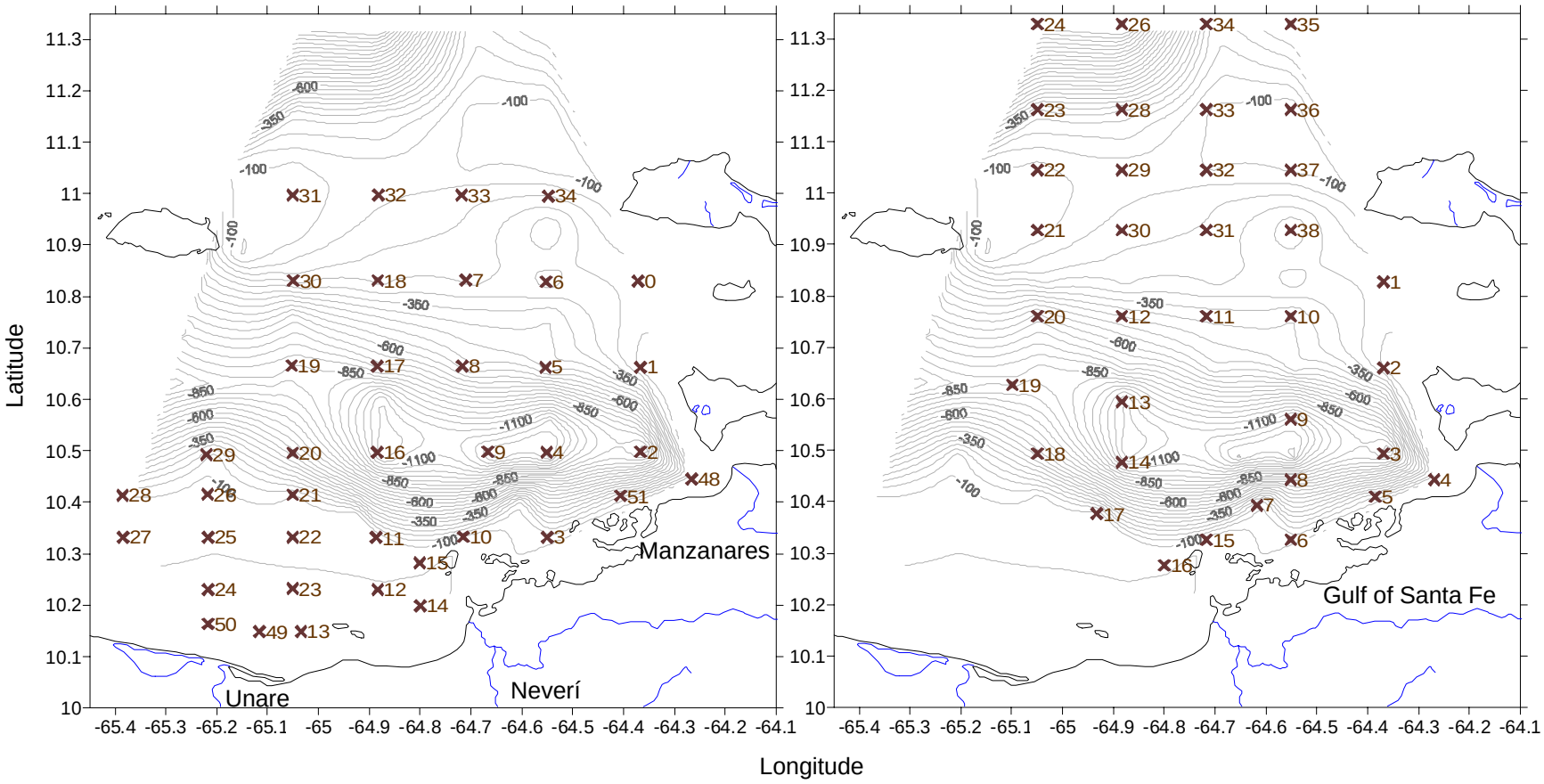

Figure 1.2: Sample map location for September 2003 (A) and March 2004 (B). Major local rivers are shown.

The samples were stored in Nalgene wide-mouthed translucent 60 ml acid-cleaned HDPE polyethylene bottles and frozen to -20 °C until analysis. Between casts, both the filter holders and tubing were rinsed with 10% HCl and distilled water. They were then sent to the Rosenstiel School of Marine and Atmospheric Science (RSMAS) at the University of Miami (Dr. Dennis A. Hansell) for analysis.

2.1 Data processing

AC-9 processing and validation

AC-9 data were corrected for temperature and salinity following Pegau et al. (1997). A scattering correction was also applied to the absorption data. The scattering correction was done by subtracting a reference wavelength (715 nm) from all data (hypothesis 3 in the AC-9 WetLabs User's Guide, 2003). As a data quality check, the AC-9 beam attenuation data at 650 nm were compared to c660 taken with the transmissometer at all stations.

Absorption Spectroscopy

Water samples from the March 2004 cruise were transported back to the University of South Florida (USF), and analyzed within one month of the cruise. Samples were re-filtered once thawed to remove any remaining particles. The data were scanned between 200 and 800 nm at 1 nm intervals using a Perkin-Elmer Lambda 18 spectrophotometer equipped with 10 cm quartz cells. The detection limit of the instrument was ± 0.002, or equivalent absorption of 0.046 m^{-1}. Milli-Q water was used as blank. For each sample, two scans were performed. Running means were used to smooth the data prior to comparison, and, where necessary, the blank absorption values were subtracted from the sample. The criterion used for the subtraction of the blank was quantitative: at 650 nm the absorption had to be zero. If the curve was above the zero line, the blank was subtracted from the sample. Each sample was looked at individually, and the best of the two scans selected. The selection of the best scan was based on the smoothness and shape of the curve, whether it had suspicious features, and whether it had been necessary to subtract the blank from the sample. Those scans where no subtractions had been done were preferred.

Absorption coefficients were calculated from absorbance, according to the relationship:

$$a(\lambda) = 2.303\ A(\lambda)/r$$

where A is the absorbance or optical density and r is the pathlength. Light absorption by CDOM decreases exponentially from the UV to the visible part of the spectrum, and can be approximated by:

$$a_g(\lambda) = a_g(\lambda_o)\exp[-S(\lambda - \lambda_o)]$$

where $a_g(\lambda)$ and $a_g(\lambda_o)$ are the absorption coefficients at wavelength λ and at a reference wavelength λ_o; λ_o was set to 400 nm. S is the spectral slope, which describes the decrease in absorption of a_g with increasing wavelength (Blough et al, 1993; Green and Blough, 1994; Ferrari, 2000, Blough and Del Vecchio, 2002). Each spectrum was plotted in two ways: through a linear least squares regression of the log-transformed data (ln(a) vs. λ, J. Cannizzaro, pers. comm.) and in an exponential form, using a non-linear least squares fitting (Dr. C. Hu, pers. comm.). The method that provided the single best fit for each individual spectrum was selected. The slope S was calculated between 330 and 400 nm. Beyond 400 nm, the signal to noise ratio was too large. Absorption coefficients at 370 nm, 400 nm, and 412 nm ($a_g(370)$, $a_g(400)$ and $a_g(412)$; Table 1.2) were used for the different characterizations. 3 stations sampled in March 2004 are shown in Table 1.2. These stations were selected because they are located outside the Basin (station 35), at the northern sill (station 29) and inside the Basin, at the upwelling focus (station 6).

Table 1.2: a_g, DOC and S values for selected stations sampled during March 2004

Station	Depth (m)	$a_g(370)$ (m^{-1})	$a_g(400)$ (m^{-1})	$a_g(412)$ (m^{-1})	*S* (330-400) (nm^{-1})	DOC (μM of C)	Temp. (°C)	Salinity
35	1	0.1349	0.0619	0.0492	0.0234	66.42	24.73	36.76
35	35	0.1096	0.0447	0.0342	0.0254	56.75	22.40	36.75
6	1	0.0823	0.0407	0.0334	0.0191	59.29	22.90	36.94
6	35	0.0626	0.0442	0.0393	0.0127	53.58	21.94	36.92
29	1	0.1352	0.0673	0.0532	0.0215	65.75	25.21	36.84
29	35	0.1116	0.0624	0.0517	0.0184	59.83	22.65	36.88
29	55	0.0758	0.0354	0.0278	0.0236	-	21.60	36.91

Satellite imagery

Two SeaWiFS (Sea-viewing Wide Field-of-View Sensor) images were processed for chlorophyll using the OC-4 algorithm (O'Reilly et al., 1998). The dates of the images were chosen as close as possible to the dates of the cruises. The only image with low enough cloud cover for September 2003 was of September 30. For March 2004, the image of March 10 was selected. Sea Surface Temperature (SST) images were also processed. Sea Surface Temperature (SST) was derived from infrared (IR) observations collected by the Advanced Very High Resolution Radiometer (AVHRR) sensors flown on the National Oceanic and Atmospheric Administration's (NOAA) Polar Orbiting Environmental Satellite (POES) series. SST was computed using the multi-channel sea-surface temperature (MCSST) algorithm developed by McClain et al. (1985). Due to cloud cover, three-day composites were used instead of daily images. Running means were used to generate the composites of September 2003 (using September 29, 30 and October 1st), and March 2004 (using March 9, 10 and 11th).

3. Results

3.1. Hydrography

3.1.1 Surface Hydrography

A marked seasonal difference was found in the Cariaco Basin in both surface temperature and salinity distribution between the sampling carried out in the dry (March 2004) and the rainy seasons (September 2003). The patterns and seasonal differences were similar to those observed in previous studies (Herrera and Febres-Ortega, 1975; Herrera et al., 1980; Astor et al. 1998; Scranton et al, 2001, Muller-Karger et al, 2001; Astor et al., 2003).

Figure 1.3 shows the surface distribution of temperature and salinity during September 2003 and March 2004. During the rainy season, surface temperatures ranged between ~26 to ~28 °C (Figures 1.3A and B). Salinities offshore varied from ~36.4 to ~36.8. Influence from local rivers was visible as lower salinity near the coast. In Figure 1.3A, the water coming from the Unare River was warmer than the Cariaco Basin water by ~0.5 °C; this river's signal was also visible as a low (~35.5) salinity area near the coast (Figure 1.3B). In contrast, the waters in the region of the plume of the Neverí River were approximately 0.2-0.3 °C colder than the surrounding Cariaco Basin water (Figure 1.3A). During September 2003 winds were weaker and the water was stratified.

During the rainy season (September 2003), warm water was observed immediately to the southwest of Margarita Island. Figure 1.4A is a current velocity profile, measured at the CARIACO time series station (see Figure 1.1 for reference), for the period of September 2003. During this month, moderate to strong (8-18 cm/s) eastward currents were observed between 30-40 m. The depth of the thermocline at this location was around 100m, and because the wind was weak, it was possible to use these observations to infer the approximate flow closer to the surface (Dr. R. Weisberg, pers. comm.). The eastward current apparently helped contain warm surface water over the continental shelf in the northeastern part of the basin.

In the dry season (March 2004, Figure 1.3C and D), temperatures in the basin ranged from ~22 to ~26 °C, and salinity from 36.7 to ~37. Colder water was observed near the coast, and the lowest temperatures in March 2004 were recorded near the Gulf of Santa Fe (22.86 °C, Figure 1.3C. These results are in agreement with model predictions of the location of the upwelling focus (Walsh et al., 1999). In March 2004, a slight decrease in surface salinity to ~36.83 (relative to >36.86 in most of the Basin) was seen near the northern sill. This was part of the CSW (<36.75) observed in the Caribbean Sea north of the sill.

Figure 1.5 shows SeaWiFS images from the sampling periods, processed for chlorophyll *a* and CDOM absorption (a_g). In Figure 1.5A the combined plume of the Orinoco and Amazon is visible on the extreme eastern margin of the image (right side of image) as a red patch, but it was distant from Margarita Island and the Cariaco Basin and

extended to the northwest. Its inclination is very pronounced, almost completely in a northward direction. In the SST image, the sliver of lower temperature (~ 26 °C) visible corresponds to the patch of low color in the chlorophyll image. The Orinoco/Amazon river plume is of higher temperature (~27-28 °C) located in the upper right-hand side of the image.

In March 2004, the patch extending from the east to the west just north of Margarita Island shows the high (> 4 mg/m^3) chlorophyll concentrations that occur in the region due to upwelling. The Orinoco River plume is in a similar location as seen in September 2003, but it is much smaller and inclined towards the northwest. SST shows a pattern of colder water similar to that of chlorophyll, indicating that this cold (~24 °C) water was upwelled water and not riverine water, which is warmer. The Orinoco/Amazon plume is harder to see in this SST image, as compared to September 2003, probably due to the occurrence of some degree of mixing between warmer river waters and cold, upwelled ones.

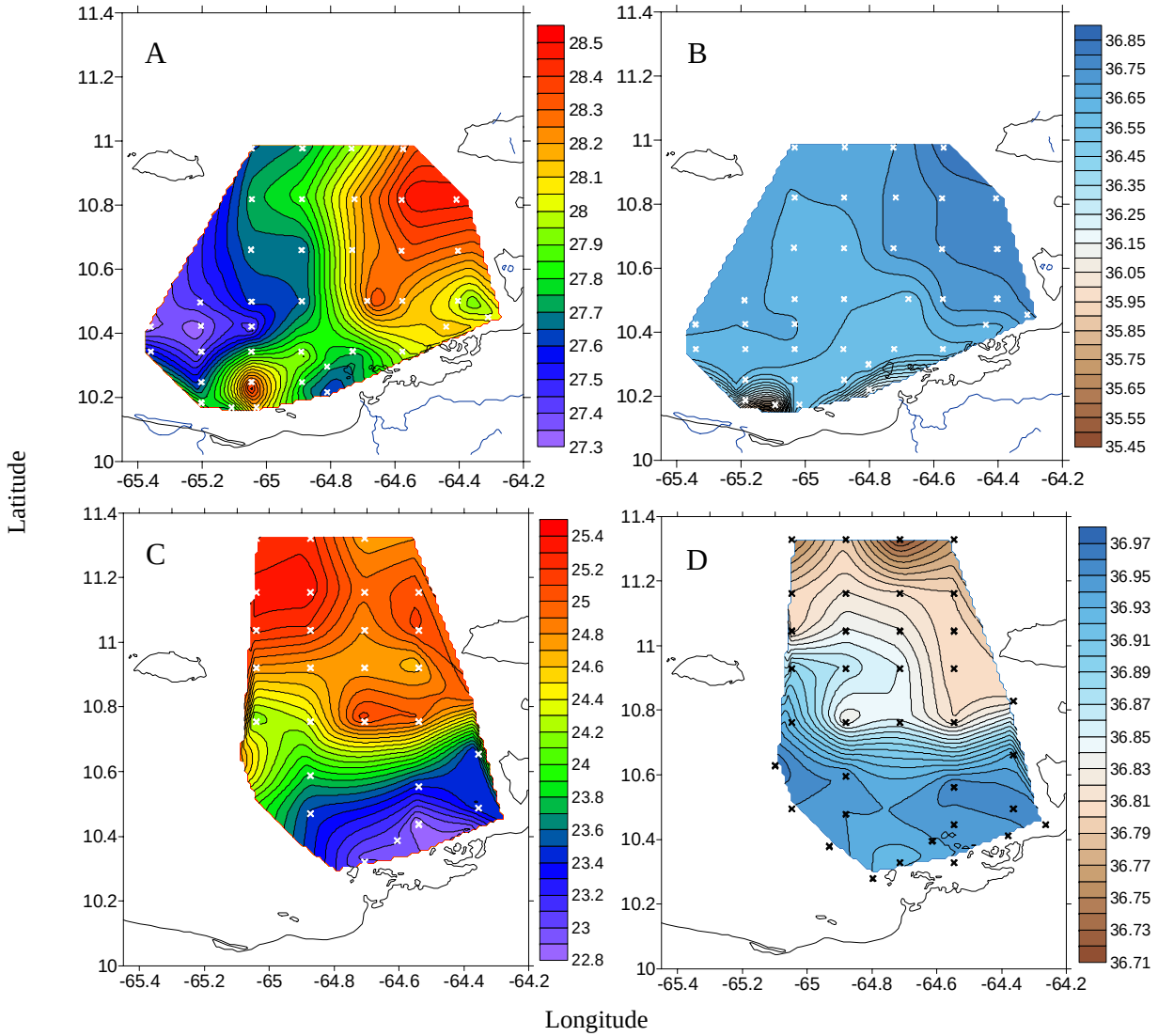

Figure 1.3: Surface temperature (A, C) and salinity (B, D) of the Cariaco Basin during September 2003 and March 2004, respectively. Note the different scales used for each cruise.

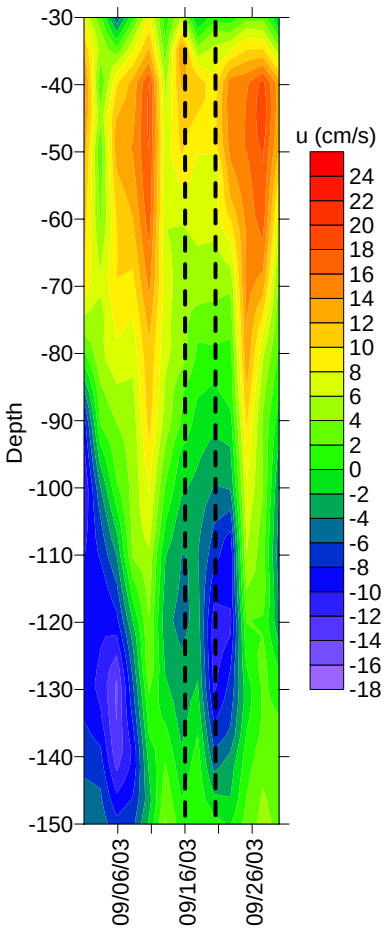

Figure 1.4: Vertical distribution of the east/west component of current velocity (cm/s), measured at the CARIACO time-series station (see Figure 1.1 for location) for September 2003. Positive (yellow/red) is eastward flow. Black lines indicate cruise dates.

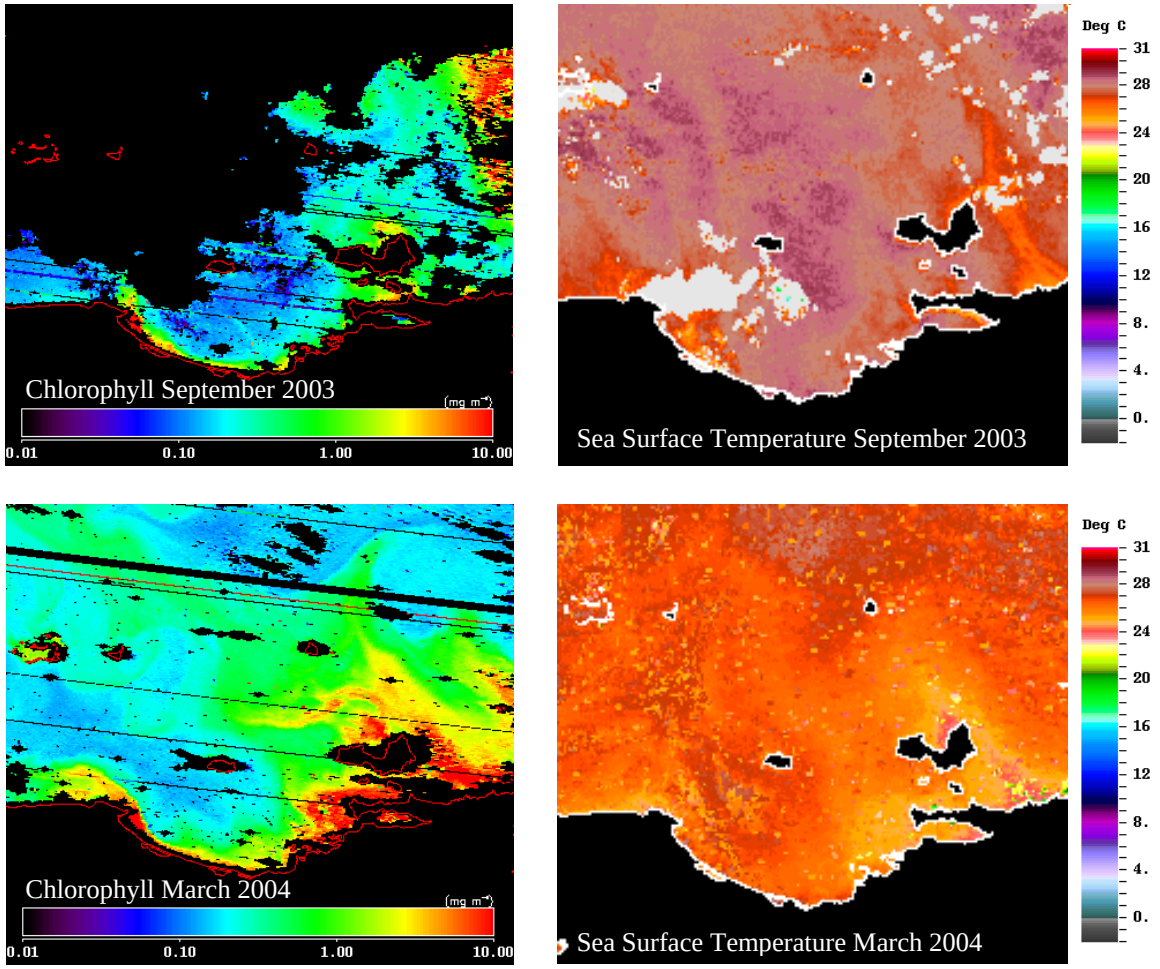

Figure 1.5: SeaWiFS images chlorophyll concentration for September, 30 2003 and March 10, 2004. Sea Surface Temperature composites are also shown.

3.1.2. Water mass distribution

Figure 1.6 is a temperature/salinity (T/S) diagrams for stations 9 (September 2003) and 26 (March 2004, see Figure 1.2 for reference). Following Herrera et al. (1980) and Morrison and Nowlin (1982), the water masses visible in these diagrams are: (1) CSW, surface waters with high temperatures (>25 ^{o}C) and lower salinity (~ 36.6) (2) SUW, characterized by a salinity maximum (~ 37) (3) TACW, monotonically decreasing temperature and salinity below the SUW (4) Antarctic Intermediate Water (AAIW), seen as a salinity minimum (~ 34.7) (5) Upper North Atlantic Deep Water (NADW), visible in the lower portion of the diagram as a salinity maximum (~ 35).

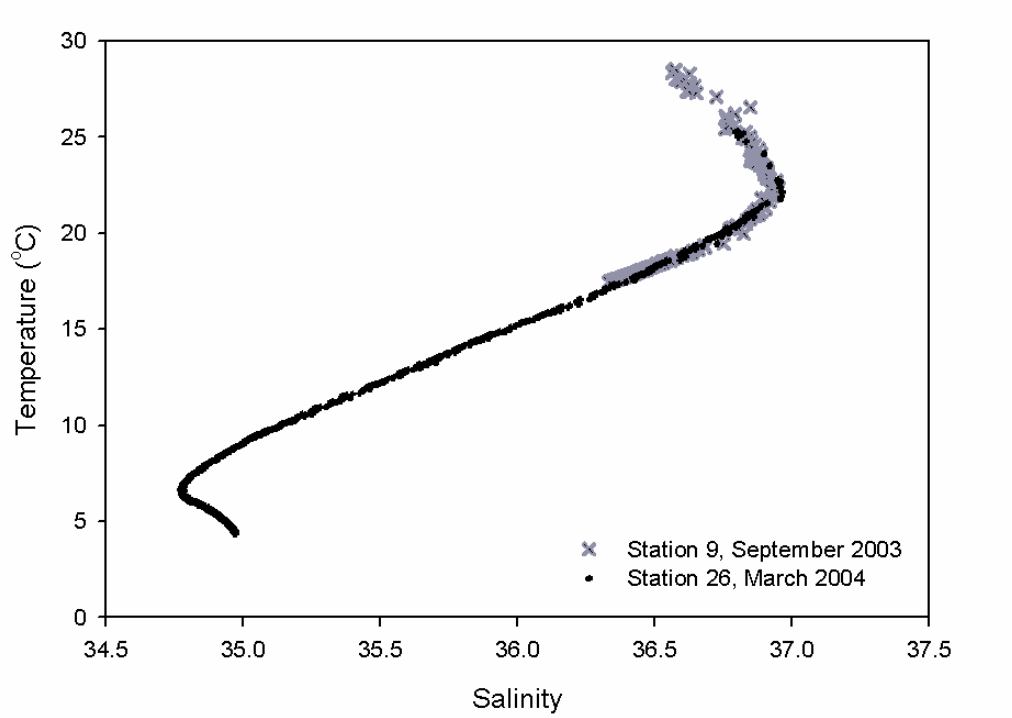

Figure 1.6: T/S diagrams for station 9, September 2003 (x) and station 26, March 2004 (●). Maximum sampling depth: 1300 m and 1382 m, respectively

Figure 1.7 is a meridional transect along 64.88°W showing salinities in September 2003 (7A) and March 2004 (7B). The depth of the SUW varied with season. During September 2003, it lay below the CSW, while in March 2004 it occupied the upper 100 m. Herrera et al. (1980) and Astor et al. (2003) also noted that the SUW reached its shallowest depths during the first months of the year. Surface salinities were therefore higher during this period (Figure 1.3D).

Figure 1.8 shows T/S diagrams from different stations in September 2003 (Figure 1.8A) and March 2004 (Figure 1.8B). In any one cruise, variations between stations at temperatures above 21^{o}C (depths above 200 m) were visible mainly in salinity. The most

pronounced variations (Figure 1.8B) were caused by differences between stations inside (19, 6, 14, red and yellow colors) vs. stations outside the basin(35, 26, blue colors; station 29 was located at the sill). Okuda (1976) observed similar differences between surface waters inside and outside the basin, and attributed such variations in salinity to the influences of large South American Rivers on Caribbean waters. The smaller differences visible in Figure 1.8A were mostly caused by the influence of local rivers, such as in station 11 (gray squares; see Figure 1.2A for reference).

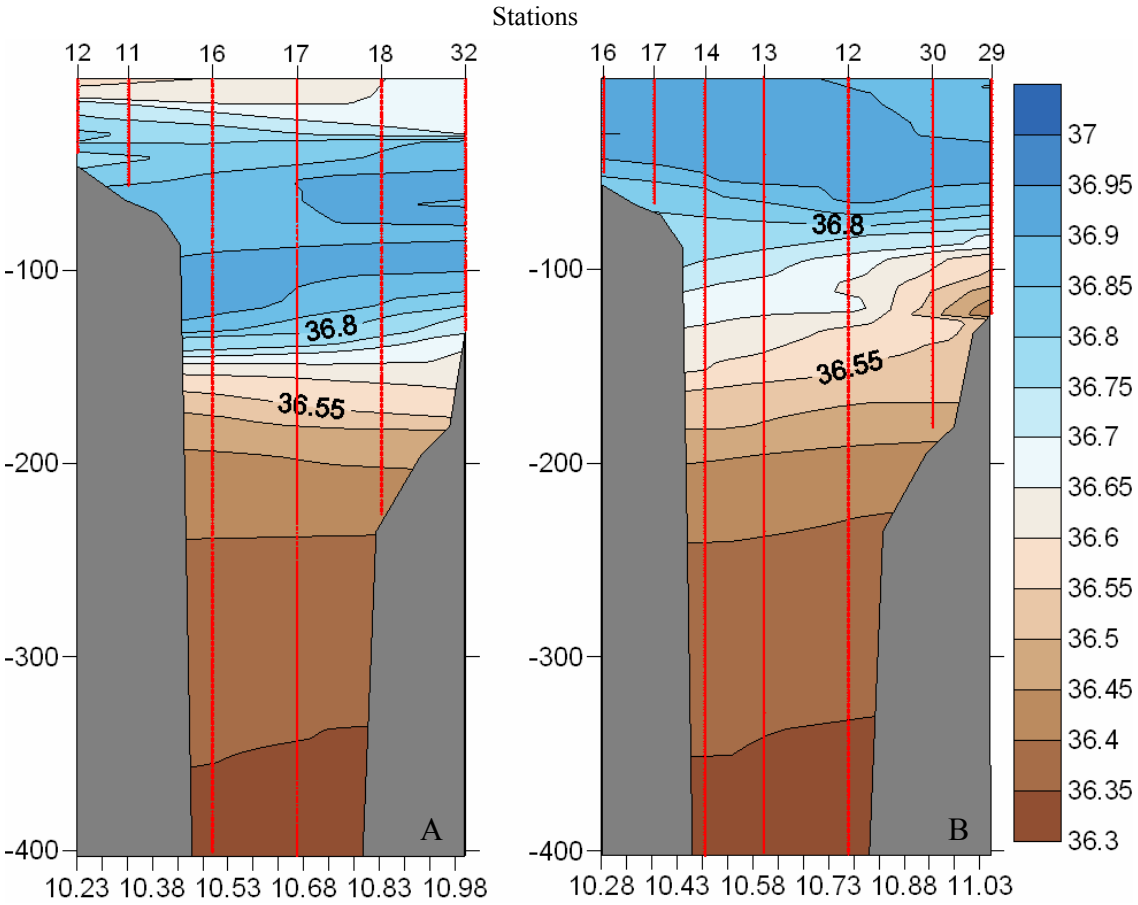

Figure 1.7: Salinity transects for September 2003 (A) and March 2004 (B). Red lines correspond to casts performed at stations.

Temperature and salinity between 250 m and 400 m in the Cariaco Basin were higher than in the Caribbean stations north of the sill by approximately 4°C and ~0.5. No spatial temperature or salinity changes were noted below the 17-degree, 36.3 salinity values inside Cariaco (Figure 1.8A).

Figure 1.8 C and D, respectively, show the predicted and measured temperature and salinity increase according to Scranton et al. (1987) for waters below 1200m. Table 1.3 lists the sources of *in situ* historical data used. The temperature measured during March 2004 followed Scranton et al's prediction. However, March 2004 values exceed the expected salinity. In Figure 1.8D there is a noticeable change in the salinity slope in

the past 6 years, which cannot be attributed to errors in the measurements. Salinity for the CARIACO project is measured by duplicates, automatically using a CTD and with discrete samples; both sets of measurements are consistent.

During September 2003, dissolved oxygen intrusions were observed at stations 19, 17, 16 and 8 (Figure 1.9). At station 19, at least two intrusions are apparent between 200 and 300 m. In stations 16 and 17 they were smaller single peaks at ~ 250 and 280 m, respectively. At the CARIACO time-series station, oxygen intrusions have been reported (Scranton et al., 2001; Astor et al., 2003). These intrusions, or ventilations, manifest themselves as peaks of dissolved oxygen concentration between 5 and 50 μM. Until now, the only information regarding these ventilations was what could be observed in the CARIACO time-series records.

During March 2004, subsurface oxygen peaks were also observed throughout the basin (Figure 1.10). Two well-defined subsurface oxygen maxima were recorded at station 19 (at ~100 and 160 m). Other subsurface oxygen maxima were seen at other stations throughout the basin (e.g. stations 13, 14, 11, 20, Figure 1.10). The oxygen profile for station 26 is also shown. Station 26 was located outside the Basin. The Cariaco Basin is anoxic below~250m. The small offset observed in both Figures 1.9 and 1.10 (ca. 4 μM of oxygen) is caused by the CTD's oxygen sensor, which, despite the fact that there is no oxygen in part of the basin, still provides a minimal reading. Calibration with discrete measurements has been difficult, and discrete measurements are not enough in numbers to pick up small vertical features like the oxygen intrusions.

Table 1.3: Sources of historical temperature and salinity measurements for waters below 1200 m in the Eastern Cariaco Basin. The CARIACO time series measurements are yearly averages

Year	Potential temperature (θ)	Salinity	Reference
1955	16.667	-	Richards and Vaccaro (1956)
1965	16.742	-	Richards (1970)
1968	16.724	-	Fanning and Pilson (1972)
1971	16.752	-	Spencer and Brewer (1972)
1973	16.765	36.196	Bacon et al. (1980)
1982	16.825	36.204	Scranton et al. (1987)
1986	16.864	-	Casso et al. (1986)
1990	17.041	36.212	Zhang and Millero (1993)
1995	16.881	36.223	CARIACO time series
1996	16.915	36.224	CARIACO time series
1997	16.924	36.225	CARIACO time series
1998	16.934	36.227	CARIACO time series
1999	16.944	36.231	CARIACO time series
2000	16.952	36.232	CARIACO time series
2001	16.961	36.236	CARIACO time series
2002	16.968	36.239	CARIACO time series
2003	16.978	36.240	CARIACO time series
2004	16.989	36.242	This study/CARIACO time series

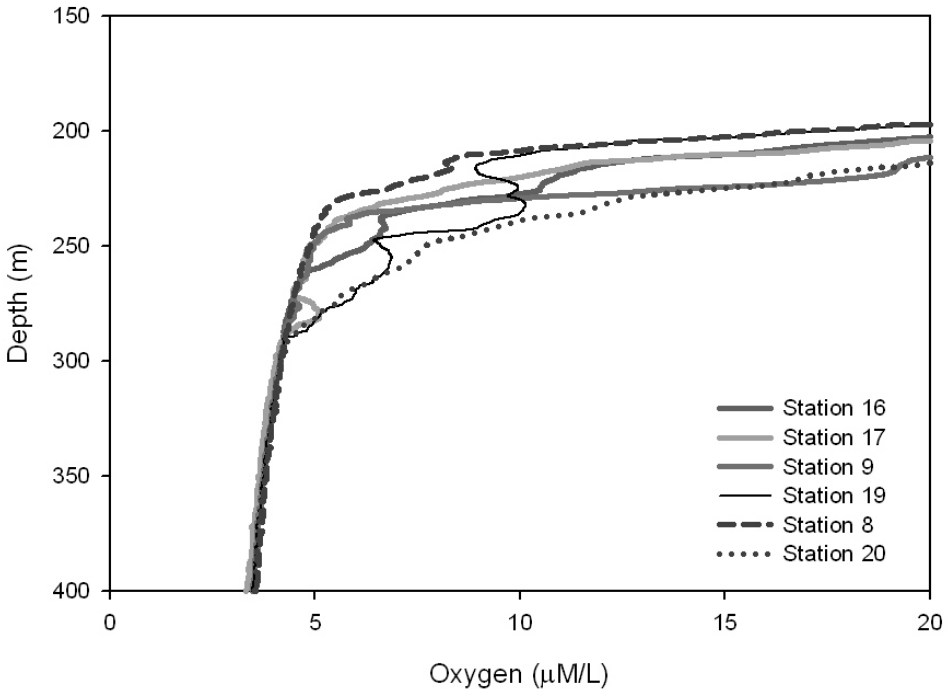

Figure 1.9: Oxygen profiles for selected stations during September 2003

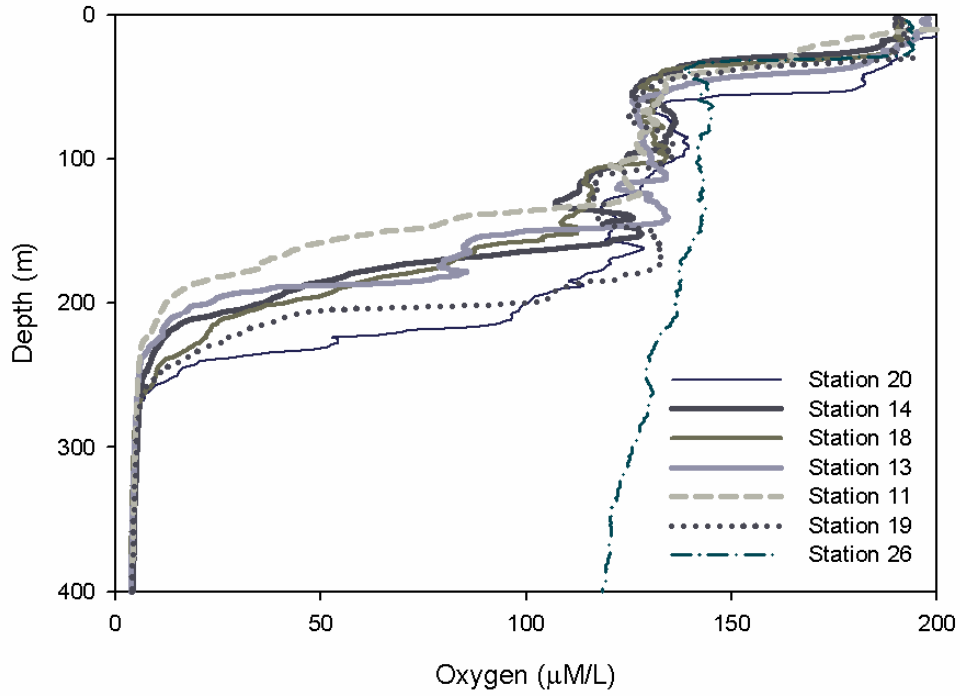

Figure 1.10: Oxygen profiles for selected stations during March 2004

3.2. Distribution of DOC and CDOM around the Cariaco Basin

Concentrations of dissolved organic carbon (DOC) at the surface ranged from ~70 μM C (Table 1.2) in stations outside the basin to ~60 μM C near the Gulf of Santa Fe (see Figure 1.2 for reference). Surface DOC sampled at locations outside the basin came from the Subtropical Underwater mass (Figure 1.7). Concentrations of DOC measured outside the basin agreed with SUW DOC concentration measured by Del Castillo (1998) near Trinidad. There was a correlation (r^2 = 0.87) between temperature and DOC concentration (Figure 1.11A), where highest values of DOC were associated with warmer water, and lower values with colder, recently upwelled, waters.

Figure 1.11B shows the relationship between DOC and CDOM in the Cariaco Basin for March 2004 (r^2 = 0.8). Similar high correlations have been noted elsewhere, especially in systems under riverine influence, like the West Florida Shelf (r^2 = 0.8, Del Castillo et al., 2000), in the Orinoco River plume (r^2 = 0.7, Del Castillo et al., 1999) and the Baltic Sea (r^2 ~ 0.9, Ferrari et al., 1996). However, no evidence of riverine influence was observed in the basin during March 2004. No DOC samples were collected during the rainy season, and therefore the relationship between DOC and a_g could not be examined.

Figure 1.12 shows CDOM fluorescence (FCDOM) and a_g sampled during March 2004. Samples collected below 35 m showed a linear correlation between these parameters (r^2 = 0.9). However, surface samples showed no clear relationship between the variables. Surface CDOM (1-25 m) had a different fluorescence yield than that immediately below the surface at 35 m depth, due to possible photochemical alterations and different sources.

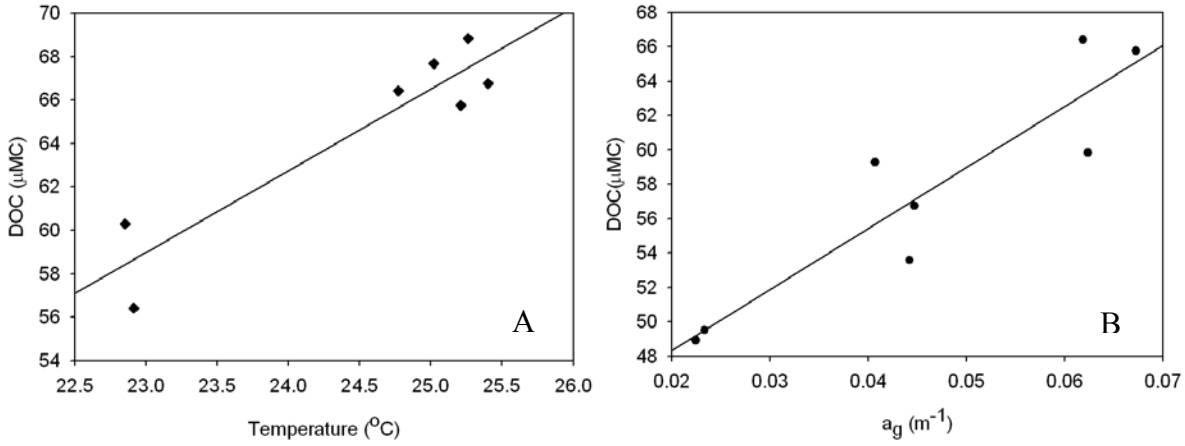

Figure 1.11: Property-property plot of (A) DOC (μMC) and Temperature (°C) (B) $a_g(400)$ and DOC (μM C) (Stations used are shown in Table 1.2). Both figures refer to March 2004 samples

Surface (1-25 m) CDOM fluorescence showed a linear correlation (r^2 > 0.8) with chlorophyll fluorescence (FChl) measurements (Figure 1.13), indicating that most of the CDOM observed at this depth range was autochthonous, i.e. released by phytoplankton and bacteria in the water column (Mague et al, 1980; Bricaud et al, 1981; Carder et al., 1986; Coble et al., 1998).

Figure 1.14 is a temperature/FCDOM diagram for stations sampled during March 2004. The low FCDOM values observed in the upper 25 m of the water column, associated with the highest temperatures (21-24°C), correspond to that portion of the water column where there was high chlorophyll fluorescence. This was observed at all stations except station 26. From SeaWiFS images of chlorophyll and CDOM absorption, it was possible to see how, during March 2004 (Figure 1.5B), there was a front located between stations east and west of the channel between Tortuga and Margarita Islands. Waters located to the west, such as at station 26 showed significantly lower nutrient concentration (Table 1.4). This suggests that they also had lower primary production and hence lower CDOM production and a_g values.

Below 19°C, there was a considerable difference between stations inside the basin (stations 14, 19, 20 and 38) and those outside (stations 35 and 26). Inside the basin, FCDOM increased rapidly immediately below the oxic-anoxic interface (~200 m), and temperature remained more or less constant. Outside the basin, the increase in CDOM was observed deeper, around ~250-270 m. There was a correlation between nutrient concentration and CDOM fluorescence both inside and outside the basin (data not shown), supporting the idea that nutrients in the Cariaco Basin were remineralized simultaneously with CDOM (Chen and Bada, 1992).

Figure 1.15A and 1.15B show profiles of FCDOM and oxygen with depth for stations 19 and 14 in March 2004. The relationship between oxygen and CDOM is useful for understanding origins of water masses. Refractory CDOM is altered with exposure to

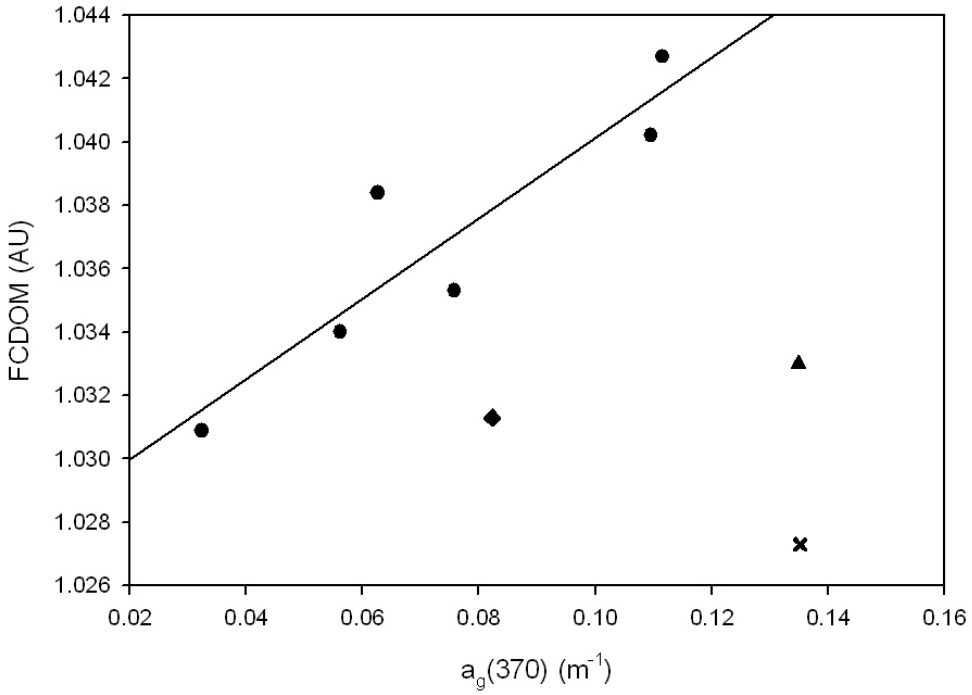

Figure 1.12: Correlation plot of CDOM absorption coefficient, a_g (m^{-1}) at 370 nm, and corresponding fluorescence emission (expressed in arbitrary units, AU) for stations 6, 29 and 35, sampled during March 2004. Circles (●) correspond to sampled stations at depths of 35m, 55m and 100m. Other symbols correspond to surface measurements: × Station 35, 1m. ♦ Station 6, 1m. ▲ Station 29, 1m.

Table 1.4**:** Temperature, salinity, CDOM fluorescence and nutrient data for selected stations sampled during March 2004

Station	Depth (m)	NO_2 (μM)	NO_3 (μM)	PO_4 (μM)	$Si(OH)_4$ (μM)	Salinity	Temp. (°C)	CDOM Fl. (AU)
6	1	0.13	5.91	0.35	3.27	36.94	25.44	1.0313
6	35	0.12	6.50	0.38	3.07	36.92	25.69	1.0385
6	55	0.07	7.98	0.48	3.72	36.85	25.83	1.0406
6	75	0.03	8.33	0.53	4.55	36.80	25.94	1.0387
6	100	0.03	9.66	0.69	6.43	36.71	26.09	1.0425
8	1	0.15	3.72	0.17	1.57	36.94	25.45	1.0208
8	100	0.05	7.47	0.49	4.04	36.77	26.03	1.0287
8	200	0.02	10.09	1.69	24.49	36.45	26.37	1.0403
8	225	0.05	5.10	1.92	33.14	36.42	26.39	1.0481
8	300	0.00	0.15	2.70	45.83	36.37	26.41	1.0857
8	350	0.11	0.19	2.70	46.05	36.35	26.42	1.1004
8	400	0.00	0.15	2.81	54.03	36.34	26.43	1.1086
26	1	0.03	0.10	0.03	0.36	36.80	24.62	-
26	35	0.24	5.78	0.34	2.39	36.93	25.49	1.0265
26	55	0.22	6.84	0.37	2.48	36.85	25.90	1.0183
26	100	0.02	8.35	0.46	2.83	36.64	26.21	1.0214
26	125	0.02	9.66	0.55	3.27	36.51	26.35	1.0236
26	150	0.06	10.86	0.62	3.77	36.42	26.44	1.0224
26	175	0.01	13.10	0.77	4.88	36.22	26.56	1.0248
26	200	0.00	14.02	0.83	5.18	36.12	26.64	1.0275
26	400	0.00	26.74	1.73	13.96	35.12	27.06	1.0637
35	1	0.03	0.07	0.02	0.46	36.76	24.75	-
35	35	0.38	7.40	0.51	6.55	36.75	25.43	1.0353
35	55	0.11	7.74	0.44	3.45	36.80	26.03	1.0287
35	100	0.07	8.79	0.49	3.30	36.64	26.24	1.0293
35	230	0.04	16.03	0.98	6.71	35.87	26.74	1.0325
35	350	0.02	25.98	1.68	13.64	35.18	27.02	1.0798

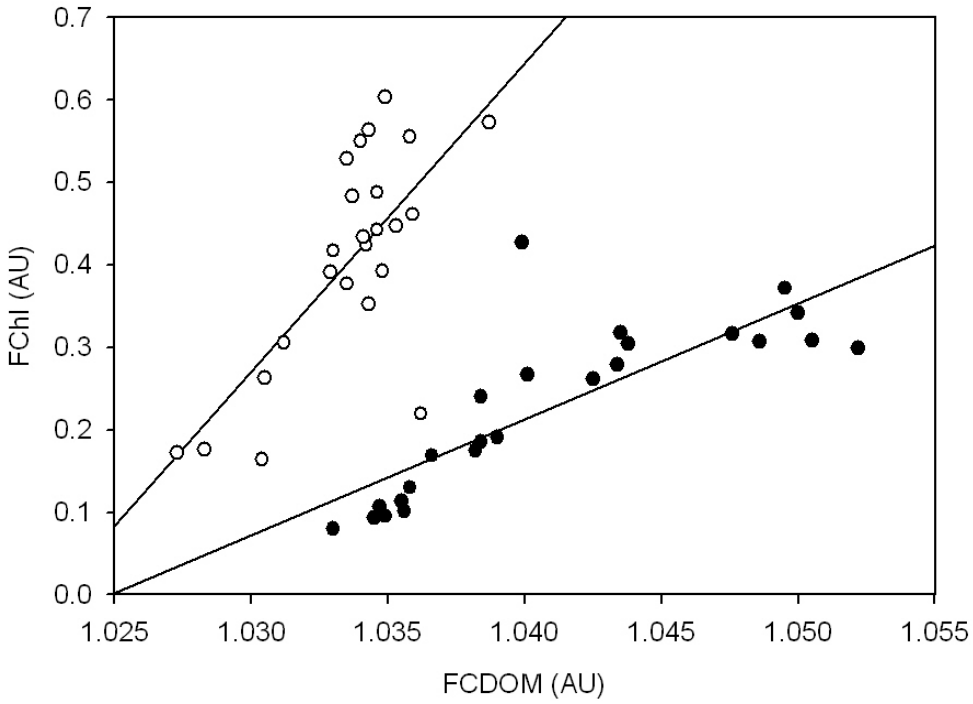

Figure 1.13: Correlation plot of FCDOM (Arbitrary Units, AU) and FChl (Arbitrary Units, AU) for surface (1-25 m) waters sampled during March 2004. Stations 29 (●) and 35 (○) are shown

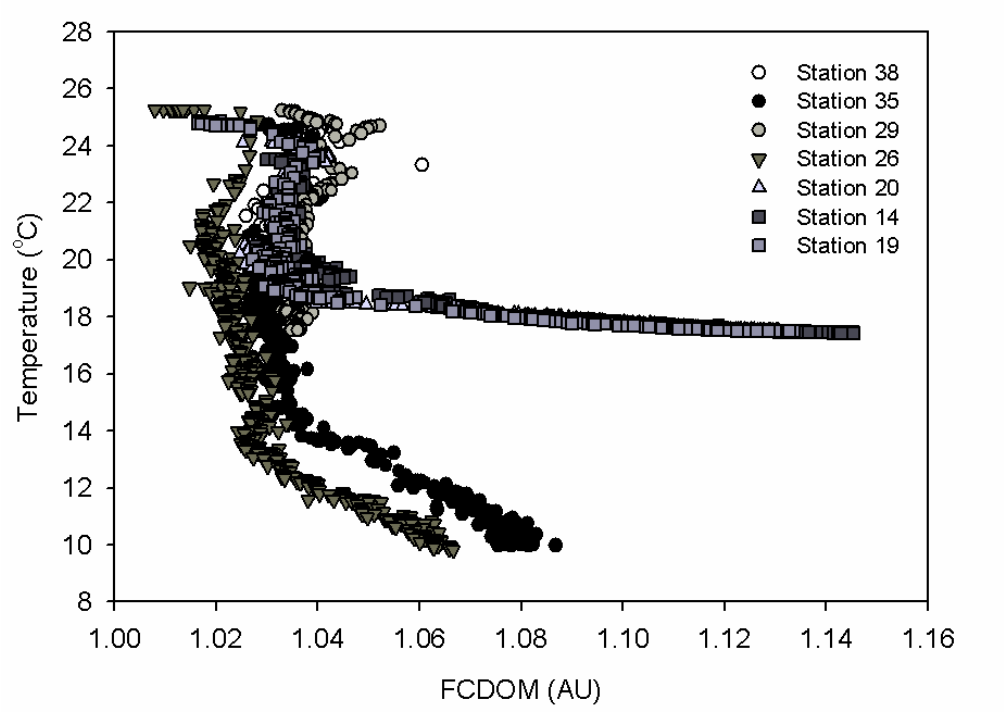

Figure 1.14: CDOM fluorescence (FCDOM) and temperature for stations inside (14, 19, 20, 29, 38) and outside (26, 35) the Cariaco Basin in March 2004.

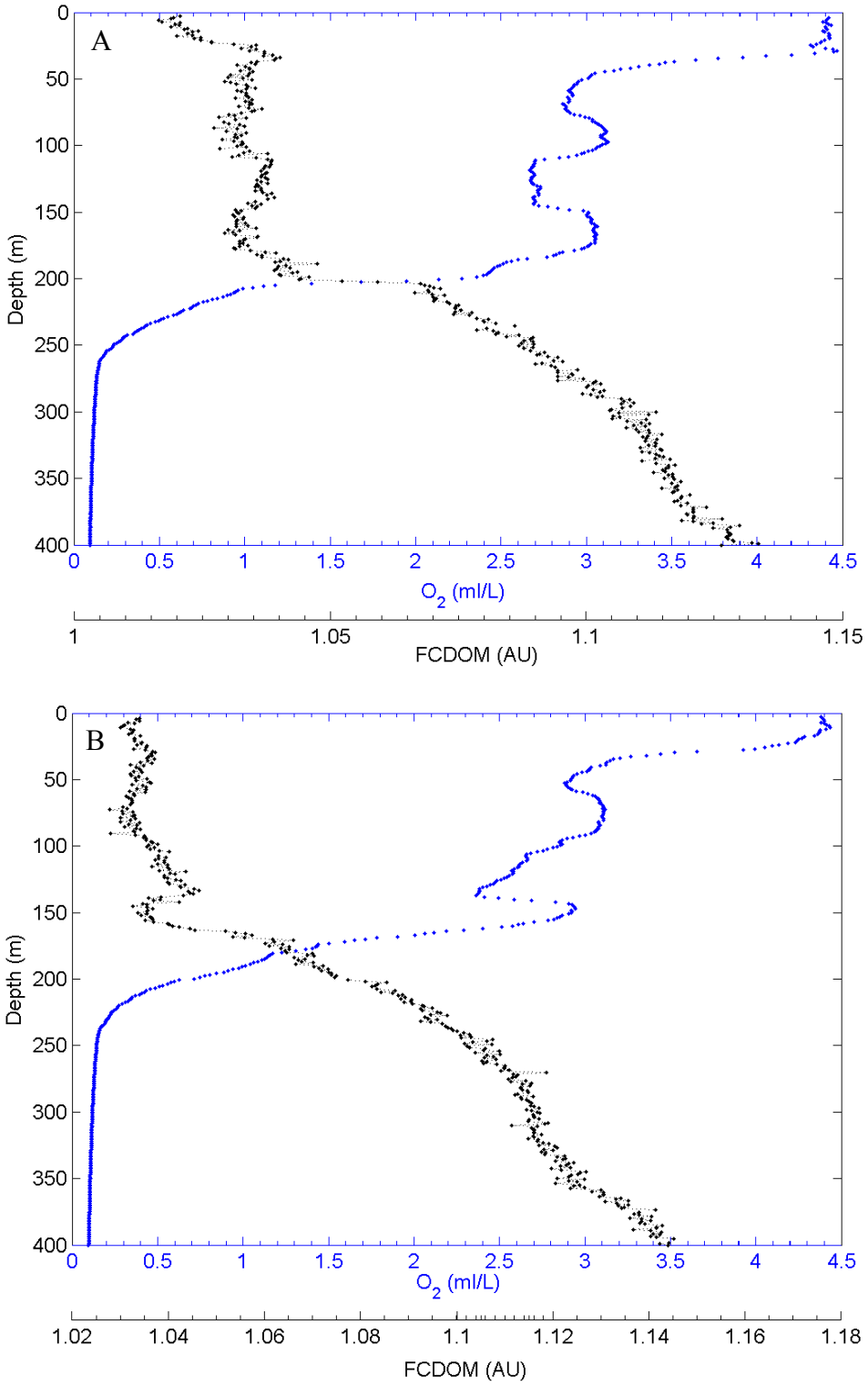

Figure 1.15: Vertical profiles of oxygen and FCDOM at stations 19 (A) and 14 (B) in March 2004

light only or slow decomposition, although labile CDOM is also affected by microbial decomposition or algae uptake (Bricaud et al., 1981; Carder et al., 1989; Blough and Del Vecchio, 2002). Vertical dissolved oxygen concentrations change in relation to different water masses (Morrison and Nowlin, 1982) and in situ biological processes. Inside the Cariaco Basin during March 2004, average fluorescence values for the upper 5 m were ~1.03 arbitrary units (AU). Between 5 - 150 m they increased to ~ 1.04 AU. Values in stations outside the sill varied from ~ 1.01 AU at station 26 to 1.03 AU at station 35 for the upper 5 m. Between 5 - 200 m, these values ranged from 1.02 (station 26) to 1.03 AU (station 35). The low FCDOM peaks associated with the oxygen intrusion (Figure 1.15A and B) were of approximately 1.03 AU.

3.3. Vertical distribution of particulate and dissolved matter

Figure 1.16A shows absorption and beam attenuation coefficient (a, c) profiles collected during the September 2003 cruise at the CARIACO time-series station (station 9). The wavelength for absorption observations was 412 nm., which is strongly affected by both CDOM and phytoplankton. At 650 – 660 nm, there is minimal absorption by CDOM and particles in the water, and attenuation at this wavelength is commonly used as a descriptor of bulk particle concentration (Boss et al., 2001; Bricaud et al., 2002). The peaks in absorption (blue dots) in the upper 50 m of the water column were caused by phytoplankton. The a and c maxima located at 130-150 m in Figure 1.16A coincided with the bottom of the pycnocline that exists in the basin at this depth (Figure 1.16B) (Scranton et al., 1987; Zhang and Millero, 1993). Stratification inhibits vertical mixing above this depth, and at the bottom of the pycnocline particles may be temporarily retained before sinking.

The series of peaks observed between 200 m and 300 m in Figure 1.16A in the beam attenuation profile corresponded to bacterial layers (Taylor et al., 2001). Similar observations were made by Naqvi et al. (2001) in the Arabian Sea and Garfield et al. (1983) and Spinrad et al. (1989) off the coast of Peru. Absorption at 412 nm also showed a maximum between 200-300 m that marked the location of the oxic-anoxic interface. This absorption peak was observed throughout the Eastern basin (Figure 1.17).

Figure 1.18 shows the relationship between beam attenuation and γ, the beam attenuation slope. The spectral shape of the beam attenuation coefficient can be linked to the particle size distribution (PSD) approximately through

$$\gamma = \xi - 3 \text{ (Diehl and Haardt, 1980)}$$

where ξ is the exponent of the PSD, which in the ocean can be well approximated by a hyperbolic distribution (Junge-like) (Diehl and Haardt, 1980; Boss et al., 2001). As particles become larger, γ decreases according to the concentration and size of the particles. In the Cariaco Basin, γ at the surface was larger than at 150 m, suggesting that particles at the surface were smaller than those at the bottom of the pycnocline. It is likely that particles retained at the pycnocline were combined to form larger aggregates (Curran et al., 2003).

Below ~200 m, the absorption of CDOM at 412 nm increased (Figure 1.19, dotted line). The a_g (412) calculated based on FCDOM measurements in March 2004 was matched to the total absorption measurements (a(412)) taken with the AC-9 during September 2003, in stations sampled at the same locations. Water below the oxic-anoxic interface is very stable (Deuser, 1973); due to slow turnover, absorption observed below the interface should be similar year-round. Below 300 m, a_g(412) values from March 2004 matched the total absorption measurements at 412 nm taken during September 2003 (Figure 1.19), indicating that below the oxic-anoxic interface most of the absorption was caused by CDOM. The a_g (412) profile, as estimated from fluorescence measurements, did not exhibit a maximum at the oxic-anoxic interface. However, a(412) did present a maximum of absorption at the interface (Figure 1.17).

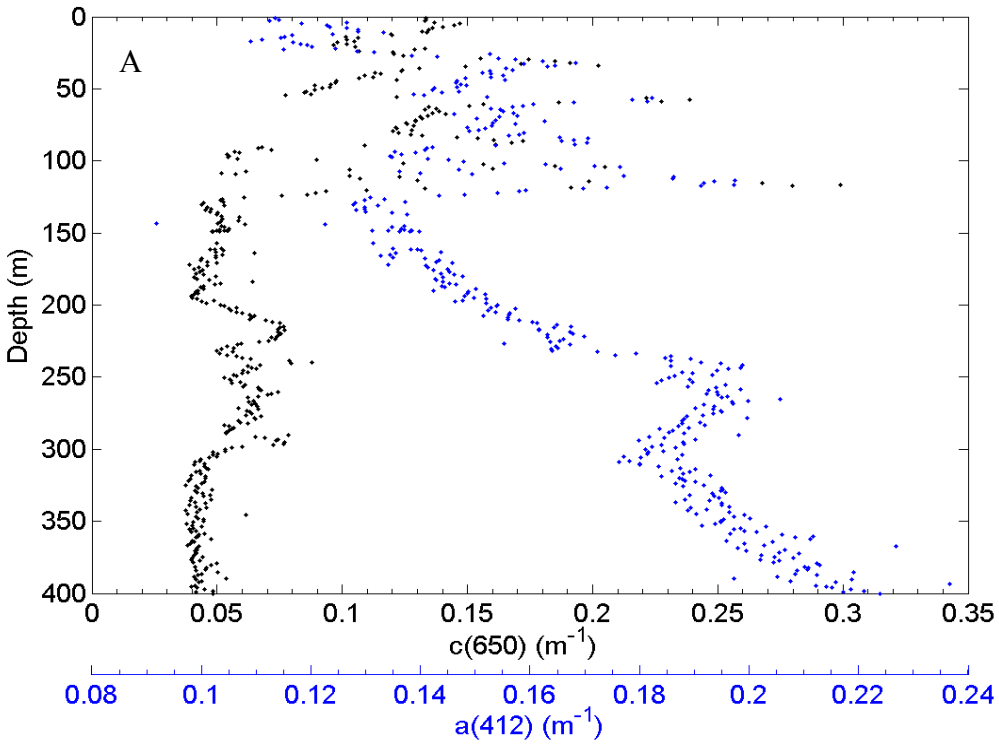

Figure 1.16: (A) Profile of total absorption at 412 nm (a412) and attenuation at 650 nm (c650) (B) Profiles of total absorption at 412 nm (blue), salinity (black) and density (red). Both profiles were measured at station 9 in September 2003. (continued next page)

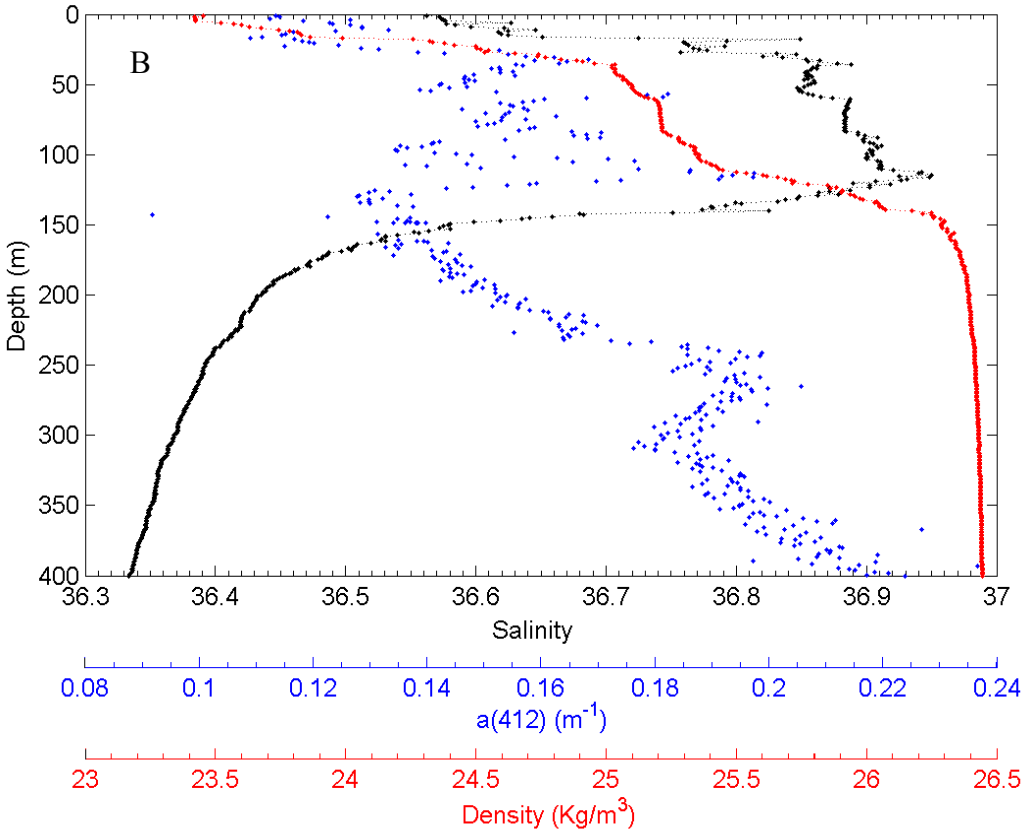

Figure 1.16 (Continued)

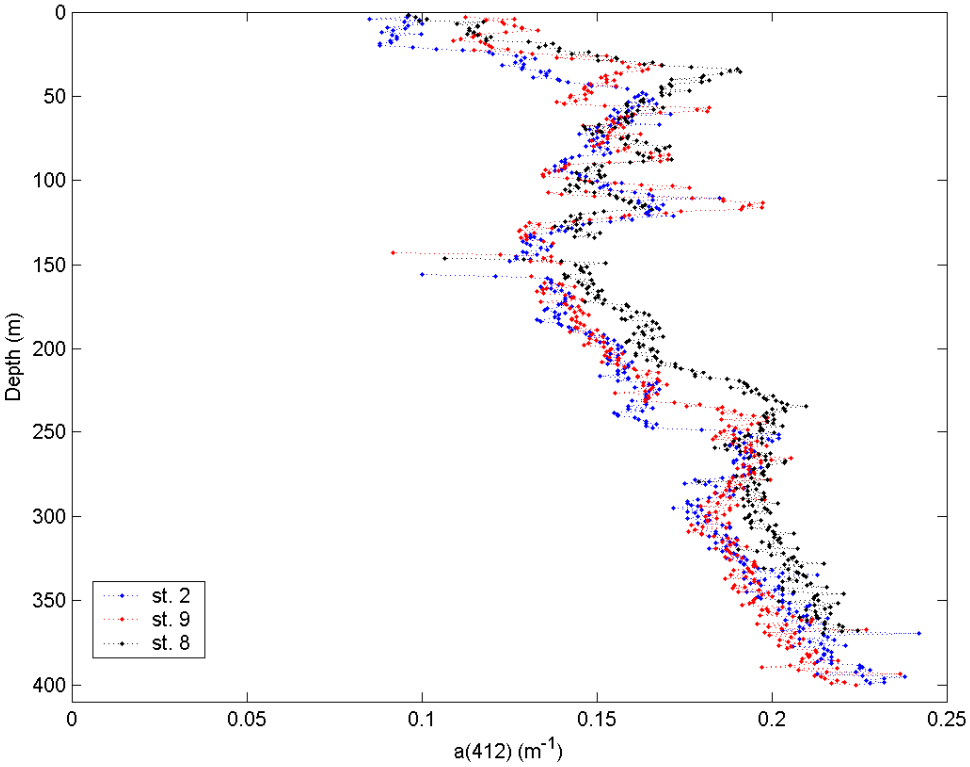

Figure 1.17: Profiles of total absorption at 412 nm (a412) for different stations inside the basin, sampled during September 2003

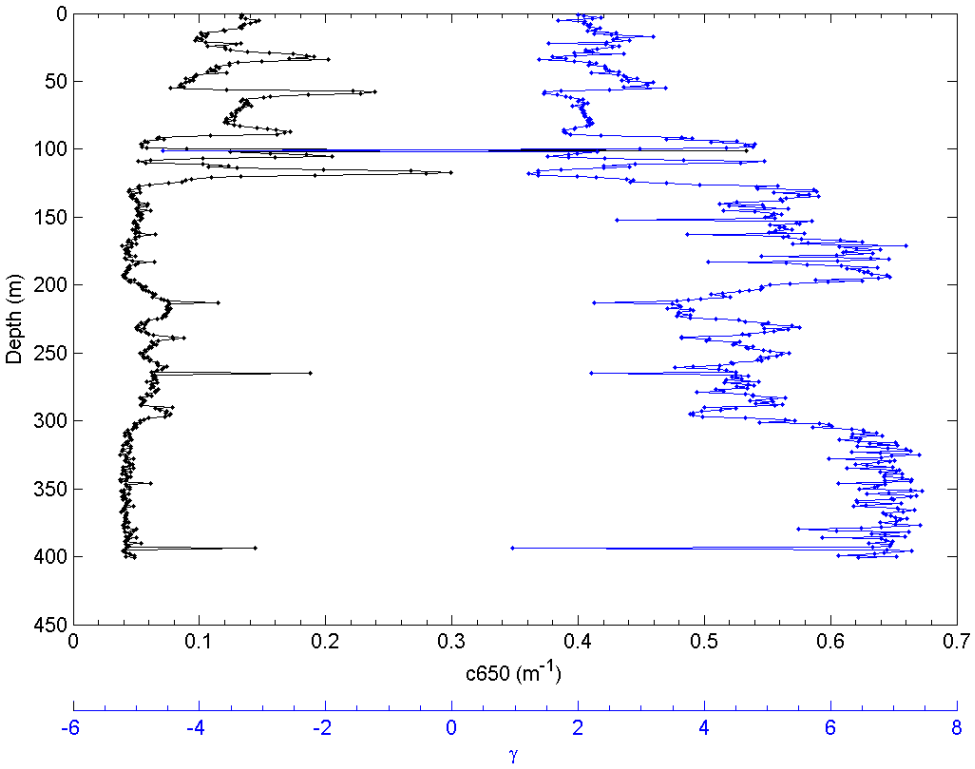

Figure 1.18: Total beam attenuation coefficient at 650 nm (c650, black) and beam attenuation spectral slope (g - blue) measured at station 9 in September 2003.

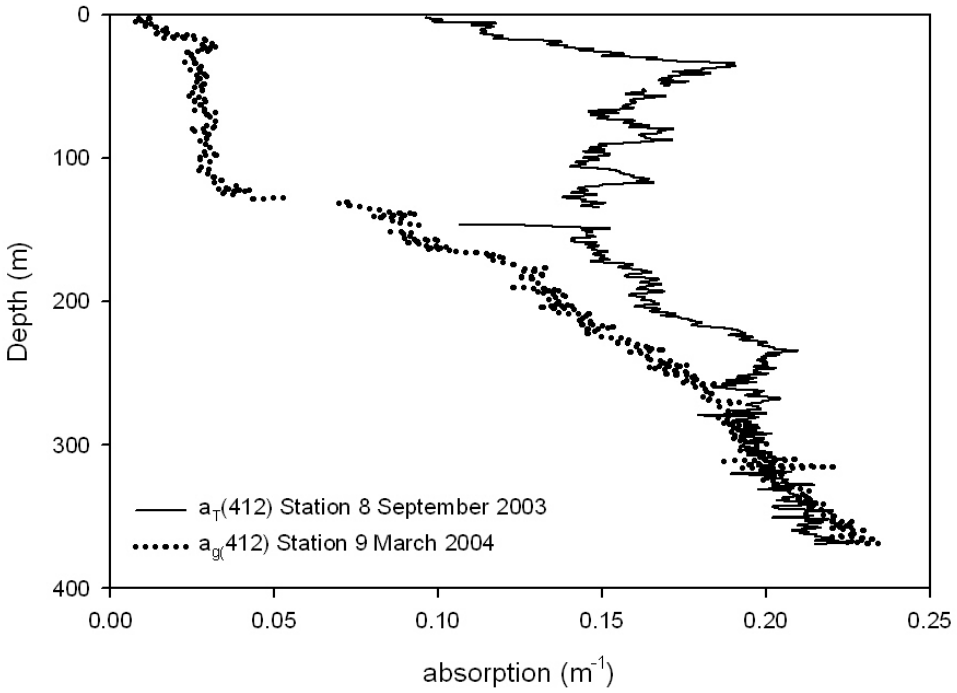

Figure 1.19: Profiles of total absorption at 412 nm (a412) measured with the AC-9 (solid line), in September 2003 and CDOM absorption derived from CDOM fluorescence at 412 nm ($a_g(412)$, dotted line), in March 2004 for stations samples at the same location. (Continued next page)

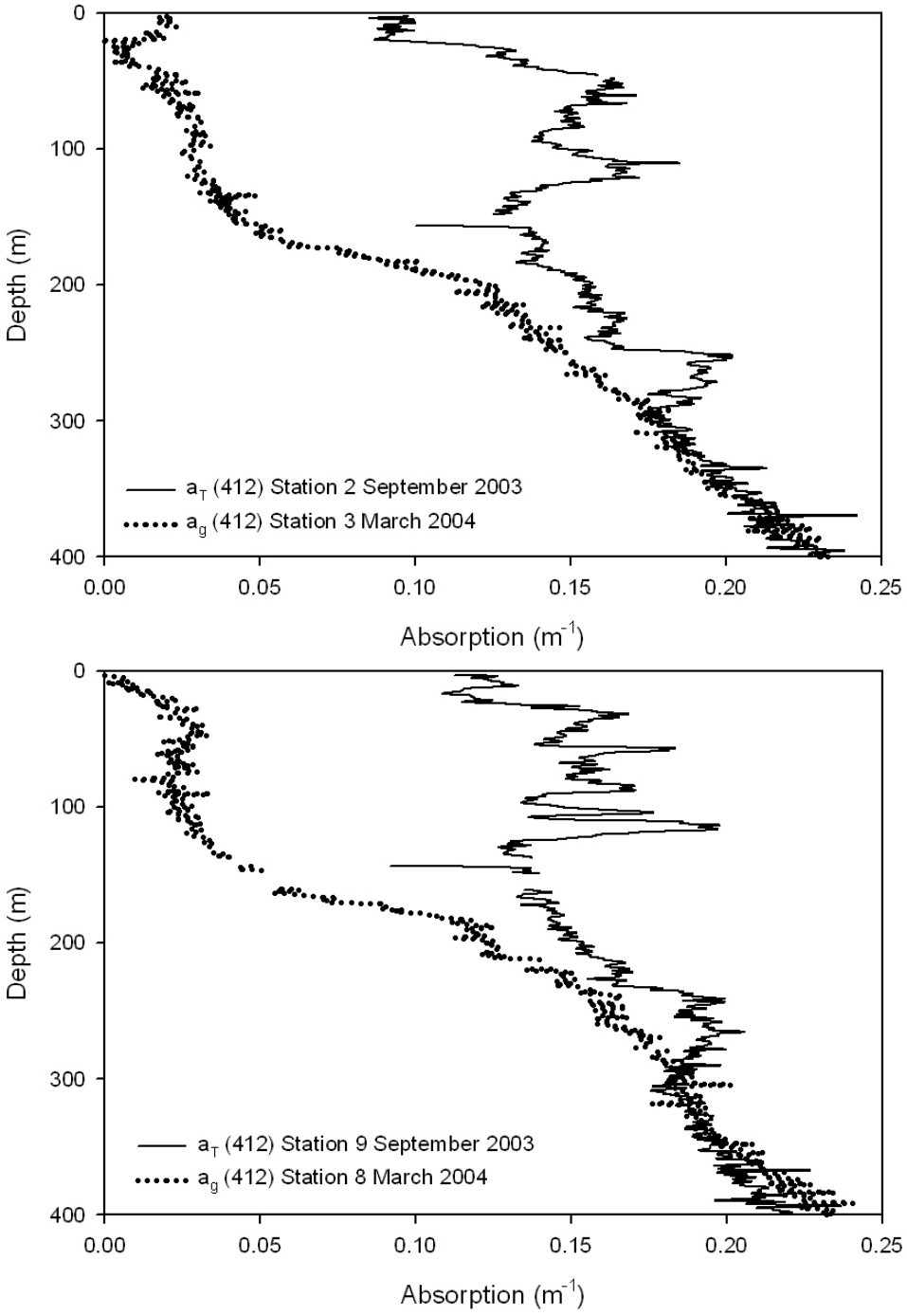

Figure 1.19: (Continued)

4. Discussion

4.1 Water mass exchange between the Cariaco Basin and the Caribbean Sea

Water exchange between the Cariaco Basin and the Caribbean Sea is restricted by a series of sills. The deepest pass on the sill between Tortuga and Margarita Islands is about 140 m. Because of this restriction, only CSW, SUW and TACW can move into the basin (Okuda, 1969; Richards and Vaccaro, 1956). During September 2003, all three water masses were observed inside the Cariaco Basin. However, during March 2004, no trace of CSW was found. In March 2004, the SUW entering the basin was being pushed to the surface, occupying the upper 100 m of the water column. Herrera et al. (1980) and Astor et al. (2003) also noted that the SUW reached its shallowest depths during the first months of the year. Higher salinities in March 2004 were associated with the upwelled, colder water, which was the surface expression of the SUW. Subsurface water intrusions were observed throughout the basin, both during September 2003 and March 2004. These intrusions manifested themselves as peaks of higher dissolved oxygen and lower CDOM concentration than surrounding water. Intrusions were observed both above (March 2004) and below (September 2003) the oxic-anoxic interface. Intrusions of oxygenated water below the oxic-anoxic interface have been observed before (Scranton et al., 1987; Astor et al., 2001) and the working hypothesis is that this water originates outside the sill, forced inside the Basin by processes occurring in the Caribbean Sea. The observations made by the CARIACO time series program and during these cruises suggest that subsurface intrusion of oxygenated water into the basin may be more frequent than previously believed. The fact that these events can be traced with both CDOM and oxygen may allow better estimates of volumes of water mixing between the Caribbean Sea and the Cariaco Basin.

The above paragraphs indicate that, despite the fact that the major influence exerted on the Cariaco Basin by the Caribbean Sea seem to be limited to the upper 200 m, the deep waters of the Basin are far from a steady-state. Slight increases with time in the deep temperature and salinity of the basin have been noted by several authors (Scranton et al., 1987; Holmen and Rooth, 1990; Zhang and Millero, 1993, Scranton et al., 2001). Scranton et al. (1987) calculated that the temperature below 1200 m increased by 0.006 °C per year. This would predict an increase of 0.132 °C from 1982 to 2004. Similarly, Scranton et al. (1987) noted an increase in salinity of approximately 8.89 x10-4 per year. March 2004 values follow Scranton's et al (1987) temperature prediction, but exceed the expected salinity. Scranton et al. (1987) attributed the increase in temperature and salinity to the diffusive mixing of warm, saline water from the upper layers downwards; they also suggested that geothermal heating plays a small role in the warming process. Holmen and Rooth (1990) modeled the effect of episodic water injection into the deep basin. They determined that, in order to explain the temperature and salinity changes at depth, water penetration into the deep was necessary. The difference in salinity slope observed during the past 6 years suggests that there may have been an increase in the input of saltier water from the surface to the deep basin in more recent years (Scranton, pers. comm.).

4.2. Influence of the Orinoco and Amazon Rivers on the Cariaco Basin and role of small, local rivers

During September 2003 and March 2004, no major intrusions of low salinity water were observed from the north, indicating that, while Amazon and Orinoco river water was present immediately to the north of the sill, it did not have major direct influence on the Cariaco Basin. The presence of Orinoco and Amazon river water outside the Cariaco Basin was evident as part of a low salinity plume (<36.75) observed in the Caribbean Sea north of the sill during March 2004. However, the Orinoco plume during this time was small and spread west along the northern coast of Venezuela, flowing north of Margarita Island (Muller-Karger and Varela, 1990). Caribbean surface waters are regularly influenced by fresh water inputs from the large South American rivers. During the period of high discharge of the Amazon, in May and June (Froelich and Atwood, 1978; Hellweger and Gordon, 2002), the surface NECC is not active and waters along the Brazilian coast flow straight into the Caribbean (Halliwell et al. 2003). The combined plume of the Orinoco and Amazon rivers was visible through SeaWiFS images, but even during the rainy season (September 2003), it was distant from Margarita Island and the Cariaco Basin. Waters outside the sill were more exposed to such influences, whereas those inside the Cariaco Basin seemed isolated. Within the Cariaco Basin, CDOM and chlorophyll concentrations measured in March 2004 were mostly the result of local upwelling.

Influence from local rivers was visible as lower salinity near the coast. Though the low salinity plumes of local rivers were limited mostly to the coast, less saline water was transported by local currents eastward towards the center of the basin, influencing directly the CARIACO time-series station. Regularly in the CARIACO time-series station, the lowest salinity is recorded in the month of September (Astor et al., 1998). Currents in the Cariaco Basin are still poorly characterized, and though the observations of September 2003 support the above statement, further research is necessary to fully understand water movement in and around the basin.

4.3. Vertical distribution of CDOM in the Cariaco Basin

Inside the Cariaco Basin, the upper 200 m of the water column are affected by both open exchange with the Caribbean Sea and local processes, such as local river discharge and primary production. During September 2003, most of the CDOM observed in the SeaWiFS image was located near the coast, and areas near the northern sill had very low concentrations of both CDOM and chlorophyll *a*, indicating that there is no significant amount of CDOM entering the basin from the Caribbean Sea during this period. In March 2004, most of the CDOM observed in the upper 25 m of the water column was autochthonous, i.e. released by phytoplankton and bacteria in the water column (Mague et al, 1980; Bricaud et al, 1981; Carder et al., 1986; Coble et al., 1998). Surface DOC concentrations declined from outside the basin to the coast by approximately 10 μM. The relationship between temperature and DOC suggests that higher DOC concentrations were associated with waters that had already sustained

prolonged primary productivity. DOC is released by phytoplanktonic organisms upon breakdown and decomposition, accumulating during the decline of phytoplankton blooms (Chen et al. 1996; Hansell and Waterhouse, 1997). Alvarez Salgado et al. (1999) observed a similar DOC surface distribution in waters off the coast of the Iberian Peninsula, and associated this pattern to wind relaxation and upwelling "spin down". In Figure 1.5, high (> 4 mg/m^3) chlorophyll concentrations are visible near the eastern coast of the Cariaco Basin. This chlorophyll was associated with colder temperatures and higher salinities, indicating this water was recently upwelled SUW water. To the North of Margarita Island high chlorophyll was also visible, with some filaments extending towards the West. This chlorophyll was in warmer waters, most likely an older plume that was already being degraded .

Below 200 m, there was a difference in CDOM distribution between stations located inside and outside the Cariaco Basin. Inside the basin, CDOM concentration, measured as CDOM fluorescence, increased rapidly immediately below the oxic-anoxic interface (~200 m), whereas outside the basin, the increase in CDOM concentration was observed at depths of around ~250-270 m. CDOM fluorescence has been shown to increase with depth, in part due to the regeneration of fluorescence in the absence of high radiation (Kouassi and Zika, 1990, Kouassi et al, 1990), to remineralization (Chen and Bada, 1992) and to microbial activity (Nelson et al., 1998; Mague et al.1980, Coble et al., 1998). The correlation between nutrient concentration and CDOM fluorescence both inside and outside the basin supported the idea that nutrients in the Cariaco Basin were remineralized simultaneously with CDOM (Table 1.4) (Chen and Bada, 1992).

At the oxic-anoxic interface, between 200 and 300 m, the peaks observed in the beam attenuation coefficient corresponded to bacterial layers (Taylor et al., 2001). Similar observations were made by Naqvi et al. (2001) in the Arabian Sea and Garfield et al. (1983) and Spinrad et al. (1989) off the coast of Peru. Absorption at 412 nm also showed a maximum between 200-300 m that marked the location of the oxic-anoxic interface, suggesting the presence of particles at the interface with pigments that absorb blue light, most likely bacteria and viruses. Repeta and Simpson (1991) measured a suite of pigments in bacteria inhabiting the redoxcline of the Black Sea, associated with bacterial anoxygenic photosynthesis. The Cariaco Basin's bacteria may have a similar suite of pigments, but its purpose would not be photosynthetic, since the Cariaco redoxcline is located much deeper than in the Black Sea (Taylor et al., submitted).

Below 300 m, most of the absorption in the Basin was caused by CDOM. This supports the idea that CDOM is generated throughout the water column and accumulates below the interface due to the lack of mixing. The age of this material and its cycling period remains to be determined. The lack of a maximum in the a_g (412) profile at the oxic anoxic interface suggests that either CDOM is not produced at a faster rate in this location in the water column, or the CDOM produced by the bacterial population is labile and used up immediately.

5. Conclusion

Water exchange between the Cariaco basin and the Caribbean Sea is restricted by a series of sills. Because of this restriction, only CSW, SUW and TACW can move into the basin (Okuda, 1969; Richards and Vaccaro, 1956). Waters deeper than ~160 m in the Caribbean Sea do not access the basin. In March 2004, water from outside the Cariaco Basin was observed entering the basin at depth and upwelling near the coast. Surface waters were pushed offshore, eliminating CSW from the study site. The water entering the Basin brought in DOC and dissolved oxygen. Oxygen intrusions similar to those documented by Scranton et al. (2001) and Astor et al. (2003) were observed at different locations around the basin in September 2003, between 200 and 300 m. During March 2004, subsurface oxygen peaks were also observed throughout the basin. Oxygen intrusions into the anoxic portion of the basin may be more frequent in time than previously believed.

A seasonal difference in both surface temperature and salinity distribution was found between September 2003 and March 2004. During September 2003, surface temperatures in the basin ranged from ~26 to ~28 ^{o}C, and salinity from ~36.4 to ~36.8. The influence of local rivers on the basin, as contributors of less saline water, was seen in September 2003 near the coast. During March 2004, temperatures were ~3 ^{o}C lower than in September 2003; salinities were higher on average by 0.2 throughout the entire study region. No major intrusion of low salinity waters was observed from the north during either the rainy or dry season, indicating that the Amazon and Orinoco rivers do not have major direct influence on the Cariaco Basin.

There is a difference in temperature and salinity between the Cariaco Basin and the open Caribbean Sea below 200 m. Inside the basin, temperatures and salinities averaged between 200 and 400 m were higher by ~4^{o}C and by ~0.5. Scranton et al. (1987) calculated that deep (~1200 m) temperature and salinity inside the basin were rising by 0.006 ^{o}C and 8.89 x 10^{-4} per year. Temperature measurements in March 2004 agree with these observations. However, salinity at 1200 m was higher than predicted by Scranton et al. (1987), indicating an input of saltier water to the deep basin (Scranton, pers. comm.).

Concentrations of dissolved organic carbon (DOC) at surface ranged from ~70 μM C in stations outside the basin to ~60 μM C near the Gulf of Santa Fe. The lower DOC concentrations were associated with cold, recently upwelled water, while the higher ones were observed in warmer waters where phytoplankton blooms were likely already in decline.

CDOM concentrations increased rapidly below the oxic-anoxic interface (~200 m) inside the Cariaco Basin. Outside the basin, the increase in CDOM was observed around ~250-270 m. Below 300 m, $a_g(412)$ values from March 2004 match the total absorption measurements at 412 nm taken during September 2003, indicating that below the oxic-anoxic interface most of the absorption is caused by CDOM. This supports the idea that CDOM is generated throughout the water column, and accumulates below the

interface due to the lack of mixing. Total absorption profiles exhibited an absorption maximum at the oxic-anoxic interface, suggests the presence of particles with pigments that absorb blue light, most likely bacteria and viruses. The a_g (412) profile did not exhibit a maximum at the oxic-anoxic interface, making it unclear whether CDOM is produced faster at the redoxcline than elsewhere in the water column or the majority of the CDOM produced is labile.

CHAPTER II

THE INFLUENCE OF LOCAL RIVERS ON THE BIO-OPTICAL PROPERTIES OF THE EASTERN CARIACO BASIN

1. Introduction

Continental margins play an important role in the global cycles of carbon and other biogeochemical elements. Most land materials enter the sea through river runoff in particulate or dissolved form (Liu et al., 2000), and some fraction is deposited on the adjacent continental shelf. The delivery of terrigenous materials via rivers varies according to changes in weather patterns, such as seasonal rainfall and ocean circulation. Ultimately, climate changes have impacts on all of these processes.

The Cariaco Basin, because of its anoxic condition and high sedimentation rate, conserves one of the best sediment records available in the marine environment (Hughen et al., 1996; Lin et al., 1997; Black et al., 1999; Peterson el al. 2000; Goñi et al., 2003). In order to carry out an accurate interpretation of past climate variation based on this record, it is necessary to understand the sources of particulate matter to the basin. Here we examine the contributions of dissolved and detrital material of local rivers to the Cariaco Basin, in an effort to help provide such information.

The Cariaco Basin is situated on the continental shelf off Venezuela (Figure 2.1), and is composed of two depressions of ~ 1400 m each. It is connected to the Caribbean Sea by a shallow sill (~140 m maximum depth; Richards, 1975). The CARIACO oceanographic time series project has collected over 9 years of data, including sediment traps, optics and hydrography in the Cariaco Basin (Muller-Karger et al., 2005). The lowest surface salinities and highest terrigenous inputs at the CARIACO time series station occur in September (Astor et al., 1998). There has been a lingering question as to whether these changes are associated with local rivers or to influence of the larger Orinoco plume that enters the Caribbean Sea (see Muller-Karger et al., 1989).

Three main rivers discharge onto the southern Cariaco shelf known as the Unare Platform: the Manzanares, Neverí and Unare Rivers (Figure 2.1), all originating in the nearby Coastal Mountain Range (Cordillera de la Costa). These rivers show high discharge during the rainy season (July to November) with maximum discharge in August and September. The Unare is the largest of these rivers, with a drainage basin area of 22.3 Km^2 and an approximate average discharge rate of 56 m^3/sec (Zinck, 1977). The Neverí and Manzanares are smaller (drainage basin of 3.9 and 1.0 km^2, respectively), discharging approximately 35 and 22 m^3/sec, respectively, into the Cariaco Basin (Zinck, 1977). Discharge rates were measured during 1958-1967. Unfortunately, data are not available to assess more recent discharge or even variation in flow. Several of the rivers have since been dammed, while others now receive contributions from sewer systems, industry and urban areas.

In this study we examine the distribution of riverine material near the coast and around the Cariaco basin to help address the question of the relative importance of local vs. remote river inputs.

1.1 Objectives

The main objective of this chapter is to understand the impact of local rivers on the Cariaco Basin, and whether this is more important than the Orinoco River with respect to sediment delivered to the basin. Specifically, we asked the following questions:

- What is the distribution of colored dissolved organic matter (CDOM) near the coast?
- What is the distribution of particulate material near the coast?
- What is the accuracy of regional CDOM and chlorophyll satellite observations?

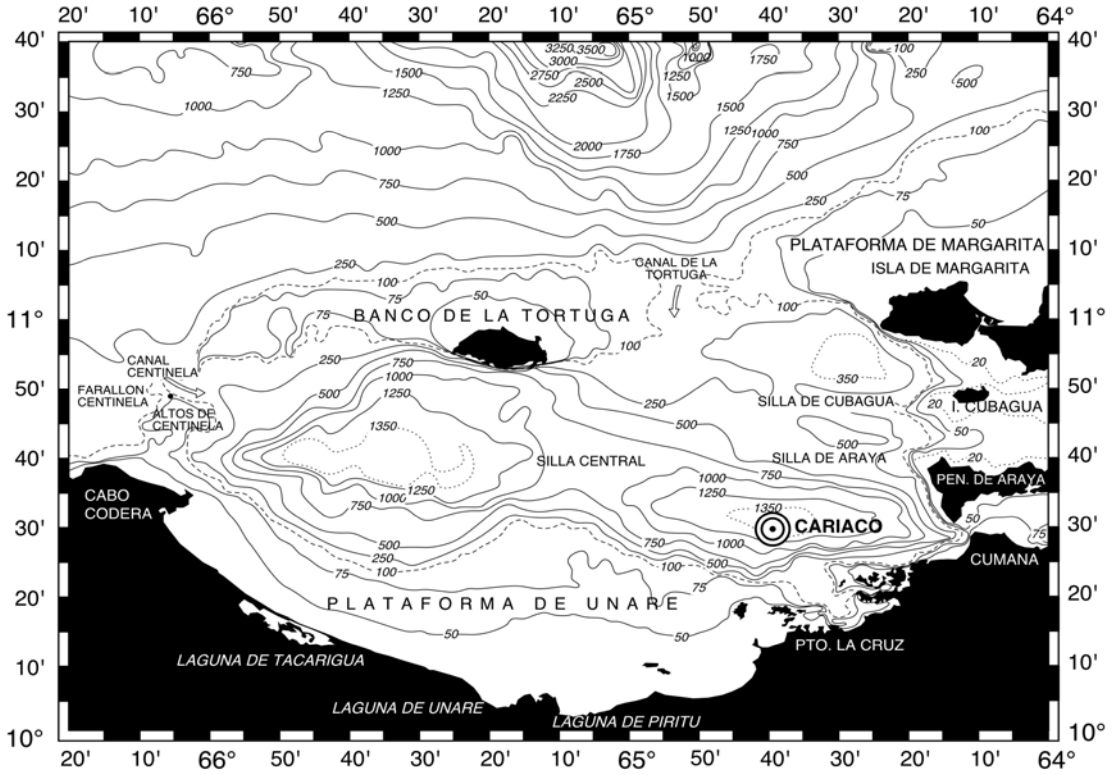

Figure 2.1: Schematic of the Cariaco Basin, showing location of the CARIACO time series station (from Astor et al., 2003)

2. Methods

Two cruises (Table 2.1) were conducted to the Cariaco Basin in different seasons using the *R/V Hermano Gines* of the Fundacion La Salle de Ciencias Naturales de Venezuela. The first cruise was conducted in September 2003 (COHRO – Campaña Optica e Hidrografica Región Oriental; Figure 2.2A). The objective of this cruise was to study the impact of rivers, both local and distant, specifically the Orinoco and Amazon, on the Cariaco Basin. 19 stations were placed between the coast and the 200 m isobath (Figure 2.2A). The rest of the stations were placed in a grid-like pattern, separated by a distance of approximately 20 km.

The second cruise was carried out in March 2004 (COHRO2; Figure 2.2B). The objective was to study the distribution of upwelling waters within the Cariaco Basin, and to help understand the characteristics of waters entering the basin from the Caribbean Sea. Eight stations were located outside the basin, north of the Tortuga-Margarita sill.

Salinity and temperature profiles were measured using a Seabird SBE25 CTD, deployed at each station in a rosette ensemble. Oxygen data and chlorophyll fluorescence were obtained with a Seabird SBE 43 oxygen sensor and a Chelsea fluorometer (Chelsea, Inc.), respectively, attached to the CTD. The ensemble also had a C-Star transmissometer (WetLabs) that measured beam attenuation at 660 nm (c660). The data were processed using SeaBird's SBE Data Processing software.

During the September 2003 cruise, one absorption/attenuation meter (AC-9 - WetLabs) was deployed as part of the hydrocasts. A pump was used to draw water through the absorption and attenuation tubes. At 14 stations, double casts were performed, one with an unfiltered AC-9, and the second using a 0.2 μm filter (Propor PES filter capsules) attached to the inlet of the absorption tube. The instrument was calibrated before, during, and after the cruise using distilled water as a reference.

Optical measurements were taken during both cruises in and above the water, using a PRR-600 submersible radiometer and a surface Spectrascan PR-650 spectroradiometer, respectively.

Samples for optical measurement of absorption of light due to colored dissolved organic matter (CDOM) were collected at 15 stations during September 2003 (depth of 1, 10, 15, 25, 50, 100; depth of sampling varied in some stations due to depth constrains or features of interest), and at 4 stations during March 2004 (depths of 1, 35 and 100 m). During September 2003, samples were filtered onboard the ship with a 0.2 μm pore-size anotop filter, using a glass syringe and measured immediately (see section 2.1). During March 2004 samples were also filtered on board in the same manner as described above, but were later stored in acid cleaned amber-colored bottles and frozen for transportation. Absorption measurements were conducted within one month of sample collection at the University of South Florida using an Ocean Optics spectrophotometer (see section 2.1)

2.1. Data processing

AC-9 processing and validation

AC-9 data were corrected for temperature and salinity, following Pegau et al. (1997). A scattering correction was also applied to the absorption data. The scattering correction was done by subtracting a reference wavelength (715 nm) from all data (hypothesis 3 in the AC-9 WetLabs User's Guide, 2003). As a data quality check, the AC-9 beam attenuation data at 650 nm were compared to c660 taken with the transmissometer at all stations. In the filtered samples, a lag in the data was observed, caused by the reduction in flow due to the filter. This lag was adjusted by comparing patterns and features between the ac-9 and the transmissometer data. Only those spectra where this procedure was possible were used.

Because attenuation at 412 nm was lower than absorption at 412 nm, caused most likely by a lack of internal calibration of the instrument or filter degradation, a new c value was calculated for 412 nm, according to the hyperbolic model

$$c(\lambda) = c(\lambda_o)*(\lambda/\lambda_o)^{-\gamma} \qquad (1)$$

where $c(\lambda)$ is the beam attenuation, $c(\lambda_o)$ is the attenuation at the reference wavelength and γ is the spectral slope of c (Boss and Zaneveld, 2003), computed here using all bands except 412 nm; λ_o was 440 nm.

Absorption Spectroscopy

In September 2003, absorption spectra were measured between 200 and 800 nm, with a 0.3 nm interval, using a dual fiber optic spectrometer (Ocean Optics) equipped with 10-cm quartz cuvettes. The detection limit of the spectrophotometer was ± 0.002, or equivalent absorption of 0.046 m^{-1}.

Distilled water was used as a blank. The distilled water was collected the day prior to the start of the cruise and kept in Nalgene polycarbonate carboys inside the air-conditioned wet lab of the ship. A running mean was used to smooth the absorption spectra, which was later binned in 1-nm intervals. Each spectrum was examined individually, and the blank absorption was subtracted from the sample absorption when absorption at 650 nm was greater than zero.

March 2004 CDOM samples were transported to the University of South Florida (USF), and analyzed within one month of the cruise. Samples were refiltered once thawed to remove any particles. Samples were scanned between 200 and 800 nm at 1 nm intervals, using a Perkin-Elmer Lambda 18 spectrophotometer equipped with 10 cm quartz cells. The detection limit of the instrument was ± 0.002, or equivalent absorption of 0.046 m^{-1}. Milli-Q water was used as blank, and for each sample two scans were performed. Running means were used to smooth the data, and, where necessary, the blank absorption values were subtracted from the sample. The best of two scans was selected. The selection of the best scan was based on the smoothness and shape of the curve, whether it had features out of the ordinary, and if it had been necessary to subtract

the blank from the sample. Those scans where no subtractions had been done were preferred.

Absorption coefficients were calculated from absorbance, according to the following relationship:

$$a(\lambda) = 2.303\ A(\lambda)/r \qquad (2)$$

where A is the absorbance or optical density and "r" is the pathlength. Light absorption by CDOM was approximated by

$$a_g(\lambda) = a_g(\lambda_o)\exp[-S(\lambda-\lambda_o)] \qquad (3)$$

where $a_g(\lambda)$ and $a_g(\lambda_o)$ are the absorption coefficients at wavelength λ and at a reference wavelength λ_o. S is the spectral slope, which describes the decrease in absorption of a_g with increasing wavelength (Blough et al, 1993; Green and Blough, 1994; Ferrari, 2000, Blough and Del Vecchio, 2002). Each spectrum was plotted in two ways: through a linear least squares regression of the log-transformed data (ln(a) vs. λ, J. Cannizzaro, pers. comm.) and in an exponential form, using a non-linear least squares fit (Dr. C. Hu, pers. omm..). The method that provided the single best fit for each individual spectrum was selected. The slope S was calculated between 350 and 450 nm.

Absorption by phytoplankton (a_{ph}) was obtained from in situ fluorometric measurements. The CARIACO project has over nine years of data, which include chlorophyll fluorescence and absorption from filter pads. These measurements were used to calibrate the chlorophyll fluorometer and obtain, for the September 2003 cruise, quantitative values of $a_{ph}(\lambda)$ from fluorescence. a_{ph} for the CARIACO dataset was measured in situ through filtration following Kishino et al. (1985). The β from Mitchell and Kiefer (1988) was used for the correction of the optical path elongation due to filter pads.

Reflectance observations

PRR and Spectrascan data were collected following the NASA Ocean Optics Protocols for SeaWiFS Validation (Mueller and Austin, 1995). The data were processed with software developed in-house (Dr. Chuanmin Hu, USF, personal communication). The diffuse attenuation coefficient, K_d, was computed from downwelling irradiance profiles (E_d) at 412, 443, 490, 532, 555, 665 and 683 nm, following the relationship:

$$E_d(z) = E_d(0^-)\, e^{-K_d * z} \text{ (Baker and Smith, 1979)} \qquad (4)$$

Where z is depth and $E_d(0^-)$ refers to downwelling irradiance just below the ocean's surface. Remote sensing reflectance, Rrs, defined as

$$R_{rs} = L_w/E_d \quad \text{(Mobley, 1992)} \qquad (5)$$

Table 2.1: Station location and cast depth for COHRO and COHRO2

COHRO, September 16-20, 2003				COHRO2, March 15-20, 2004			
Latitude	Longitude	Station	Maximum profiling depth (m)	Latitude	Longitude	Station	Maximum profiling depth (m)
10.83	-64.37	0	225	10.83	-64.36	1	217
10.66	-64.36	1	157	10.66	-64.36	2	160
10.50	-64.36	2	400	10.50	-64.36	3A	400
10.33	-64.55	3	120	10.50	-64.36	3B	1220
10.49	-64.55	4	400	10.45	-64.26	4	120
10.66	-64.55	5	400	10.41	-64.38	5	190
10.83	-64.55	6	220	10.33	-64.55	6	127
10.83	-64.70	7	225	10.40	-64.61	7	160
10.66	-64.71	8	400	10.45	-64.55	8A	521
10.49	-64.66	9	400	10.45	-64.55	8B	798
10.33	-64.71	10	40	10.56	-64.55	9A	400
10.33	-64.88	11	56	10.56	-64.55	9B	1220
10.23	-64.88	12	37	10.76	-64.55	10	400
10.14	-65.03	13	15	10.76	-64.71	11	383
10.19	-64.79	14	26	10.76	-64.88	12	400
10.28	-64.8	15	45	10.60	-64.88	13	403
10.49	-64.88	16	400	10.48	-64.88	14	400
10.66	-64.88	17	400	10.33	-64.71	15	50
10.83	-64.88	18	224	10.28	-64.80	16	50
10.66	-65.05	19	400	10.38	-64.93	17	76
10.49	-65.05	20	400	10.50	-65.05	18	400
10.41	-65.05	21	63	10.63	-65.10	19	400
10.33	-65.05	22	59	10.76	-65.05	20	400
10.23	-65.05	23	25	10.93	-65.05	21	67
10.23	-65.21	24	24	11.05	-65.05	22	75
10.33	-65.21	25	56	11.16	-65.05	23	276
10.41	-65.21	26	75	11.33	-65.05	24	400
10.33	-65.38	27	55	11.33	-64.88	26A	400
10.41	-65.38	28	77	11.33	-64.88	26B	1382
10.49	-65.21	29	113	11.16	-64.88	28	276
10.83	-65.04	30	220	11.05	-64.88	29	123
11.00	-65.04	31	80	10.93	-64.88	30	181
11.00	-64.88	32	130	10.93	-64.71	31	310
11.00	-64.71	33	174	11.05	-64.71	32	90
10.99	-64.54	34	273	11.16	-64.71	33	90
10.44	-64.26	48	70	11.33	-64.71	34	210
10.14	-65.11	49	15	11.33	-64.55	35	380
10.16	-65.21	50	10	11.16	-64.55	36	50
10.41	-64.40	51	180	11.05	-64.55	37	84
				10.93	-64.55	38	350

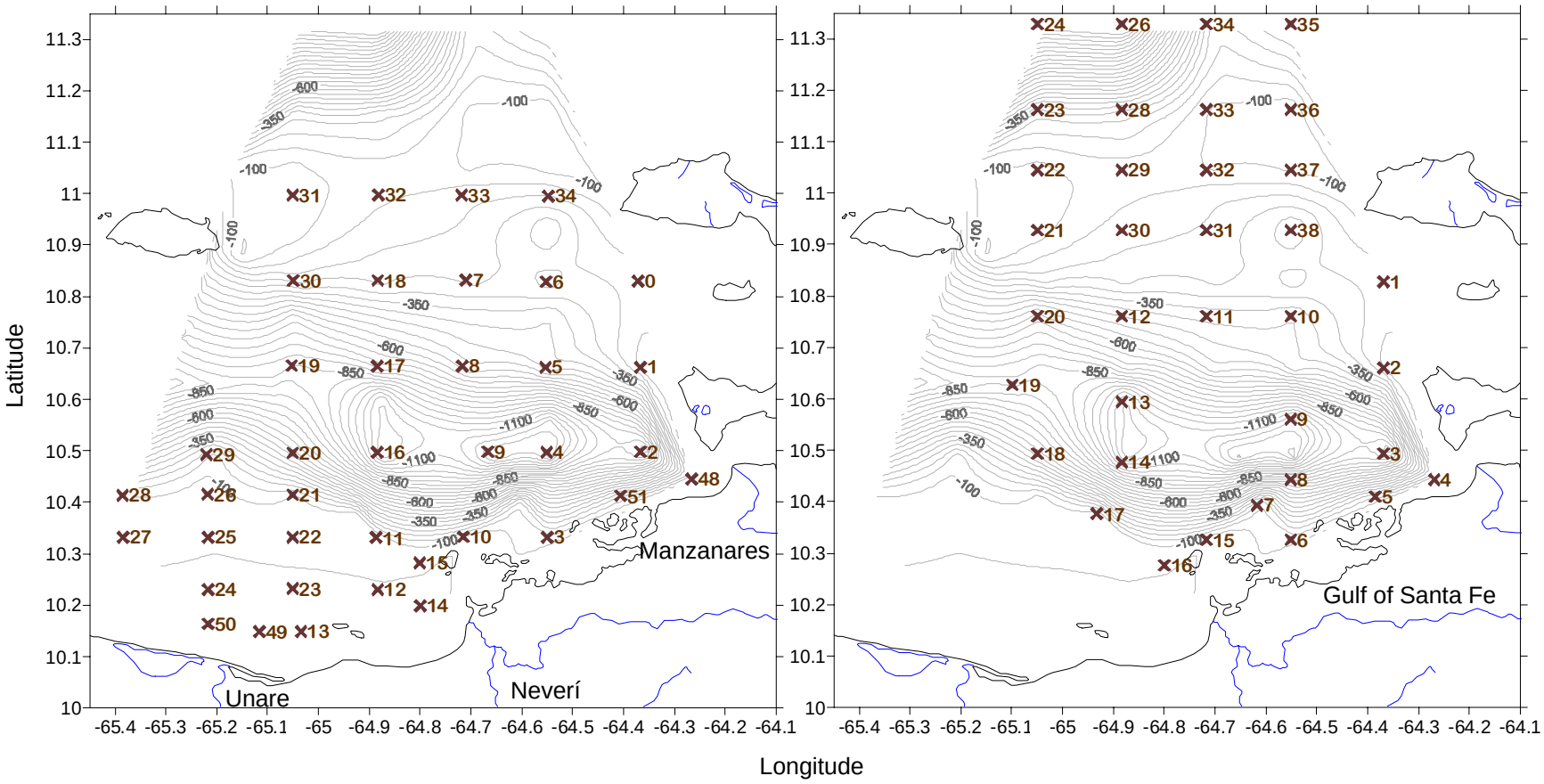

Figure 2.2 Sample location for the September 2003 (A) and March 2004 (B) cruises. Major local rivers are shown.

was derived from above-water measurements for wavelengths between 380-780 nm, at 1 nm intervals.

Beam attenuation profiles taken with the WetLabs CStar transmissometer were used to study the three-dimensional distribution of particulate matter across the basin. A statistical analysis was conducted to determine possible relationships between the beam attenuation and chlorophyll fluorescence profiles, to identify variability corresponding to inorganic or detrital particles as opposed to phytoplankton.

Satellite imagery

Two SeaWiFS (Sea-viewing Wide Field-of-View Sensor) images were processed for chlorophyll and CDOM absorption (a_g) at 440 nm, using the optimization algorithm of Lee et al. (1999) and the Carder et al. (1999) MODIS algorithm (Dr. C. Hu, Pers. Comm). The dates of the images were chosen as close as possible to the dates of the cruises. For September 2003, the only image with low enough cloud cover was for September 30, almost 2 weeks after the cruise. For March 2004, the image of March 10 was selected.

3. Results

3.1. Surface distribution of CDOM near the coast

Observations collected during September 2003 show that the two main contributors of CDOM to the Cariaco Basin were the Neverí and Unare rivers. There were low (~0.04 m^{-1} at 400 nm) concentrations of CDOM in surface waters near the mouth of the Manzanares river (Figure 2.3). Traces of leaves, plastic and other types of debris were seen at station 48 off the Manzanares (see Figure 2.2 for reference), but the water was blue, similar to what is expected in open ocean areas away from the coast with no visible suspended matter.

Figure 2.4 shows the relationship between CDOM absorption (a_g) and salinity for stations sampled during September 2003. A linear, conservative mixing is expected between salinity and CDOM concentration from rivers if there are no additional sources or sinks of CDOM (Carder et al, 1989; Del Castillo et al., 1999; Boss et al., 2001; Boss et al., 2001; Cauwet, 2002, Hu et al., 2003). The relationship between CDOM and salinity observed near the coast in Cariaco was not robust, in part due to the quick mixing of the river water with the coastal seawater. The lowest salinity recorded near the coast was close to 36, indicating that at that location there was mostly seawater. A relationship between CDOM and salinity probably exists closer to the river mouths. Despite the fact that even near the coast salinity was not lower than ~ 36, at the CARIACO time-series station lower than average (~36.5) salinity is always observed during September (Figure 2.5 A) (Astor et al., 1998). This was also the case for September 2003. Figure 2.5B is a current profile measured near the CARIACO time-series station for September 2003; a relatively strong eastward current (~22 cm/s) was observed between 30-50m. The depth of the thermocline at this location was around 100m, and because the wind was weak (~2-4 m/s as measured from the R/V Hno. Gines in stations near the coast), it was possible to use these observations to infer the approximate flow at the surface (Dr. R. Weisberg, pers. comm.). Less saline water from local rivers is the cause of the low salinity observed yearly at the CARIACO time-series station, which is transported by local currents as far north as 10°30'.

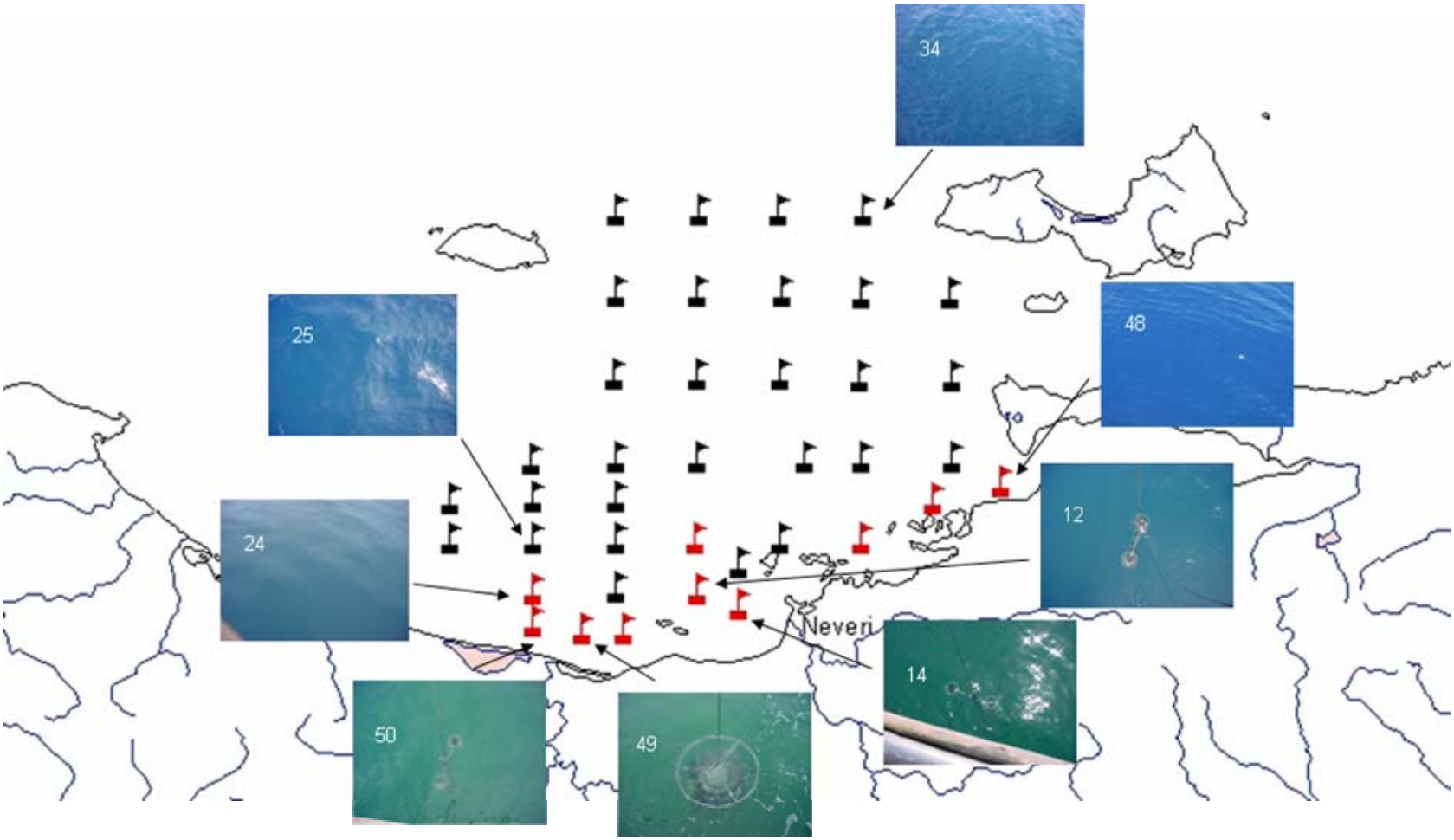

Figure 2.3: Visible changes in water color in September 2003. Station 48 is located near the Manzanares River, station 14 close to the Neverí River and stations 49 and 50 near the Unare River

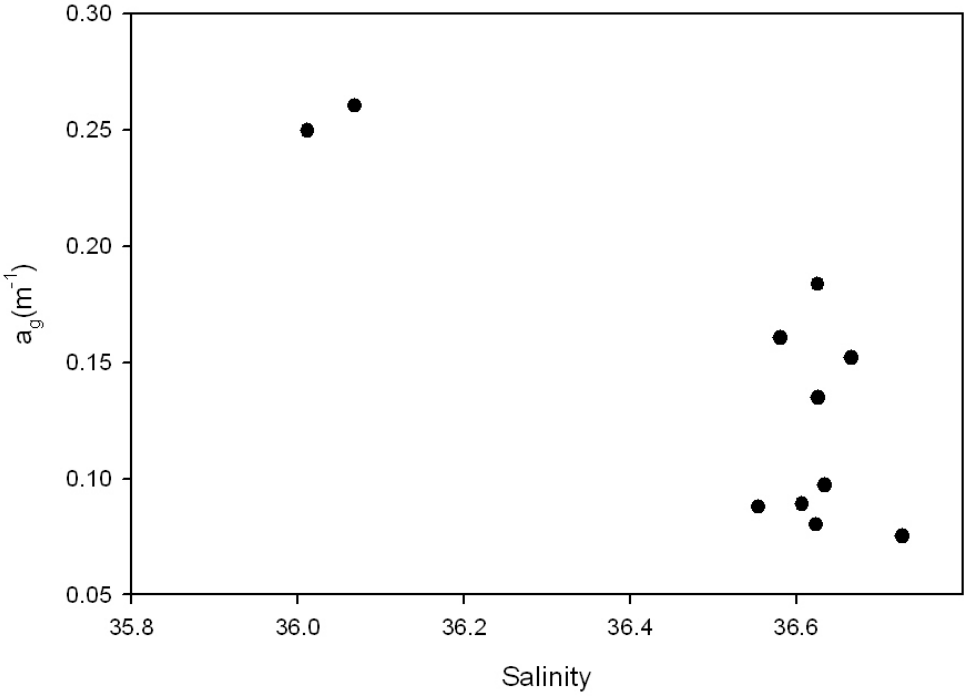

Figure 2.4: Relationship between CDOM absorption coefficient ($a_g(400)$) and salinity for stations 4, 11, 12, 13, 14, 16, 20, 21, 22, 50, and 51 sampled in September 2003.

Figure 2.6 shows the relationship of S, the slope of a_g (equation 3), and $a_g(400)$ in the Cariaco Basin. Variations in S contain information about the nature of CDOM (Nelson et al., 1998; Blough and Del Vecchio, 2002). Farther offshore, in the central and northern Cariaco Basin, S was higher (>0.02 nm^{-1}) than in coastal regions under the influence of rivers (0.010-0.018 nm^{-1}). Offshore waters not affected by rivers, sampled during March 2004, showed low $a_g(400)$ (~0.03 m^{-1}) and high S (0.024 nm^{-1}). Areas near the coast, sampled during September 2003, showed high $a_g(400)$ (~0.25 m^{-1}) and low S (~0.011 nm^{-1}). Table 2.2 compares the range of S observed in the Cariaco Basin during September 2003 and March 2004 with data from other locations. The range of S measured was similar to that reported by other authors, both for coastal and open waters (Bricaud et al., 1981; Nelson and Guarda, 1995; Carder et al., 1999; Cannizzaro, 2004). Some extreme slope values (e.g. 0.0105 nm^{-1}) were associated with high (~ 0.25 nm^{-1}) concentrations of CDOM, suggesting that the estimate of S was sensitive to particle scattering and baseline offsets (Green and Blough, 1994). When a_g values were too low (~0.02 m^{-1}) there was a signal to noise problem, in which the instruments used to measure a_g was not sensitive enough for such low concentrations. This yielded a higher than normal S (e.g. 0.028 nm^{-1}) (Dr. K. Carder, pers. comm.). Such extremes should be treated carefully.

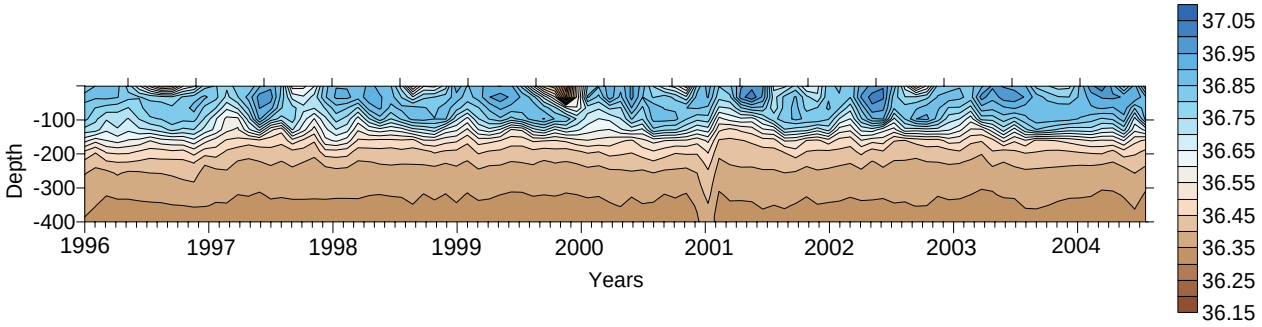

A

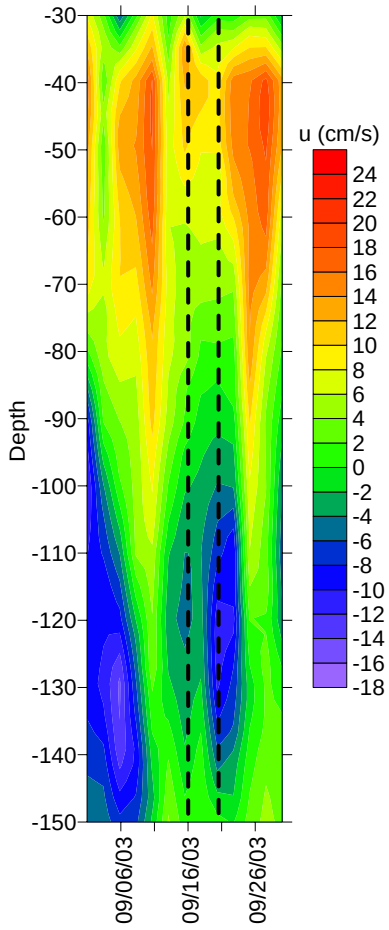

B

Figure 2.5: (A) Vertical profile (from 1-400m) of salinity at the CARIACO time-series station from January 1996 to July 2004. Contour lines are interpolated between measurements. (B) Vertical distribution of the east/west component of current velocity (cm/s), at the CARIACO time-series station (see Figure 2.1 for location) for September 2003.

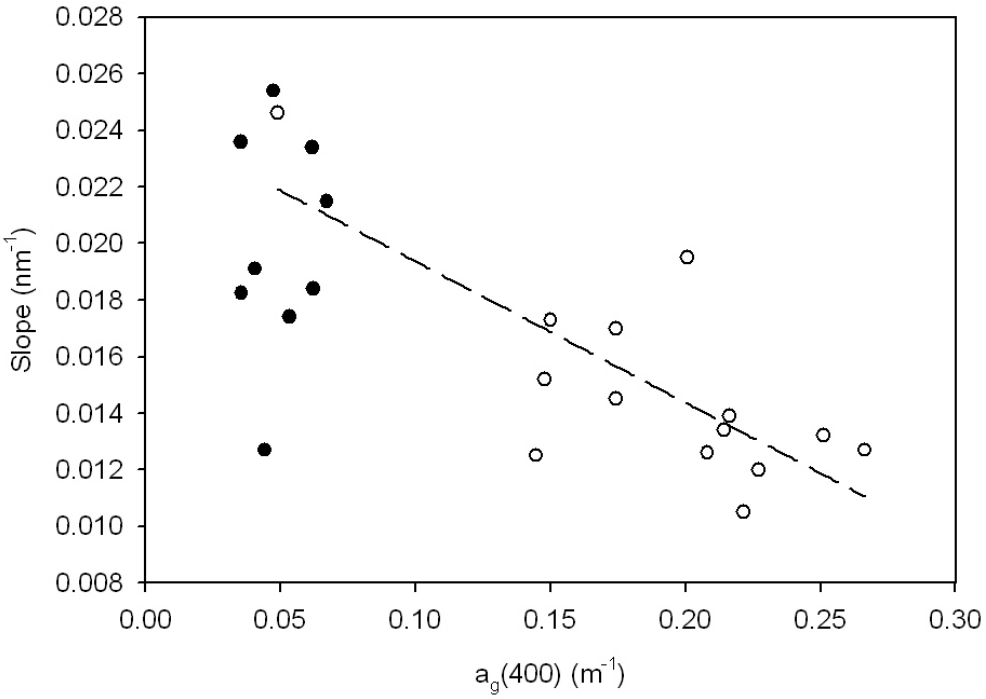

Figure 2.6: Relationship between the spectral slope (S) and CDOM absorption (a_g) at 400 nm. Samples used include those collected during September 2003 (○) and March 2004 (●)

Table 2.2: CDOM absorption slopes, S

Location	*S* (nm $^{-1}$)	Reference	Range (nm)
Mediterranean and Baltic Sea	0.012-0.018	Bricaud et al. 1981	375-500
GOM	0.011-0.017	Carder et al. 1989	370-440
South Atlantic Bight	0.017-0.023	Nelson and Guarda, 1995	300 - ~500
West Florida Shelf	0.014-0.025	Cannizzaro, 2004	350-450
Cariaco Basin	0.011-0.026	This study	330-400

3.2. River influence on the optical properties of Cariaco's coastal waters

Optical properties of the water can be used to determine the spatial variability of riverine influence in the Cariaco Basin. Total absorption at depths of 1, 5, 10, and 25 m, measured during September 2003, are shown in Figure 2.7. Changes in absorption of light in natural waters are caused mainly by phytoplankton (a_{ph}), CDOM (a_g) and detritus (a_d) (Roesler and Perry, 1995; Green et al., 2003). Absorption by water (a_w) is well know and constant (Pope and Fry, 1997). The absorption of light in the ocean is additive:

$$a_T = a_{ph} + a_{CDOM} + a_d \quad [m^{-1}]$$

where a_T stands for total absorption (Roesler et al., 1989; Green et al., 2003). At stations near the coast (22, 21 and 11, Figure 2.7) small absorption peaks were noted in all depths

at 676 nm. These peaks indicated the presence of phytoplankton. The typical absorption shape of phytoplankton in the blue part of the spectrum was masked by CDOM. Chlorophyll concentrations in the coastal area varied between 0.04-1.58 mg/m^3; concentrations were highest between 10-20 m, where the deep chlorophyll maximum was located. Station 21 showed some of the strongest absorption at 10 and 25 m, which corresponded to higher chlorophyll concentrations.

The combined percentage contribution of detritus and CDOM (a_{CDM}) to total absorption was assessed and compared to the contribution by phytoplankton. The relationship between a_{ph} at 676 nm and chlorophyll fluorescence was calculated using data from the CARIACO time-series project. This regression resulted in the following equation:

$$a_{ph}(676) = 0.05778 * FChl + 0.00003 \qquad (r^2 = 0.92)$$

Absorption at 676 nm was linearly related ($r^2 = 0.98$) to $a_{ph}(412)$ by

$$a_{ph}(412) = 1.5719 - a_{ph}(676) + 0.0071$$

Other authors have used power functions in these relationships (Claustre et al., 2000), to account for packaging effects and accessory pigments.

Because the concentration of phytoplankton was very low, in this case a linear relationship is probably more accurate. $a_{ph}(412)$ was subtracted from total absorption to obtain the absorption at 412 nm effected by detrital and dissolved matter. The percentage contribution of CDM at 412 nm to total absorption at 412 was then calculated (Claustre et al., 2000):

$$\%CDM(412) = a_{CDM}/a_T(412) * 100$$

At some stations, absorption estimates by CDOM at 412 nm were available from the AC-9 filtered data, and the actual percentage contribution only by CDOM was calculated. In coastal areas, over 90% of the absorption was caused by detrital and dissolved matter. In stations close to the coast (22, 21 and 11) over 80% of this absorption was caused by CDOM alone.

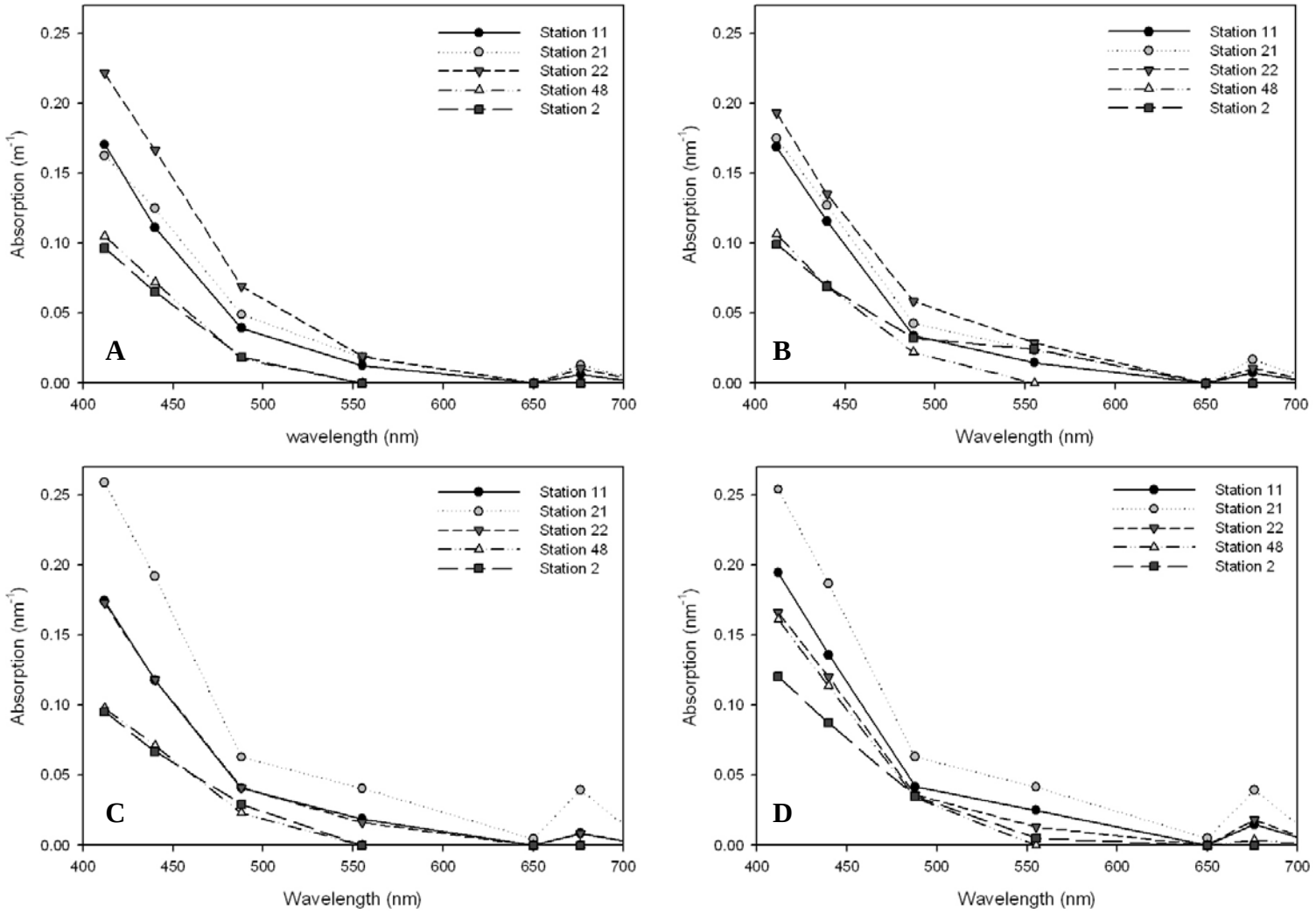

Figure 2.7: Total absorption measured during the September 2003 at (A) 1m (B) 5m (C) 10m (D) 25m

The contribution of CDOM decreased with distance from the coast. In stations away from the influence of rivers, $a_T(412)$ decreased by half (Figure 2.7, station 48 and 2), and absorption was likely dominated by CDOM and non-algal particles.

Figure 2.8 shows changes of light with depth, expressed as optical depth (OD) and derived from diffuse attenuation coefficient measurements (K_d) as follows:

$$\zeta = K_d z \qquad \text{(Kirk, 1994)}$$

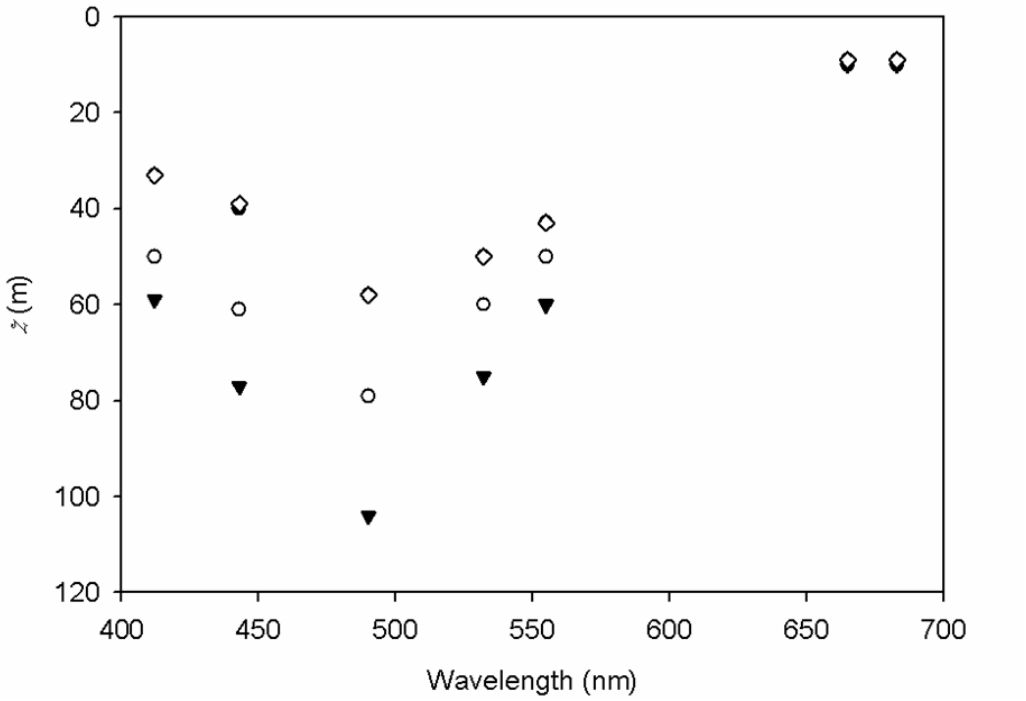

Figure 2.8: Optical depths at selected stations sampled during September 2003. Station 50 (●) Station 51 (○) Station 24 (▼) Station 14 (◊).

K_d can be used as an indicator of bio-optical state of natural waters (Baker and Smith, 1982; Farmer et al., 1993). Similar to absorption, the combined effects of dissolved and particulate matter affect K_d and optical depth. Of special interest is the OD where the downward irradiance of PAR (photosynthetically available radiation) is 1% of that just below the surface (Kirk, 1994). This depth corresponds to the bottom of the euphotic zone and is of importance for photosynthetic organisms. At this point in the water column ζ equals to 4.6 (Kirk, 1994); this depth will hereafter be referred to as $OD(z_{eu})$.

A difference in light penetration through the water column was observed in September 2003 between stations close to the coast and those farther away (Figure 2.8). Stations 50 and 14, roughly 10 km from the mouths of the Unare and Neverí rivers, respectively, reached the 1% light level at 412 nm around 30 m. Stations 51 and 24, further away from the coast, reached this point at 50 and 59 m, respectively. The

transparency window for all the stations was near the green, at 488 nm. The depths at which the 1% light level in the blue was reached far exceeded the real depth of each station, indicating that light penetrates the entire water column, despite the high concentrations of CDOM and detrital suspended matter.

Figure 2.9 shows SeaWiFS images processed for $a_g(440)$ and chlorophyll, from September 30, 2003 and March 2004. The images were processed using two different algorithms, discussed in Section 3.4. In the September 2003 images, a narrow rim of color is visible near the coast. This was most likely suspended and dissolved material ejected by the rivers into the basin.

Figure 2.10 is a cross-shelf profile of beam attenuation coefficient collected during September 2003 from station 13 (located near the mouth of the Unare River) to station 21 (see Figure 2.2A for reference). Higher attenuation (0.6 m^{-1}) was observed at ~15 m depth at station 13, as compared to station 21 (0.2 m^{-1}). At station 23, located approximately 10 Km from station 13, the attenuation was almost half of that measured at station 13 at 15 m depth (0.4 m^{-1}).

Figure 2.11A shows the distribution of the beam attenuation coefficient at the surface for September 2003. The plume from the Unare River caused high light attenuation (~ 1 m^{-1}) near its mouth (station 49), due to the suspended material carried along by the river. As distance increased from the river mouths, attenuation was reduced, suggesting that there were fewer suspended particles. Most particles associated with the rivers seem to have precipitated from surface waters within 10 km from their mouths.

3.3. Particle and sediment transport from the coast

In Figure 2.10, higher attenuation was observed near the bottom of stations 21 and 22 (~0.2-0.3 m^{-1}) compared to waters just above that (~0.15 m^{-1}). Figure 2.11B shows the distribution of beam attenuation coefficient near the bottom of each station in September 2003. Higher attenuation was observed throughout the Unare Platform, with higher values (~ 0.6 - 1 m^{-1}) near the bottom of stations 49 and 13. Figure 2.12 is a beam attenuation plot of the stations surrounding the Neverí River (see Figure 2.2 for reference). Higher beam attenuation (0.5-0.6 m^{-1}) was also visible at two stations near the bottom: station 12 and 14. The interpolation of beam attenuation values of Figure 2.11B suggests that the higher coefficients observed at station 12 were most likely caused by sediments coming from the Unare River and not the Neverí. The thickness of the bottom attenuation maximum varied. Near the Neverí River, the bottom nepheloid layer ranged from 6 to 15 m, while near the Unare it was <5m. Intermediate nepheloid layers were seen at stations 15 and 11 at depths of 35 and 45 m, respectively (Figure 2.12).

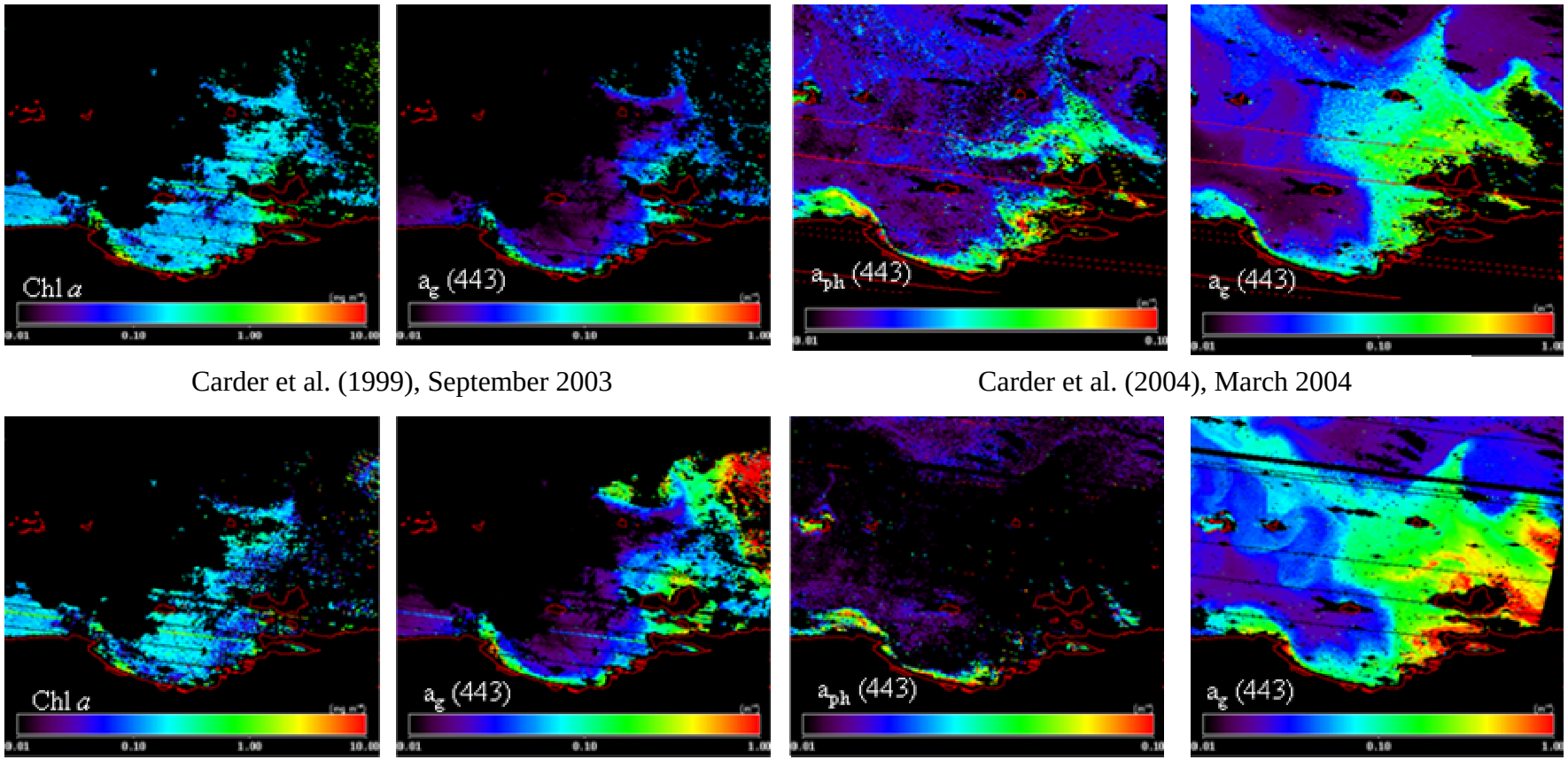

Carder et al. (1999), September 2003

Carder et al. (2004), March 2004

Lee et al. (1999), September 2003

Lee et al. (1999), March 2004

Figure 2.9: SeaWiFS images of CDOM absorption at 443 nm ($a_g(443)$), chlorophyll concentration (chl*a*) and a_{ph} (443), processed with Lee et al. (1999), Carder et al. (1999) and Carder et al. (2004) algorithms. Images are from September 30, 2003 and March 10, 2004

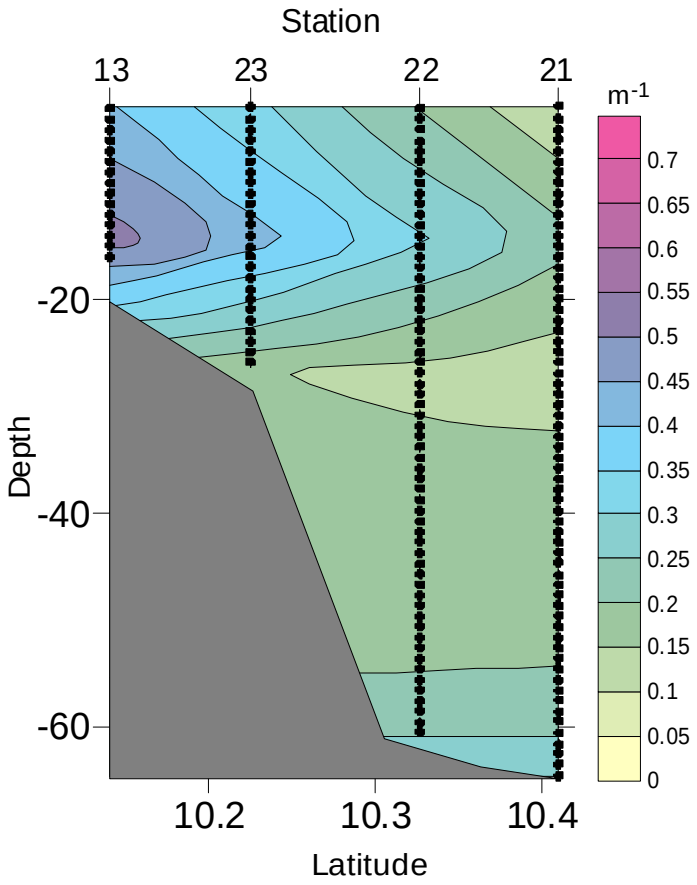

Figure 2.10**:** Beam attenuation (660nm) transect from station 13 to station 21 sampled during September 2003. Contour lines are interpolated between stations. Black lines indicate profile locations and depths.

Other stations sampled during September 2003 also exhibited attenuation maxima both near the bottom and at intermediate water column depths (stations 0, 1, 3 and 51).

The plume of the Manzanares River was less apparent than that of the Unare and Neverí Rivers. However, intermediate nepheloid layers (~0.09 m^{-1}) (INL) were observed in September 2003 near the Manzanares River at stations 48 and 2, located over a submarine canyon (Figure 2.13). These nepheloid layers were less pronounced than those observed near the southern coast at stations 15 and 11 (~0.2 m^{-1}). The peaks in beam attenuation corresponding to the INL did not show a corresponding variation in absorption.

The INL observed at 10°29’ N 64°21’ W was measured both in September 2003 (station 2, Figure 2.13A) and March 2004 (station 3, Figure 2.13B). During September 2003, this peak (located at ~220 m) was thicker (~ 50 m) than the one observed at a similar depth in March 2004 (~ 30 m). These layers were similar to those reported by Pak et al. (1980) for the West coast of South America. During March 2004, a shallower, thinner and more attenuating (~ 0.15 m^{-1}) layer was also seen around 100 m.

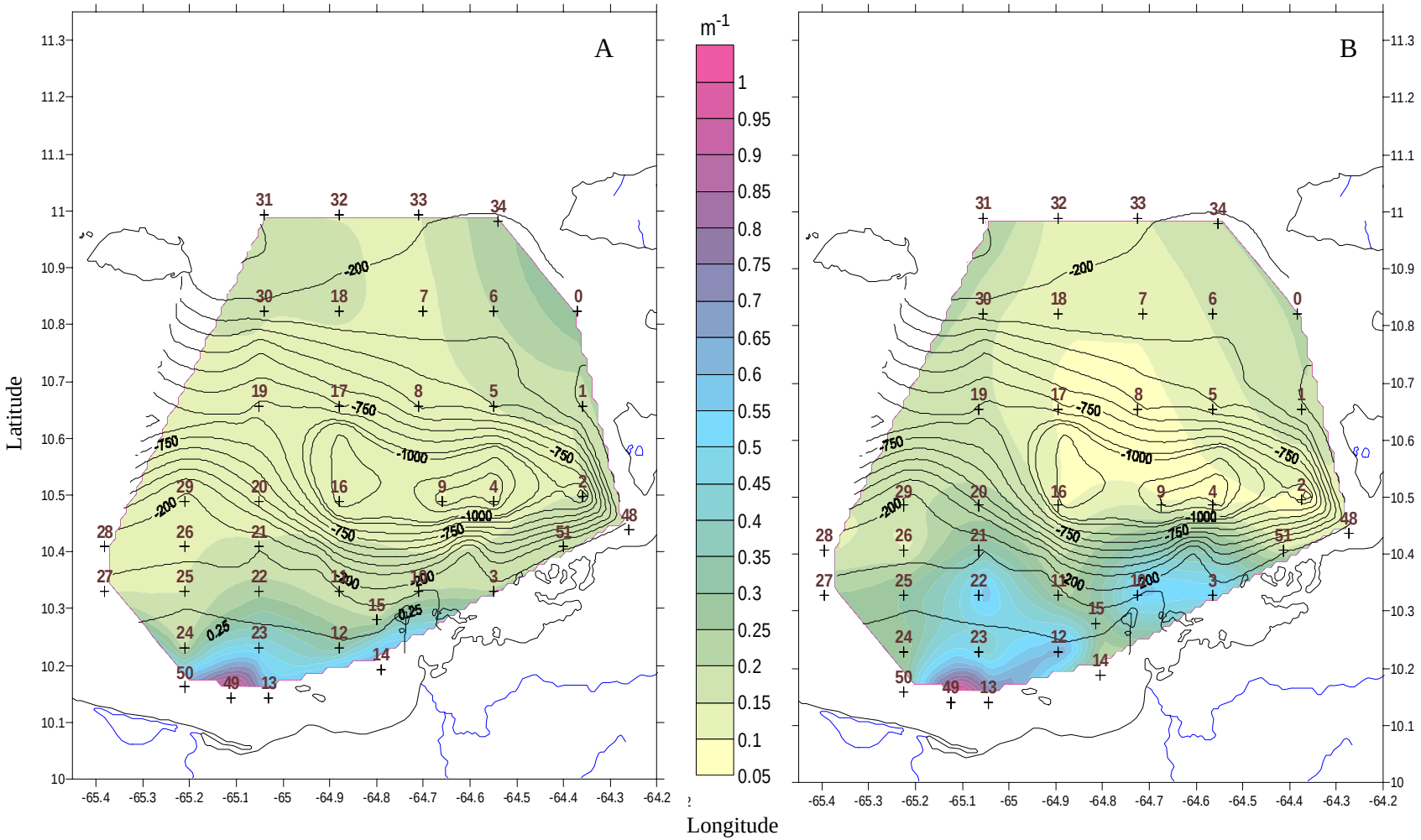

Figure 2.11: Horizontal distribution of the beam attenuation (660 nm) near the eastern coast of the Cariaco Basin during September 2003. At the surface (A) and at the maximum depth of each station (B).

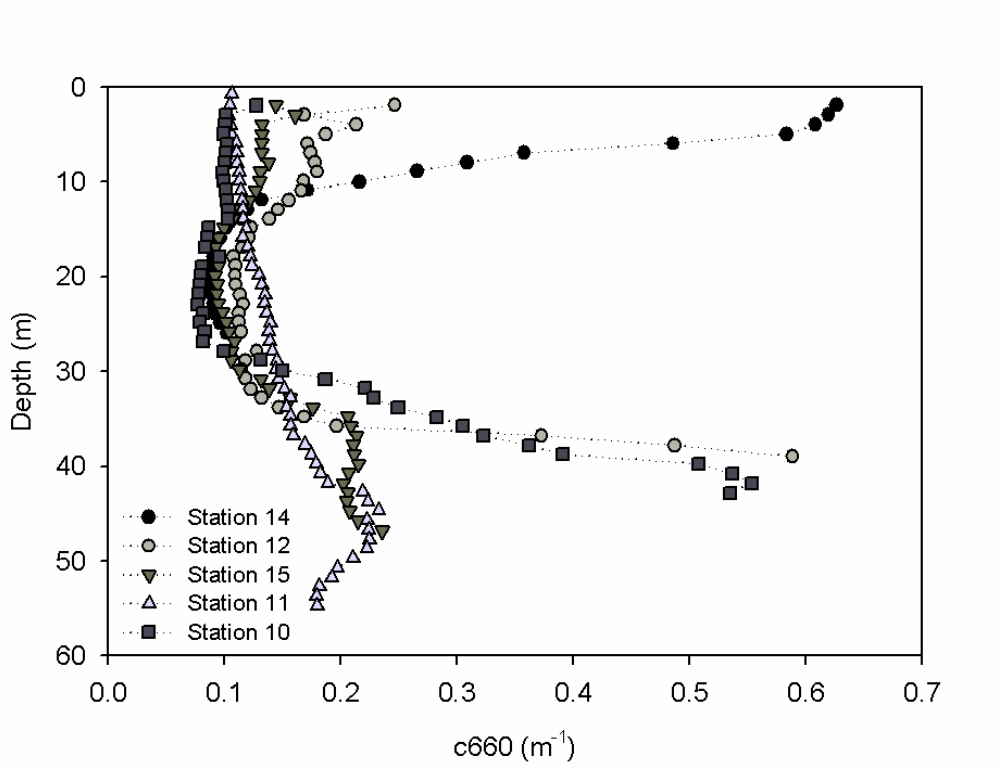

Figure 2.12: Beam attenuation (660nm) profiles near the Neverí River during September 2003. For station location refer to Figure 2.2A

The waters inside the basin during March 2004 were well mixed, due to the intense winds that blow in this region during the upwelling season, and this shallower nepheloid layer was not associated with any density structure. It was not linked to the deep chlorophyll maximum either, leaving its formation an open question.

For the nepheloid layer observed near 200 m at 10°29' N 64°21' W in September 2003, the spectral shape of the beam attenuation coefficient (γ) was calculated. γ can be linked to the particle size distribution (PSD) approximately through

$$\gamma = \xi - 3 \text{ (Diehl and Haardt, 1980)}$$

where ξ is the PSD exponent (Boss et al., 2001). As particles become larger, γ decreases according mainly to the size of the particles. γ at the nepheloid layer was smaller, indicating it was probably composed of larger particles, perhaps aggregates.

The range of attenuation coefficients observed in the water column of the Cariaco Basin in September 2003 and March 2004 varied between 0.1 and 0.22 m^{-1}. This included locations near the rivers and over the Eastern Deep, but excluded the intermediate nepheloid layers. Puig and Palanques (1998) observed attenuation between 0.5 and 0.9 m^{-1} in the Foix Canyon on the Barcelona continental margin. McPhee-Shaw et al. (in press) and Snyder and Carson (1986) observed a similar range over the California continental margin and the Quinault Canyon, respectively.

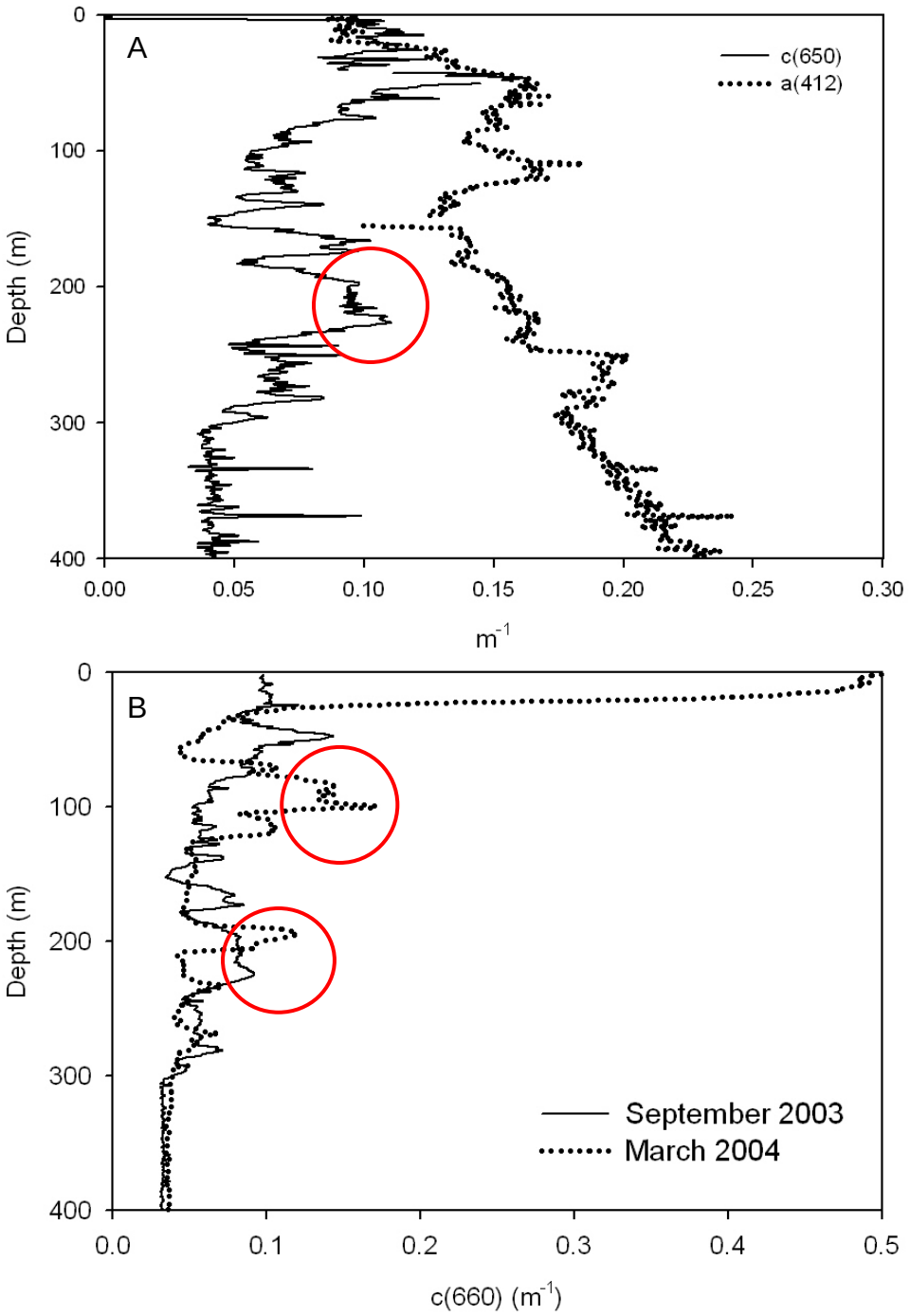

Figure 2.13: (A) Profile of total absorption at 412 nm (a412 – dotted line) and attenuation at 650 nm (c650-solid line) at station 2 (10°29' N 64°21' W) during September 2003 (B) Beam attenuation profiles at 660 nm (c660) at 10°29' N 64°21' W for September 2003 (dotted line) and March 2004 (solid line). Red circles indicate INL (Intermediate Nepheloid Layer) location (C) Total beam attenuation coefficient at 650 nm (c650, black) and beam attenuation spectral slope (γ - blue) at station 2 (10°29' N 64°21' W) during September 2003. Arrow indicates the location of the maximum phytoplankton biomass; red circle indicates location of the INL (Continued next page)

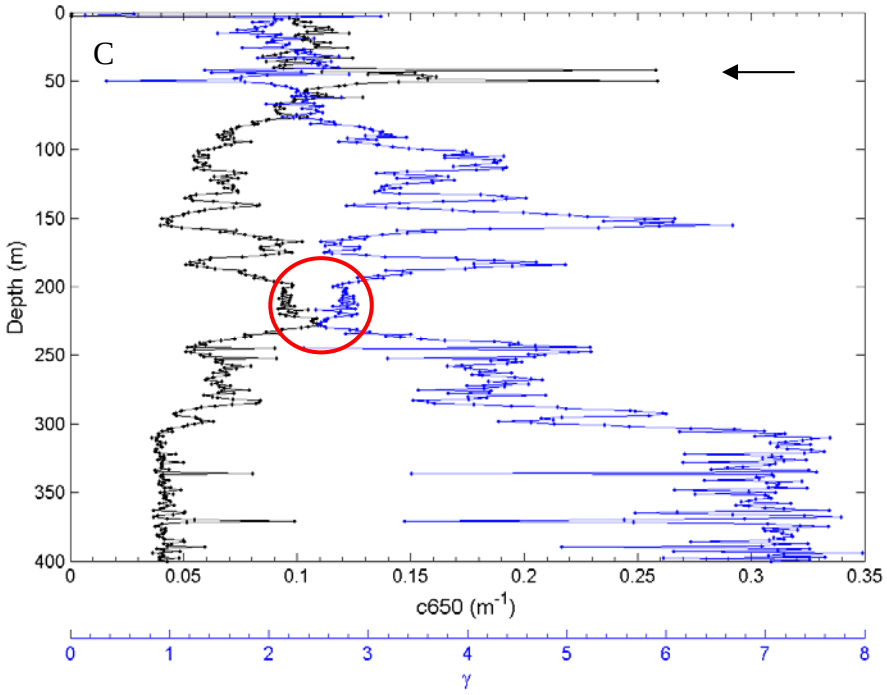

Figure 2.13 (Continued)

The low-end, or background values of beam attenuation measurements of the authors mentioned above, which would correspond to clear, particle-free waters, were close to 0.1 m^{-1} or above. The low-end in the Cariaco Basin was approximately 0.05 m^{-1}. Taking into account this offset between measurements, beam attenuation values observed in the Cariaco Basin were similar to those reported for other near shore regions.

3.4. Remote sensing reflectance of Cariaco waters

Figure 2.14 shows remote sensing reflectance (Rrs), at different stations during September 2003. Rrs(750) was used as an offset. The contribution of dissolved and suspended particulate material from local rivers to the Cariaco Basin lead to marked changes in the color of surface waters (Figure 2.3). Some coastal stations were dominated by reflectance in the green (e.g. stations 50 and 49). Rrs at 532 nm. at station 49 (0.0109 sr^{-1}) was somewhat higher than at station 50 (0.0101 sr^{-1}). At station 49, located in front of the Unare River mouth, surface (~1m) beam attenuation (~0.9 m^{-1}) was higher than at station 50 (~0.5 m^{-1}, see Figure 2.11), suggesting the concentration of suspended matter was higher. Rrs for station 14 was ~0.008 sr^{-1}, considerably lower than at stations 49 and 50. Figure 2.14 also shows low reflectance in the blue at stations near the coast. This was most likely due to the strong absorption by CDOM at these locations. Waters only a few (~30) kilometers farther offshore showed high Rrs in the blue.

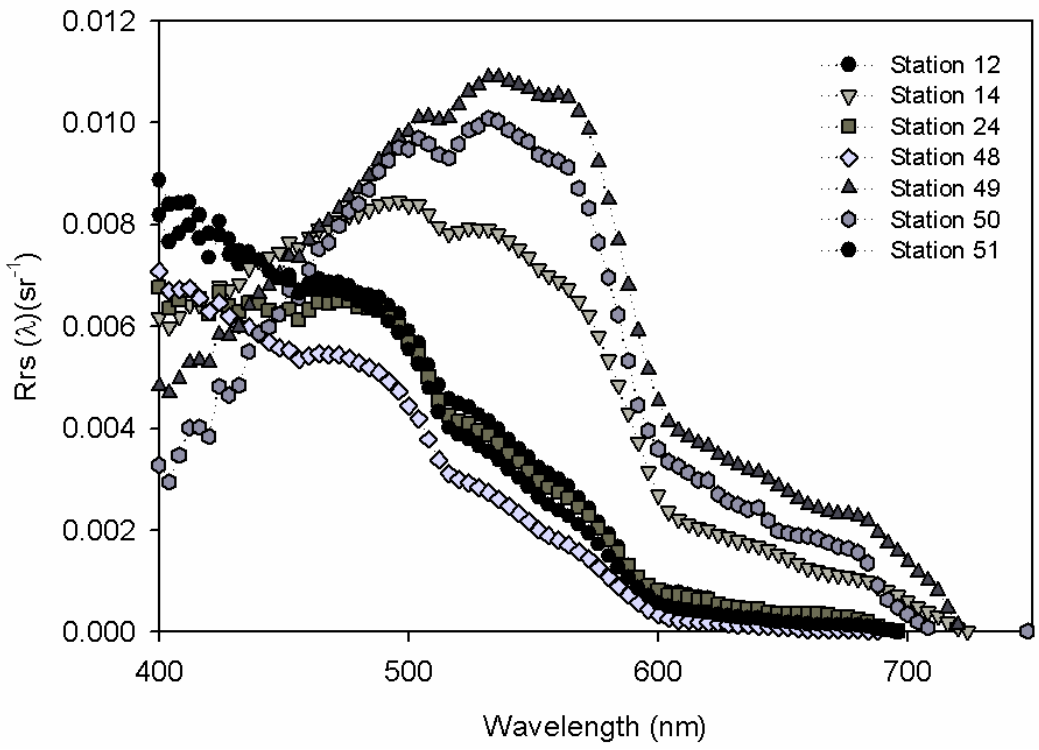

Figure 2.14: Remote sensing reflectance spectra measured in situ in September 2003

Lee's et al. (1999) bio-optical optimization model and the Carder et al. (1999) global bio-optical algorithm developed for MODIS were applied to Cariaco waters to test the retrieval of inherent optical properties (IOP's) from reflectance data. Their performances are later compared. To initially test the algorithms, Rrs and $a_{ph}(440)$ measurements from the CARIACO time-series project ($10^{o}30'$N, $64^{o}40'$W) were used. Due to the large dataset the CARIACO Project has gathered, only three years (2001, 2002 and 2003) of the CARIACO Project Rrs measurements were used for testing the model. At the CARIACO time-series station, Rrs measurements are collected monthly; a total of 34 Rrs spectra were analyzed. Each selected spectrum was carefully examined and those that were suspicious, based on the shape of the Rrs and sky reflectace curves, were discarded.

The Rrs data were compared with SeaWiFS images of the corresponding cruise day or closest available. The satellite images rarely matched the day of the in situ sampling, but the Rrs spectra measured with SeaWiFS for the available dates were always within 10% of the Rrs gathered *in situ*. a_{ph} was derived from *in situ* measurements, as described in the Data Processing section.

To obtain more accurate results using the Lee et al. (1999) model, empirical coefficients for $a_o(\lambda)$ and $a_1(\lambda)$ (Lee et al, 1998) were derived from the *in situ* data. Due to the high noise in some of the a_p and a_d measurements, averaged a_o and a_1 were used. Error to assess the models' effectiveness was calculated between the measured and the modeled data using:

$$\%Error = (a_{ph\_mo}-a_{ph\_mea})/a_{ph\_mea} *100$$

where a_{ph_mea} was the measured value of a_{ph} and a_{ph_mod} was the value obtained through the model.

Table 2.3 presents some of the results obtained using the CARIACO Project Rrs measurements. The Lee et al. (1999) model error estimated, based on the CARIACO Project data, ranged between 2 and 135%. The error was lowest when data from either the dry or the rainy season were used (Table 2.3). These months included January, February and March during the dry season, and July, August and September during the rainy season. The error obtained using the model was generally highest during "transition" months between the rainy and dry season, when there was low $a_{ph}(440)$ (e.g. 0.01 mg/m^3). a_{ph} was generally underestimated by the model during these "transition" months. The Carder et al. (1999) algorithm had less error variation between the selected dates (Table 2.3). Its errors ranged between 40 and 80%, with no clear reason for such variations. Chlorophyll was generally underestimated as well with Carder et al.'s algorithm. This systematic underestimation of aph (440) is consistent with Carder et al. (1999)

The Lee et al. (1999) and Carder et al. (1999) algorithms were then used for estimating $a_g(440)$ and chlorophyll *a* concentration directly from SeaWiFS images from September 30, 2003 and March 10, 2004 (Figure 2.9). Rrs measurements from the satellite were in good agreement (r^2 >0.9) with Rrs measured *in situ* during the September 2003 cruise. During March 2004 Rrs from SeaWiFS was one order of magnitude lower in the blue than Rrs in situ (~0.004 vs. 0.0004 sr^{-1} for stations in the upwelling plume). This problem arise most likely from errors in the atmospheric correction of SeaWiFS. When aerosols in the atmosphere are non-absorbing, atmospheric corrections using the NIR (near infrared) part of the spectrum work well, but when the aerosol absorption is not negligible in the near infrared, this technique fails (Chomko and Gordon, 2001). African dust is a strong absorber and is transported across the Atlantic year round. Though during the northern hemisphere summer months the amount of dust transported peaks, reaching altitudes of 5-7 km in the atmosphere and extending over large areas (from the Caribbean Sea and the south-east United States) (Carlson and Prospero, 1972), during the northern hemisphere winter there are also large quantities of dust carried out of North Africa and across the Atlantic, but its transport is primarily to South America (Prospero et. Al., 1981).

In September 2003, both algorithms performed very similarly (less than 10% difference from one another) for the estimation of both a_g and chlorophyll *a*. At locations away from the coast where both $a_g(440)$ and chlorophyll were low (< 0.1 m^{-1} and 0.01 mg/m^3), $a_g(440)$ and chlorophyll concentration were underestimated by more than 80% by the algorithms relative to the *in situ* validation observations (Table 2.4, stations 18 and 32). In stations located between the CDM-dominated waters and clear waters (stations 4, 20 and 21), both algorithms underestimated *in situ* CDOM observations by >50%. Chlorophyll was both under and overestimated, depending on location, by more than 80%. It is not clear what made the models under or overestimate chlorophyll concentrations in this region. In areas highly influenced by rivers (stations 11 and 13),

$a_g(440)$ was underestimated by up to 70%. The Lee et al. (1999) algorithm performed better in the estimation of chlorophyll than the Carder et al. (1999) algorithm, underestimating concentrations by less than 50% (Table 2.4).

In March 2004, in areas of high chlorophyll concentration (> 4 mg/m^3), neither the Lee et al. (1999) nor the Carder et al. (1999) algorithms were able to derive any values, mainly because the water leaving radiance in the blue was very low (~0.02 $Wm^{-2}sr^{-1}$). The Carder et al. (2004) expanded algorithm was used instead, which was able to provide values of chlorophyll and a_g for the upwelling plume.

Table 2.3: Error obtained using the Lee et al. (1999) and Carder et al. (1999) algorithms to estimate $a_{ph}(440)$ at the Cariaco time-series station

CARIACO project Month	% Lee et al. (1999) error	% Carder et al. (1999) error
Aug-01	102.492	44.891
Aug-02	109.502	60.717
Feb-03	62.179	48.185
Jan-03	23.838	65.377
Jul-00	14.608	70.744
Jul-01	135.000	57.807
Jul-02	21.607	71.058
Jul-03	-2.256	70.989
Jun-02	99.615	63.008
Jun-03	118.605	60.039
Mar-02	36.989	54.160
May-02	52.593	59.933
Oct-02	63.087	67.195

Table 2.4: Error obtained using the Lee et al. (1999) and Carder et al. (2004) algorithms to estimate chlorophyll concentration and $a_g(440)$ in waters of the Cariaco Basin during September 2003 and March 2004. Undet. refers to undetermined value

Cruise	Location			% Lee et al. (1999) error for a_g	% Lee et al. (1999) error for chl	% Carder et al. (1999) error for a_g	% Carder et al. (1999) error for chl
	Station	Latitude	Longitude				
COHRO	32	11.00	-64.88	90.95	>100	91.93	87.53
COHRO	11	10.33	-64.88	61.13	48.47	67.52	>100
COHRO	13	10.14	-65.03	17.05	19.51	20.24	>100
COHRO	20	10.49	-65.04	78.89	>100	82.26	82.20
COHRO	18	10.83	-64.88	80.79	40.83	83.53	66.85
COHRO	4	10.49	-64.55	59.61	28.38	66.00	68.71
COHRO	21	10.41	-65.04	81.07	>100	83.74	82.60
COHRO 2	14	10.48	-64.88	16.62	99.33	77.88	62.45
COHRO 2	21	10.93	-65.05	Undet.	Undet.	10.14	88.28
COHRO 2	22	11.05	-65.05	72.74	65.93	>100	25.23
COHRO 2	8	10.33	-64.55	>100	-98.99	29.53	29.53
COHRO 2	18	10.5	-65.05	>100	90.44	>100	24.06
COHRO 2	1	10.63	-64.36	Undet.	Undet.	>100	57.87

However, when chlorophyll concentrations are higher than ~1.5- 2.0 mg/m^3, when Rrs (412) is too low for the semianalytical retrievals, the algorithm defaults to an empirical expression, which uses a band ratio between Rrs(488) and Rrs(551), along with empirically derived constants, to provide chlorophyll concentrations. For high chlorophyll concentration areas, the Carder et al. (2004) algorithm underestimated chlorophyll concentrations by ~50-70%. This underestimation was caused by the problems with the atmospheric correction, which returned a lower than real Rrs. a_g was overestimated by more than 90%, in part caused by the same low water leaving radiance, and in part to the fact that absorption by detritus and CDOM are combined when retrieving them using inversion models. In areas where the in situ chlorophyll concentration was between 2 – 3 mg/m3, the Lee et al. (1999) algorithm calculated only $a_g(440)$, which was highly overestimated (> 100%). In those areas where chlorophyll concentrations and $a_g(440)$ were estimated by the Carder et al. (1999) algorithm (where chlorophyll concentrations were below 3 mg/m3 – refer to Figure 2.9), chlorophyll concentrations were underestimated by 30-90%. $a_g(440)$ was generally overestimated by >50% (Table 2.4)

4. Discussion

4.1. Colored dissolved organic matter (CDOM) distribution in the eastern Cariaco basin

The two main contributors of CDOM to the Cariaco Basin during September 2003 were the Neverí and Unare rivers. Riverine CDOM affected primarily a narrow (30-40 Km) rim of the basin along the coast. Away from the coast, CDOM concentrations in Cariaco were generally low (absorption coefficients at 412 nm of 0.03 m^{-1}). The range of S measured was similar to that reported by other authors, both for coastal and open waters (Bricaud et al., 1981; Nelson and Guarda, 1995; Carder et al., 1999; Cannizzaro, 2004). The changes in CDOM slope from the coastal area to the open basin were likely due to different sources of CDOM, and were indicative of the mixing between riverine and autochthonous material.

CDOM distribution has generally been studied in relation to light distribution and its effect on remote sensing, primary production and the carbon cycle. The presence of CDOM in surface waters of the Cariaco Basin changed significantly its color. Coastal stations affected directly by local rivers were dominated by a strong reflectance in the green, whereas waters farther offshore showed high Rrs in the blue. The contribution of CDOM to the Rrs signal will have an impact on the estimates of IOP's from satellite remote sensing data (see Section 4.4), especially in areas close to the coast.

The plume of the Manzanares River was less apparent than that of the Unare and Neverí Rivers. There appeared to be little CDOM injected to the Basin through the Manzanares River. To the north of the Basin, CDOM was low (~0.03 m^{-1}), indicating that the CDOM ejected by the Amazon and Orinoco does not influence the basin directly.

4.2 The distribution of particulate material in the eastern Cariaco basin

The Unare and Neverí rivers were the largest source of particulate matter to the Eastern Deep of the Cariaco Basin. Beam attenuation measurements suggest that the Unare River discharged more suspended particulate matter than the Neverí River. The distribution of detrital matter in the Cariaco Basin for September 2003 was similar to that of CDOM. Most particulate material was located close to the mouths of the rivers, decreasing with distance from the coast. Suspended particles associated with the river largely precipitated from surface waters within 10 km from the river mouths. Maximum beam attenuation coefficient was observed near the bottom and was associated with bottom nepheloid layers (Pak et al., 1984; Boss et al., 2001; Xu et al., 2002; McPhee-Shaw et al., in press). The Unare's bottom nepheloid layer was observable to at least 40 km from the mouth of the river, while the Neverí's was close to 23 km. This was a larger radius of influence than seen in the suspended and surface distribution of particulate matter.

Thunell et al. (2000), Goni et al. (2003) and Goñi et al. (2004) have reported terrigenous material in sediment traps located near the CARIACO times-series station. Local river water affected the salinity measured at the CARIACO time-series station. However, sediments discharged by the local rivers in September 2003 did not affect the optical properties of the waters at the time-series station. The material observed in the traps is probably derived from local rivers, but is likely transported at intermediate levels in layers moving off the bottom of the continental margin. More intensive sampling is necessary to reach a better understanding of sediment transport and distribution within the basin. Although the Unare and Neverí are likely the largest sources of terrigenous material to the Basin, contributions from the Manzanares and Tuy Rivers may also be important. The Tuy River affects mostly the western Cariaco Basin. Its drainage basin occupies an area of 6.6 km^2 and has an approximate discharge of 82 m^3/sec. (Zink, 1977). The Tuy River is larger than the Unare, and its plume has been observed flowing toward the center of the Western basin (Figure 2.15). Sediment cores analyzed by Hughen et al. (1996) were recovered from the 900m deep saddle, located between the Eastern and Western Deep. Given the distance from the southern coast to the saddle, and current observations of the Unare and Neverí River plumes, it seems unlikely that terrigeous material from the southern coast would be carried this far into the basin. The sediment observed by Hughen et al. (1996) could have been transported by the Tuy's river plume.

Nepheloid layers present at intermediate depths (150-300 m) could constitute an important pathway of coastal sediment transport to the central Cariaco Basin. Several stations sampled around the Eastern Deep exhibited turbid layers at intermediate depths. Of particular importance was a layer observed at 10^o29' N 64^o21' W over a submarine canyon. Hickey et al. (1986) determined that the dominant mode of sediment transport off the shelf in Quinault Canyon was by episodic formation of turbidity layers at intermediate depths caused by horizontal advection. Puig et al. (2003) also observed such a persistent layer, which contributed to the off-shelf sediment transport in Eel Canyon. Puig and Palanques (1998) suggested that in canyons located on continental margins, such as the Foix Canyon, sediment transport could be dominated by intermediate nepheloid layer detachments and internal waves.

The intermediate nepheloid layer observed at 10^o29' N 64^o21' W in Cariaco did not seem to be associated with any temperature or salinity feature. It is unlikely that it formed from only vertical particulate flux, and indeed waters above and below the layer were relatively devoid of suspended particles. The ~220 m turbidity layer could have been an offshore extension of a shelf-break intermediate nepheloid layer, and could constitute an important means of terrigenous sediment transport into the deeper portions of the Eastern Cariaco Basin. During glacial times, enhanced terrigenous input to the Cariaco Basin may have occurred (Peterson et al., 2000). The sources were probably local rivers and aeolian dust (Yarincik et al., 2000). Part of this enhanced sediment input could also be responsible for the large extension of the Unare platform. During glacial times the sea level would have been approximately 121 m lower (Fairbanks, 1989), exposing the Unare platform (Figure 2.16). The Unare and Neverí Rivers would have had a more direct drainage into the basin, and sediment transport through the submarine canyon near the Manzanares River would have been enhanced, driven by gravity mechanisms such as turbidity currents and debris flows.

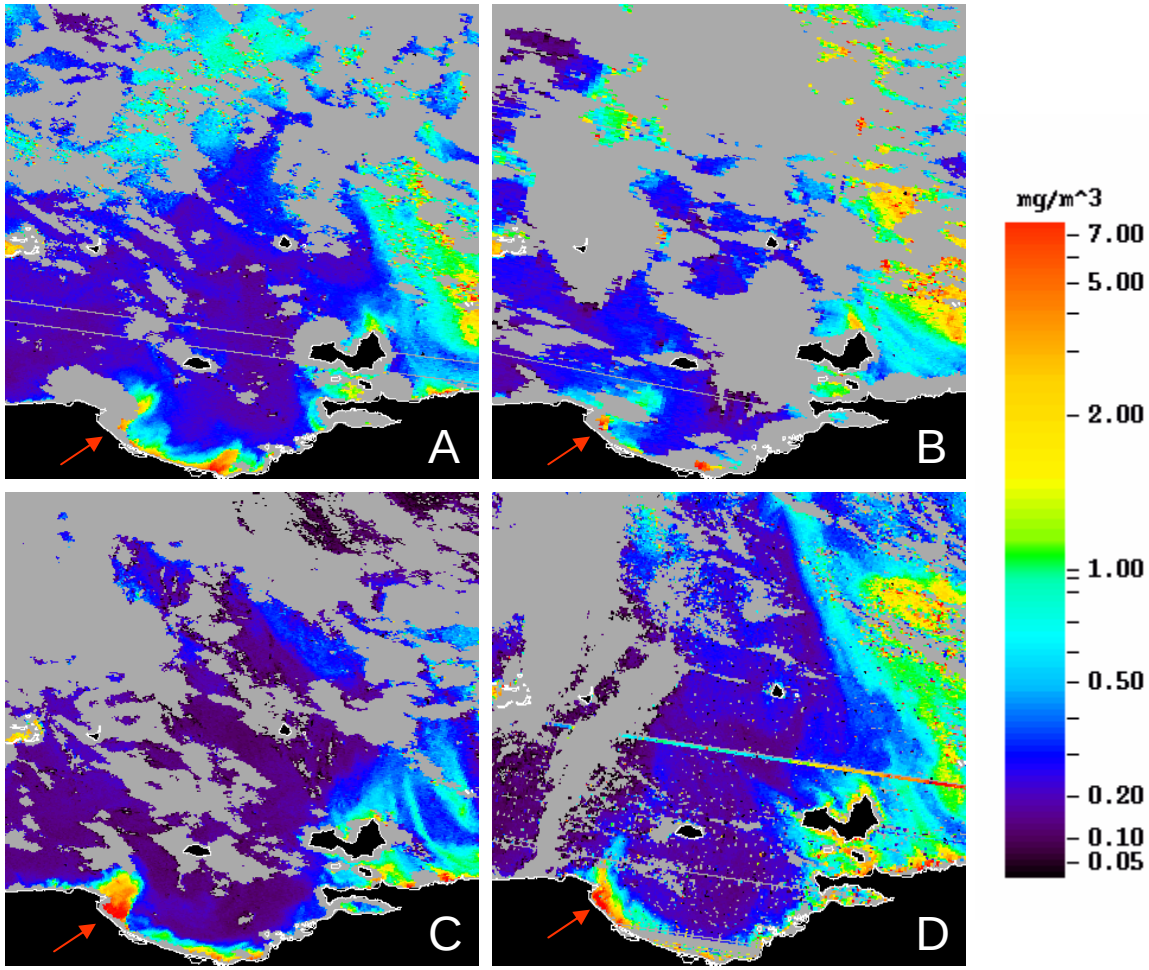

Figure 2.15: SeaWiFS images of chlorophyll *a* for the eastern coast of Venezuela (A) September 25, 2000 (B) September 26, 2000 (C) October 25, 2001 (D) October 24, 2003. The approximate location of the Tuy River is indicated by the red arrow

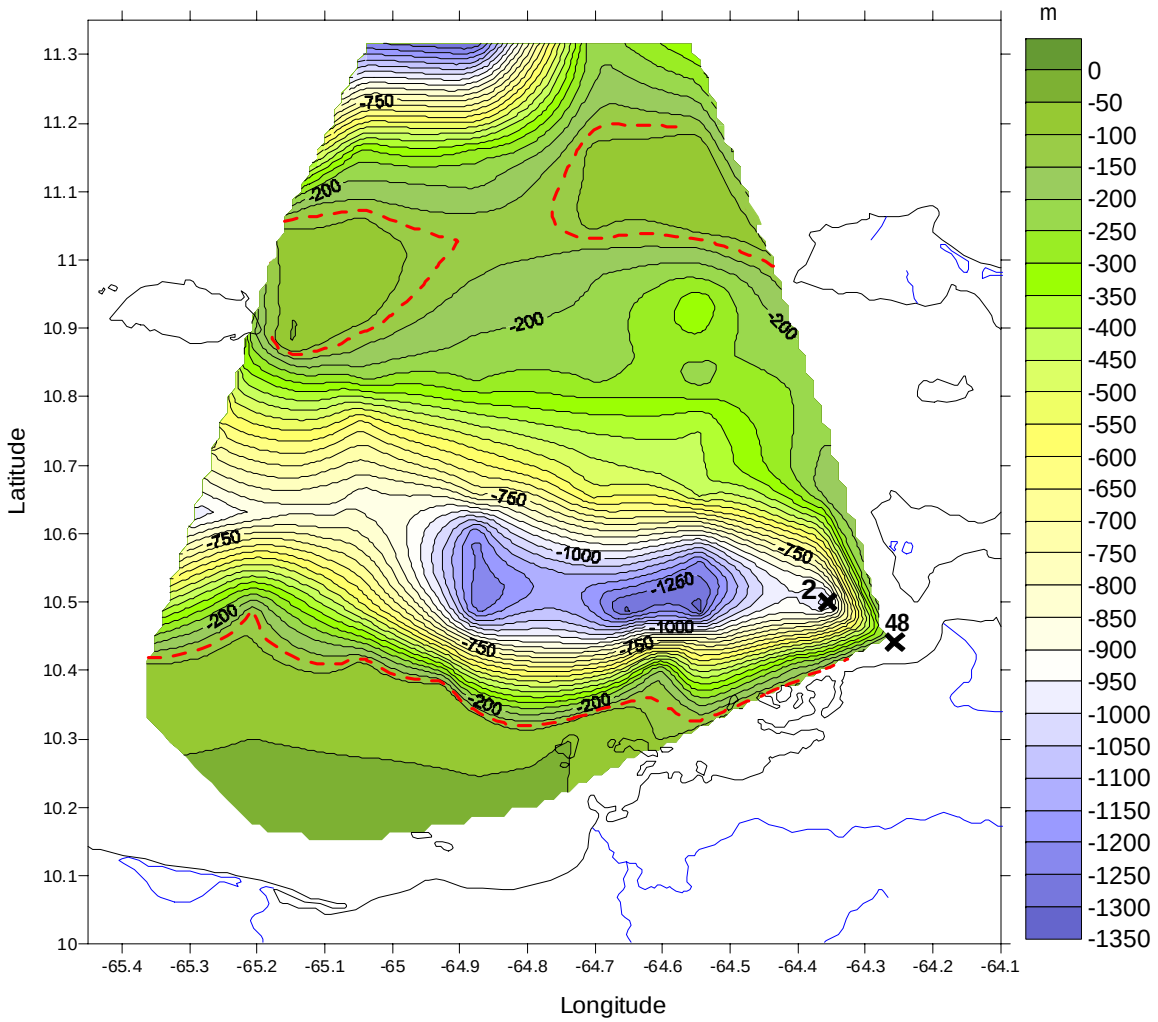

Figure 2.16: Bathymetry of the Cariaco Basin. The red segmented line marks approximate sea level during the Last Glacial Maximum (Fairbanks, 1989)

4.3. Remote sensing of CDOM and chlorophyll in the Cariaco Basin

It is a challenge to retrieve inherent optical properties using remote sensing data in coastal areas, and particularly it is difficult to properly differentiate between chlorophyll and CDOM absorption (Carder et al. 1989). In South America, an extra setback comes from Saharan Dust, which is transported year round from the Africa coast and across the Atlantic, and which affects aerosol composition in the atmosphere. Two algorithms were used in the Cariaco Basin to test retrieval of chlorophyll *a* and a_g from satellite remote sensing measurements during this study. Specifically, the Lee at al. (1999) and Carder et al. (1999) algorithms were used. Errors in the algorithms varied with season. In September 2003, both algorithms performed very similarly (<10% difference between them). Both algorithms were off by at least 50% in estimates of chlorophyll and CDOM absorption. In March 2004, the water leaving radiance measured by SeaWiFS, especially in the blue part of the visible spectrum, was very low. This was caused by the combined effects of high phytoplankton absorption and errors in the atmospheric correction, most likely due to a high concentration of Saharan Dust in the atmosphere. This lower-than-real water leaving radiance was the main culprit of erroneous estimations in both chlorophyll and a_g during March 2004. In areas of high chlorophyll concentration (>4 mg/m^3), neither algorithm was able to derive values. In areas of intermediate chlorophyll concentration (between 2 – 3 mg/m^3), the algorithm of Lee et al. (1999) attributed most of the low remote sensing reflectance to CDOM, while they were largely due to high concentrations of chlorophyll (C. Hu, pers. comm.). The Carder et al. (1999) algorithm provided an estimate of chlorophyll and $a_g(440)$ only in areas where the chlorophyll *a* concentration was below 3 mg/m^3.Chlorophyll and $a_g(440)$ were underestimated by 30-90% and overestimated by more than 50%, respectively.

In order to improve the algorithm performances for this region, it will be necessary to improve atmospheric corrections, especially taking into account the influence of absorbing aerosols, such as Saharan Dust. It will be necessary also to adjust certain parameters, such as S, the $a_g(440)$ slope, to match local values. Changes will most likely also have to be done taking into consideration the season, and it is possible one single algorithm may not suffice (Gilbes et al., in preparation). Unfortunately, there is still no single algorithm that can successfully estimate chlorophyll and CDOM concentrations in coastal areas.

One possibility, for chlorophyll retrieval in future applications, can be to use the chlorophyll fluorescence product available from sensors like MODIS (Moderate Resolution Imaging Spectroradiometer) or MERIS. MODIS bands 13, 14 and 15 (662 – 672 nm., 673 – 683 nm. and 743 – 753 nm.) provide a measure of solar-stimulated fluorescence. MODIS has been actively taking measurements since 1999 and 2002 on board of the Terra and Aqua satellites, respectively, and data processing and validation has improved significantly over the past 3 years. Figure 2.17 shows the relationship between fluorescence determined with MODIS (image from March 16, 2004) and chlorophyll, measured during March 2004, for 26 stations. The linear relationship (r^2 = 0.6266) between variables is encouraging, but further validation has to be done in order to determine the accuracy and viability of chlorophyll derivation from remote sensing images using this method.

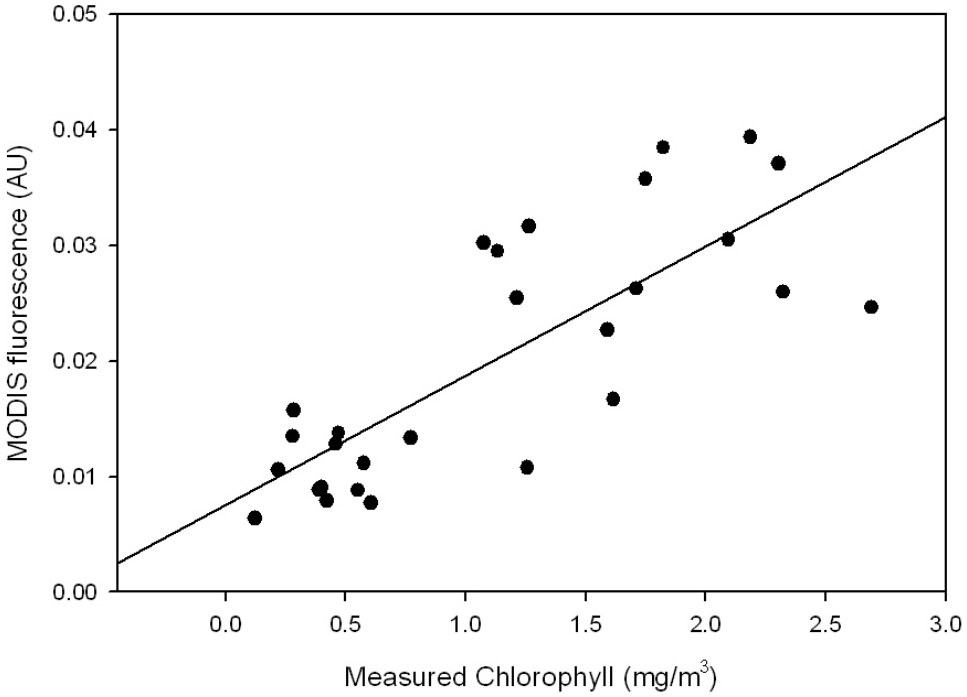

Figure 2.17: Relationship between chlorophyll measured *in situ* during March 2004 at 26 stations, and MODIS chlorophyll fluorescence for corresponding locations (image from March 16, 2004)

5. Conclusions

The two main contributors of CDOM and terrigenous particles to the Cariaco Basin were the Neverí and Unare rivers. Their influence was most pronounced along a narrow (30-40 km) band along the southern coast of the Cariaco Basin. There was only a weak relationship between CDOM and salinity when all stations were considered, but correlation improved near the mouths of rivers.The slope of a_g varied from high values (0.025 nm^{-1}) in areas depleted of CDOM away from the coast, to low values (0.011 nm^{-1}) in areas influenced by rivers. The changes observed in S were likely due to different sources of CDOM. The range of S observed in Cariaco in September 2003 and March 2004 was similar to that reported by other authors, both for coastal and open waters (Bricaud et al., 1981; Nelson and Guarda, 1995; Carder et al., 1999; Cannizzaro, 2004).

Near the coast, over 90% of the light absorption was caused by detrital and dissolved matter, particularly during September 2003. In some stations, over 80% of absorption was caused by CDOM. As distance from the coast increased, CDM absorption decreased rapidly. The contribution of suspended and particulate material from local rivers to the Cariaco Basin also lead to changes in the color of surface waters. Some coastal stations were dominated by a reflectance in the green; waters 30 Km farther offshore showed high Rrs in the blue.

The Unare River discharged into the Cariaco Basin more suspended particulate matter than the Neverí River, as seen through optical measurements. Light attenuation was higher adjacent to the rivers, as compared to offshore waters in September 2003. At 15 m, beam attenuation 20 km away from the Unare's mouth was almost half (0.4 m^{-1}), as compared to beam attenuation 10 km from the river's mouth (0.6 m^{-1}), indicating that a considerable portion of the suspended material that caused light attenuation precipitated within that distance. Bottom nepheloid layers, visible throughout the Unare Platform, were strongest near the point of discharge. The radius of influence of the Unare's bottom nepheloid layer was approximately 40 km from the mouth of the river, while the Neverí's was close to 23 km. The Manzanares River did not show any visible suspended matter or high concentrations of CDOM in surface waters. However, internal nepheloid layers (INL) were observed near the Manzanares River, over a submarine canyon, both in September 2003 and March 2004. This may be an important mechanism of sediment transport off the shelves and into the Eastern Deep.

Local rivers are the probable source of the terrigenous material to the Eastern Deep. Though the Unare and Neverí were the most obvious sources of terrigenous material in September 2003, contributions from the Tuy River should not be ignored.

Lee et al. (1999) and Carder et al. (1999) algorithms were used for estimating a_g and chlorophyll *a* concentration from SeaWiFS images from September 2003 and March 2004. Rrs measurements from the satellite were in good agreement (r^2 >0.9) with Rrs measured *in situ* during the September 2003 cruise. During March 2004, water leaving radiances measured from the satellite were lower than real *in situ* measurements, especially in the blue part of the visible spectrum. This was most likely due to the

combined effect of high absorption by chlorophyll in the blue part of the spectrum and a problem in the atmospheric correction, caused by absorbing aerosols in the atmosphere, such as Saharan Dust. In September 2003, both algorithms performed similarly. $a_g(440)$ and chlorophyll concentration were generally underestimated by at least 50%. In March 2004, neither algorithm was able to derive $a_g(440)$ or chlorophyll concentration values in highly (> 4 mg/m^3) productive areas. In areas where chlorophyll concentrations and $a_g(440)$ were calculated, using the Carder et al. (1999) algorithm (chlorophyll *a* concentrations of less than 3 mg/m^3), they were usually underestimated by 30-90% and overestimated by more than 50%, respectively. Most of the problems retrieving chlorophyll and a_g values during March can be attributed to the low water leaving radiance, and hence Rrs.

GENERAL CONCLUSIONS

The temporal variability of physical and biogeochemical oceanographic parameters of the Cariaco Basin, located along the southern margin of the Caribbean Sea, was studied using data collected during two cruises to the eastern half of the Basin in September 2003 and March 2004. Water exchange between the Cariaco basin and the Caribbean Sea was restricted to the upper ~150 m. In March 2004, water from outside the Cariaco basin was observed entering the basin and upwelling near the coast. This water brought nutrients and DOC into the basin. A marked seasonal difference in both surface temperature and salinity distribution was found between September 2003 and March 2004. During September 2003, surface temperatures in the basin ranged from ~26 to ~28 ^{o}C, and salinity from 36.4 to ~36.8. There was a difference in temperature and salinity between the Cariaco Basin and the open Caribbean in waters below 200 m. Inside the basin temperatures and salinities, averaged between 200 and 400 m, were higher by ~4^{o}C and by ~0.5, respectively. Deep (1200m) water temperature agreed with the predictions of Scranton et al. (1987). Salinity below 1200 m was higher than predicted by Scranton et al. (1987), indicating an input of saltier water to the deep basin.

The influence of local rivers on the basin, as contributors of less saline water and dissolved and detrital matter, was seen in September 2003 near the coast. No major intrusion of low salinity waters was observed from the north during either the rainy or dry season, indicating that the Amazon and Orinoco rivers do not have major direct influence on the Cariaco Basin. The two main contributors of CDOM and freshwater to the Cariaco Basin were the Neverí and Unare rivers, located on the southern coast of the Cariaco Basin. The suspended and dissolved colored matter brought by the rivers affected the optical properties of the water, but were confined to the southern margin of the basin. Near the coast, over 90% of the absorption was caused by detrital and dissolved matter, as measured during September 2003. The low salinity plumes were dispersed towards the NE, reaching the CARIACO time-series station (10^{o}30' N, 64^{o}40'W). Local rivers are responsible for the seasonal salinity variation observed in surface waters at the CARIACO time-series station. Local rivers are the probable source of the terrigenous material to the Eastern Deep. Though the Unare and Neverí were the most obvious sources of terrigenous material, contributions from the Tuy and the Manzanares River should not be ignored.

There is a deep CDOM pool below the oxic-anoxic interface (~200 m) inside the Cariaco Basin. Below 300 m, most, if not all, of the absorption measured in September 2003 and March 2004 was caused by CDOM. This supports the idea that CDOM accumulates below the interface due to the lack of mixing. The presence of light-absorbing particles was also noted at the oxic-anoxic interface, most likely bacteria and viruses.

REFERENCES

Alvarez-Salgado, X.A., M.D. Doval and F.F. Pérez. 1999. Dissolved organic matter in shelf waters off the Ría de Vigo (NW Iberian upwelling system). J. of Mar. Chem., 18: 383-394.

Astor, Y., F. Muller-Karger and M. Scranton. 2001. Seasonal and Interannual Variation in the Hydrography of the Cariaco Basin: Implications for Basin Ventilation. Cont. Shelf Res. 23:1, 125-144

Astor, Y., J. Meri, F. Muller Karger. 1998. Variabilidad estacional hidrográfica en la Fosa de Cariaco. Memoria de la Sociedad de Ciencias Naturales La Salle, 63 (149): 61-72.

Baker, K. and R. C. Smith. 1982. Bio-optical classification and model of natural waters. Limnol. Oceanogr., 27: 500- 509.

Bidigare, R. R., M. E. Ondrusek, and J. M. Brooks. 1993. Influence of Orinoco River outflow on distributions of algal pigments in the Caribbean Sea, J. Geophys. Res., 98, 2259–2269.

Black, D. E.; L. C. Peterson; J. T. Overpeck; A. Kaplan; M. N. Evans and M. Kashgarian. 1999. Eight centuries of North Atlantic ocean-atmosphere variability. Science, 286, 1709-1713.

Blough, N.V. and R. Del Vecchio.2002. Chromophoric DOM in the Coastal Environment. In: Biogeochemistry of Marine Dissolved Organic Matter. D.A. Hansell and C.A. Carlson eds. Academic Press. 774 p.

Blough, N.V., O.C. Zafiriou, and J. Bonilla 1993. Optical Absorption Spectra of Waters From the Orinoco River Outflow: Terrestrial Input of Colored Organic Matter to the Caribbean. J. Geophys. Res. 98: 2271-2278

Boss E. and J. R. V. Zaneveld, 2003. The effect of bottom substrate on inherent optical properties; evidence of biogeochemical processes. Limnol. Oceanogr., 48, 346-354.

Boss E., M. S. Twardowski and S. Herring, 2001. The shape of the particulate beam attenuation spectrum and its relation to the size distribution of oceanic particles. Applied Optics,40, 4885-4893.

Boss, E., S.W. Pegau, R. Zaneveld, and A. H. Barnard. 2001. Spatial and temporal variability of absorption by dissolved material at a continental shelf. J. Geophys. Res. 106: 9499-9507

Boss, E., W. S. Pegau,W. D. Gardner, J. R. V. Zaneveld, A. H. Barnard., M. S. Twardowski, G. C. Chang and T. D. Dickey, 2001. The spectral particulate attenuation and particle size distribution in the bottom boundary layer of a continental shelf. J. Geophys. Res., 9509-9516.

Bricaud, A., A. Morel, and L. Prieur 1981. Absorption by Dissolved Organic Matter of the Sea (Yellow Substance) in the UV and Visible Domains. Limnol. Oceanogr. 26(1): 43-53.

Bricaud, A., C. Roesler, J. Ishizaka, and J. Parslow. 2002. Bio-optical studies during the JGOFS-Equatorial Pacific program: A contribution to the knowledge of the Equatorial system. Deep Sea Res. 49: 2583-2599.

Cannizzaro, J. P. 2004. Detection and Quantification of *Karenia brevis* Blooms on the West Florida Shelf from Remotely Sensed Ocean Color Imagery. Master Thesis, University of South Florida, Florida, USA.

Carder, K. L.; R.F. Chen; J. P. Cannizzaro; J. W. Campbell and B. G. Mitchell. 2004. Performance of the MODIS semi-analytical ocean color algorithm for chlorophyll-*a*. Adv. in Space Res. 33: 1152-1159.

Carder, K.; F.R. Chen; Z. P. Lee; S. K. Hawes and D. Kamykowski. 1999. Semianalytic Moderate-Resolution Imaging Spectrometer algorithms for chlorophyll *a* and absorption with

bio-optical domains based on nitrate-depletion temperatures. J. of Geophys. Res., 104 (C3): 5403-5421.
Carder, K.L., R.G. Steward, G.R. Harve and R.B. Ortner. 1989. Marine humic and fulvic acids: their effects on remote sensing of ocean chlorophyll. Limnol. Oceanogr. 34, 68-81.
Carlson, T. N. and J. M. Prospero. 1972. The Large-Scale Movement of Saharan Air Outbreaks over the Northern Equatorial Atlantic. J. appl. Met. 11: 283–297.
Cauwet, G. 2002. DOM in the Coastal Zone. In: Biogeochemistry of Marine Dissolved Organic Matter. D.A. Hansell and C.A. Carlson eds. Academic Press. 774 p.
Chang, G.; T. D. Dickey; C. D. Mobley, E. Boss and W. S. Pegau. 2003. Toward closure of upwelling radiance in coastal waters. Applied Optics, 42(9): 1574-1582.
Chen, R. F., B. Fry, C. S. Hopkinson, D. J. Repeta, E. T. Peltzer. 1996. Dissolved organic carbon on Georges Bank. Cont. Shelf Res., 16: 409-420.
Chen, R.F., and J.L. Bada. 1992. The fluorescence of dissolved organic matter in seawater. Mar. Chem. 37, 191–221.
Chomko, R.M. and H. R. Gordon. 2001. Atmospheric correction of ocean color imagery: test of the spectral optimization algorithm with the Sea-viewing Wide Field-of-View Sensor. Appl. Optics, 40 (18): 2973-2984.
Claustre, H.; F. Fell; K. Oubelkheir; L. Prieur; A. Sciandra; B. Gentili and M. Babin. 2000. Continuous monitoring of surface optical properties across a geostrophic front: Biogeochemical inferences. Limnol. Oceanogr., 45(2): 309–321.
Coble, P. G., C. E. Del Castillo, and B. Avril. 1998. Distribution of DOM in the Arabian Sea During the SW Monsoon. Deep Sea Research II 45, 2195-2223
Coble, P.G. 1996. Characterization of marine and terrestrial DOM in seawater using excitation-emission matrix spectroscopy. Mar. Chem. 51(4): 325-346.
Curran, K. J., P. S. Hill, and T. G. Milligan. 2003. Time variation of floc properties in a settling column. J. of Sea Res., 49: 1-9.
Del Castillo, C. 1998. Optical characteristics of the colored dissolved organic matter in the Easter Caribbean, West Florida Shelf and the Arabian Sea: relationship between chemical characteristics and optical response. Ph.D. thesis, University of South Florida. 131p.
Del Castillo, C.E., Coble P.G., Morel J.M., Lopez J.M., and Corredor J.E. 1999. Analysis of the optical properties of the Orinoco River Plume by absorption and fluorescence spectroscopy. Mar. Chem. 66: 35-51.
Del Vecchio, R. and N.V. Blough. 2002. Chromophoric DOM in the Coastal Environment. In: Biogeochemistry of Marine Dissolved Organic Matter. D.A. Hansell and C.A. Carlson eds. Academic Press. 774 p.
Deuser, W. G. 1973. Cariaco Trench: Oxidation of organic matter and residence time of anoxic water. Nature, 242, 601-603.
Diehl, P. and H. Haardt. 1980. Measurement of the spectral attenuation to support biological research in a 'plankton tube' experiment. Oceanol. Acta 3, 89–96.
Fairbanks, R.G. 1989. A 17,000 year glacio-eustatic sea level record: Influence of glacial melting rates on the Younger Dryas event and deep-ocean circulation. Nature 342, 637-642.
Farmer, C.T.; C.A. Moore; R.G. Zika and R.J. Sikorski. 1993. Effects of low and high Orinoco River Flow on the Underwater Light Field of the Eastern Caribbean Basin. J. Geophys. Res., 98 (C2): 2279-2288.
Ferrari, G.M. 2000. The relationship between chromophoric dissolved organic matter and dissolved organic carbon in the European Atlantic coastal area and in the West Mediterranean Sea (Gulf of Lions). Mar. Chem. 70: 339-357.
Ferrari, G.M., M.D. Dowell, S. Grossi, and C. Targa. 1996. Relationship between the optical properties of chromophoric dissolved organic matter and total concentration of dissolved organic carbon in the southern Baltic Sea Region. Mar. Chem. 55: 299-316

Froelich Jr., P. N. and D. K. Atwood, 1978. Dissolved silicate and salinity structure of the upper waters of the Venezuela Basin, Caribbean Sea, In: Progress in Marine Research in the Caribbean and Adjacent Regions (ed. H. B. Stewart, Jr.), 1976. FAO Fisheries Report No. 200 Supplement, p. 299-314.

Froelich Jr., P. N., D. K. Atwood and G. S. Giese. 1978. Influence of Amazon River discharge on surface salinity and dissolved silicate concentration in the Caribbean Sea. Deep Sea Res., 25:735-744.

Goñi, M.A.; E. Tappa; H. Aceves; B. Benitez-Nelson; F. Muller-Karger; L. Lorenzoni; M. McIntyre; Y. Astor, R. Varela and R. Thunell. 2004. Seasonal to Climate-Scale Variability in the Vertical Flux of Terrigenous Organic Matter in the Cariaco Basin. Presented at the 2004 AGU meeting, San Francisco.

Goñi, M.A.; H. L. Aceves; R. C. Thunell; E. Tappa; Y. Astor; R. Varela and F. Muller-Karger. 2003. Biogenic fluxes in the Cariaco Basin: A combined study of sinking particulates and underlying sediments. Deep-Sea Res. I 50: 781-807.

Gordon, A.L. 1967. Circulation of the Caribbean Sea. J. of Geophys. Res., 72, 6207-6223.

Green, R. E.; H. M. Sosik and R. J. Olson, 2003. Contributions of phytoplankton and other particles to inherent optical properties in New England continental shelf waters. Limnol. Oceanogr., 48 (6), 2377-2391.

Green, S.A. and Blough, N.V., 1994. Optical absorption and fluorescence properties of chromophoric dissolved organic matter in natural waters. Limnol. Oceanogr. 38, 1903–1916.

Halliwell, Jr., G.R., R. H. Weisberg, and D.A. Mayer, 2003. A synthetic float analysis of upper-limb meridional overturning circulation interior ocean pathways in the tropical/subtropical Atlantic. Interhemispheric Water Exchange in the Atlantic Ocean, G. Goni and P. Malanotte-Rizzoli, ed., Elsevier Publishing Company.

Hansell, D.A. and T. Y. Waterhouse. 1997. Control of the distribution of organic carbon and nitrogen in the Eastern Pacific Ocean. Deep-Sea Res. I, 44:843-857.

Haug, G., Pedersen, T., Sigman, D., Calvert, S, Nielsen, B., Peterson, L., 1998. Glacial/interglacial: variations in production and nitrogen fixation in the Cariaco Basin during the last 580 kyr. Paleoceanography 13, 427–432.

Hellweger, F. L. and A. L. Gordon, 2002. Tracing Amazon River Water into the Caribbean Sea. J. Mar. Res., 60(4), 537-549.

Herrera, L.E. and G. Febres-Ortega. 1975. Procesos de surgencia y de renovación de aguas en la Fosa de Cariaco, Mar Caribe. Bol. Inst. Oceanográfico Univ. de Oriente 14, 31–44.

Herrera, L.E., G. Febres-Ortega and J. M. Andrés. 1980. Distribución de las masas de agua y sus vinculaciones dinámicas en el sector Centro-Occidental Venezolano, Mar Caribe. Bol. Inst. Oceanográfico Univ. de Oriente, 19, 93–118.

Hickey, B.; E. Baker and N. Kachel. 1986. Suspended particle movement in and around Quinault Submarine Canyon. Mar. Geol. 71, 35–83.

Hill, P. S., T. G. Milligan, and W. R. Geyer. 2000. Controls on effective settling velocity in the Eel River flood plume. Cont. Shelf Res., 20: 2095-2111.

Hill, P. S.; G. Voulgaris and J. H. Trowbridge. 2001. Controls on floc size in a continental shelf bottom boundary layer. J. of Geophys. Res., 106: 9543-9549.

Hoge, F. E., and P. E. Lyon. 1996. Satellite retrieval of inherent optical properties by linear matrix inversion of oceanic radiance models: An analysis of model and radiance measurement errors, J. Geophys. Res., 101: 16,631-16,648.

Hu, C., E. T. Montgomery, R. W. Schmitt and F. E. Muller-Karger. The Amazon and Orinoco River plumes in the tropical Atlantic and Caribbean Sea: Observation from space and S-PALACE floats. Submitted to Deep-Sea Research-II SeaWiFS special volume (in press).

Hu, C.; F. E. Müller-Karger; D. Biggs; K. L. Carder; B. Nababan; D. Nadeau and J. Vanderbloemen. 2003. Comparison of ship and satellite bio-optical measurements on the continental margin of the NE Gulf of Mexico. Int. J. of Rem. Sens., 24 (13): 2597-2612.

Hughen, K. A.; J. T. Overpeck; L. C. Peterson and R. F. Anderson. 1996. The nature of varved sedimentation in the Cariaco Basin, Venezuela, and its palaeoclimatic significance. In: Palaeoclimatology and Palaeoceanography from Laminated Sediments. A. E. S. Kemp, ed. Geological Society Special Publication No. 116, pp. 171-183.

Hughen, K.A., Overpeck, J.T., Peterson, L.C., Trumbore, S., 1996b. Rapid climate changes in the tropical Atlantic region during the last deglaciation. Nature 380, 51}54.

Karl, D.M. and G. A. Knauer. 1991.Microbial production and particle flux in the upper 350 m of the Black Sea. Deep Sea Res. Supl. 2, 38: S921-S942.

Kinard, W.F., D.K. Artwood and G.C. Giese. 1974. Dissolved oxygen as evidence for 18^{o}C Sargasso Sea Water in the Eastern Caribbean Sea. Deep Sea Res., 21: 79-82.

Kirk, J.T.O. 1994. Light and photosynthesis in aquatic ecosystems. Cambridge University Press, 401p.

Kishino, M.; M. Takahashi; N. Okami and S. Ichimura. 1985. Estimation of the spectral absorption coefficients of phytoplankton in the sea. Bull. of Mar. Sci., 37: 634-642.

Lee, Z., Carder, K.L., Mobley, C.D., Steward, R.G., Patch, J.S., 1999. Hyperspectral remote sensing for shallow waters: 2. deriving bottom depths and water properties by optimization. Applied Optics 38, 3831-3843.

Lin, H. L., L. C. Peterson, J. T. Overpeck, S. E.Trumbore and D. W. Murray. 1997. Late Quaternary climatic change from d-18 O records of multiple species of planktonic foraminifera: High-resolution records from the anoxic Cariaco basin, Venezuela. Palaeoceanography, 12(3): 415-427.

Liu, K.K; K. Iseki and S. Y. Chao. 2000. Continental margin carbon fluxes. In: The Changing Ocean Carbon Cycle: A Midterm Synthesis of the Joint Global Ocean Flux Study. R. B. Hanson, H. W. Ducklow and J. G. Field, eds. Cambridge University Press. 528 p.

McClain, E.; W. Pichel and C. Walton. 1985. Comparative Performance of AVHRR-Based Multichannel Sea Surface Temperatures. Journal of Geophysical Research (90): 11,587-11,601.

McPhee-Shaw, E. E.; R.W. Sternberg; B. Mullenbach and A. S. Ogston. 2004. Intermediate nepheloid layers and internal tide reflection on the Northern California Margin. Cont. Shelf Res. (in press)

Morrison, J., and W. Nowlin. 1982. General distribution of water masses within the eastern Caribbean Sea during the winter of 1972 and fall of 1973. J. of Geophys. Res., 87: 4207-4229.

Morrison, J.M., and O.P. Smith. 1990. Geostrophic transport variability along the Aves Ridge in the eastern Caribbean Sea during 1985-1986. J. of Geophys. Res., 95: 699-710.

Mueller, J. L. and R.W. Austin (1995). Ocean Optics Protocols for SeaWiFS Validation, Revision 1, SeaWiFS Technical Report Series, Vol. 25, S. B. Hooker, E. R. Firestone and J. G. Acker (eds.),NASA Technical Memorandum 104566, Greenbelt, Maryland.

Muller-Karger, F. E. R. Varela, R. Thunell, M. Scranton, R. Bohrer, G. Taylor, J. Capelo, Y. Astor, E. Tappa, T. Y. Ho, and J. J. Walsh. 2001. Annual Cycle of Primary Production in the Cariaco Basin: Response to upwelling and implications for vertical export. J. Geophys. Res. 106 (C3): 4527-4542

Müller-Karger, F. E., and R. Aparicio. 1994. Mesoscale Processes Affecting Phytoplankton Abundance in the Southern Caribbean Sea. Cont. Shelf Res. (14:2/3). 199-221.

Müller-Karger, F. E., C. R. McClain, T. R. Fisher, W. E. Esaias, and R. Varela. 1989. Pigment distribution in the Caribbean Sea: Observation from space. Prog. Oceanogr. 23: 23-64.

Muller-Karger, F., R. Varela, R. Thunell, M. Scranton, R. Bohrer, G. Taylor, J. Capelo, Y. Astor, E. Tappa, T.- Y. Ho, M. Iabichella, J. J. Walsh, and J. R. Diaz. 2000. Sediment record linked to surface processes in the Cariaco Basin. EOS. AGU Transactions. American Geophysical Union, 81 (45): 529, 534-535

Muller-Karger, F.E., and R.J. Varela. 1989/1990. Influjo del Río Orinoco en el Mar Caribe: observaciones con el CZCS desde el espacio. Mem. Soc. Cienc. Nat. La Salle 49/50: 361-390.

Nelson, J.R. and S. Guarda. 1995. Particulate and dissolved spectral absorption on the continental shelf of the southeastern United States. J. of Geophys. Res. 100, 8715-8732.

Nelson, N.B., D.A. Siegel, and A.F. Michaels. 1998. Seasonal dynamics of colored dissolved material in the Sargasso Sea. Deep-Seas Res. I. 45:931-957

O'Reilly, J.E.; S. maritorena; B.G. Mitchell; D.A. Siegel; K. L. Carder; S.A. Garver; M. Kahru and C. McClain. 1998. Ocean color algorithms for SeaWiFS. J. of Geophys. Res. (103): 24937-24953.

Okuda, T. 1978. Condiciones hidroquímicas de las aguas superiores de la Fosa de Cariaco y áreas adyacentes. In: Progress in Marine Research in the Caribbean and Adjacent Regions (ed. H. B. Stewart, Jr.), 1976. FAO Fisheries Report No. 200 Supplement, p. 349-362.

Pak, H.; J.R.V. Zaneveld and R.W. Spinrad. 1984. Vertical distribution of suspended particulate matter in the Zaire River, Estuary and Plume. Neth. J. of Sea Res., 17 (2-4):412-425.

Pak, H.; L.A. Codispoti and J. R. V. Zaneveld. 1980. On the intermediate particle maxima associated with oxygen-poor water pff west South America. Deep Sea Res., 27A: 783-797.

Pegau, W. S.; D. Gray and J. R. V. Zaneveld. 1997. Absorption and attenuation of visible and near-infrared light in water: dependance on temperature and salinity. Applied Optics 36: 6035-6046.

Peterson, L. C., G. H. Haug, R.W. Murray, K. M. Yanicik, J. W. King, T. J. Bralower, K. Kameo, S. D. Rutherford and R. B. Pearce. 2000. Late Quaternary stratigraphy and sedimentation at site 1002, Cariaco Basin (Venezuela). In: Leckie, R. M., Sigurdson, H., Acton, G. D. & Draper, G. (eds.), Proceedings of the Ocean Drilling Program, Scientific Results, 165: 85-99.

Peterson, L.C., Overpeck, J.T., Kipp, N.G., Imbrie, J., 1991. A high-resolution late quaternary upwelling record from the anoxic Cariaco Basin, Venezuela. Paleoceanography 6, 99–119.

Prospero, J., R.; Glaccum and R. Nees. 1981. Atmospheric transport of soil dust from Africa to South America. Nature (289): 570 – 572.

Puig, P. and Palanques, A. 1998. Nepheloid structure and hydrographic control on the Barcelona continental margin, northwestern Mediterranean. Mar. Geol. 149, 39–54.

Puig, P., Ogston, A.S., Mullenbach, B.L., Nittrouer, C.A., Sternberg, R.W. 2003. Shelf-to-canyon sediment-transport processes on the Eel continental margin (northern California), Mar. Geol. 193, 129-149.

Repeta, D.J. and D.J. Simpson. 1991. The distribution and recycling of chlorophyll, bacteriochlorophyll and carotenoids in the Black Sea. Deep Seas Res. Suppl. 2, 38: S969-S984

Richards, F. A. 1975. The Cariaco Basin (Trench). Oceanogr. Mar. Biol. Ann. Rev., 13, 11 –67.

Roesler, C. S. and M. J. Perry. 1995. *In situ* phytoplankton absorption, fluorescence emission, and particulate backscattering spectra determined from reflectance. J. of Geophys. Res., 100:13279-13294.

Roesler, C. S., M. J. Perry, and K. L. Carder. 1989. Modeling in situ phytoplankton absorption from total absorption spectra. Limnol. Oceanogr. 34: 1512-1525.

Scranton, M. I., Y. Astor, R. Bohrer, T.-Y. Ho, and F. E. Muller-Karger. 2001. Controls on temporal variability of the geochemistry of the deep Cariaco Basin. Deep Sea Res. I, 48: 1605-1625.

Snyder, G. W. and B. Carson. 1986. Bottom and suspended particle sizes: implications for modern sediemtn transport in Quinault Submarine Canyon. Mar. Geol., 71:85-105.

Taylor, G., M. Scranton, M. Iabichella, T.Y. Ho and R. Varela. 2001. Chemoautotrophy in the redox transition zone of the Cariaco Basin, a significant source of midwater organic carbon production. Limnol. Oceanogr., 46:148-163

Thunell, R., R. Varela, M. Llano, J. Collister, F. Muller-Karger, and R. Bohrer. 2000. Organic carbon flux in an anoxic water column: sediment trap results from the Cariaco Basin. Limnol. Oceanogr., 45: 300-308

Thunnell, R. 1997. Continental margin particle flux: Seasonal cycles and archives of global change. Oceanus. 40: 20-24

Vodacek, A., N.V. Blough, M.D. DeGramdpre, E.T. Peltzer, and R.K. Nelson. 1997. Seasonal variation of CDOM and DOC in the Middle Atlantic Bight: Terrestrial inputs and photooxidation. Limnol. Oceanog. 42: 674-686

Walsh, J.J., D.A. Dieterle, F.E. Muller-Karger, R. Bohrer, W.P. Bissett, , R. Aparicio, R.J. Varela H.T. Hochman, C. Schiller , R. Diaz, R. Thunell, G.T. Taylor, M.I. Scranton, K.A. Fanning, and E.T. Pelzer. 1999. Simulation of carbon/nitrogen cycling during spring upwelling in the Cariaco Basin. J. Geophys. Res., 104 (C4):7807-7825.

WetLabs AC-9 User's Guide. Revision L, January 10, 2003. (D. Stahlke and H. Van Zee). 37p.

Wust, G. 1964. Stratification and circulation in the Atillean-Caribbean Basins. Columbia University Press, Palisades, NY, 201 pp.

Xu, J.P., M. Noble, S. L. Eittreim, L. K. Rosenfeld, F. B. Schwing and C. H. Pilskaln. 2002. Distribution and transport of suspended particulate matter in Monterey Canyon, California. Mar. Geol. 181: 215-234.

Yarincik K. M., Murray R. W., and Peterson L. C. 2000. Climatically controlled eolian and hemipelagic deposition in the Cariaco Basin, Venezuela, over the past 578,000 years: Results from Al/Ti and K/Al. Paleoceanography, 15: 210-228.